



HAL
open science

Stochastic multilevel reduced-order computational model in vibroacoustics applied to automobiles

Justin Reyes

► **To cite this version:**

Justin Reyes. Stochastic multilevel reduced-order computational model in vibroacoustics applied to automobiles. Mechanical engineering [physics.class-ph]. Université Paris-Est, 2020. English. NNT : 2020PESC2077 . tel-03364131

HAL Id: tel-03364131

<https://theses.hal.science/tel-03364131>

Submitted on 4 Oct 2021

HAL is a multi-disciplinary open access archive for the deposit and dissemination of scientific research documents, whether they are published or not. The documents may come from teaching and research institutions in France or abroad, or from public or private research centers.

L'archive ouverte pluridisciplinaire **HAL**, est destinée au dépôt et à la diffusion de documents scientifiques de niveau recherche, publiés ou non, émanant des établissements d'enseignement et de recherche français ou étrangers, des laboratoires publics ou privés.

Université Paris-Est Marne-la-Vallée
École doctorale Sciences, Ingénierie et Environnement

THÈSE

présentée et soutenue publiquement le 5 Novembre 2020

pour l'obtention du

Doctorat de l'Université Paris-Est Marne-la-Vallée

Discipline: mécanique

par

Justin Paul Reyes

Stochastic multilevel reduced-order computational model in vibroacoustics applied to automobiles.

Composition du jury

| | | |
|----------------------------|-----------------------|---|
| <i>Rapporteurs :</i> | Jérôme Antoni | Professeur – INSA Lyon |
| | Jean-François Deü | Professeur – CNAM |
| <i>Examineurs :</i> | Didier Clouteau | Professeur – CentraleSupélec |
| | Christophe Desceliers | Professeur – Université Gustave Eiffel |
| | Béatrice Faverjon | Maître de Conférence – INSA Lyon |
| | Laurent Gagliardini | Expert acoustique-vibrations – Groupe PSA |
| <i>Directeur de thèse:</i> | Christian Soize | Professeur – Université Gustave Eiffel |

Mis en page avec la classe thesul.

Acknowledgment

Je souhaite remercier les Professeurs Jérôme Antoni et Jean-François Deü de m'avoir fait l'honneur de rapporter mon manuscrit de thèse, et pour le temps qu'ils ont consacré à la lecture de ce manuscrit. Je remercie également le Professeur Didier Clouteau et Béatrice Faverjon pour leur participation au jury de thèse.

Mes remerciements vont maintenant à mon directeur de thèse, le Professeur Christian Soize qui m'a offert un environnement de travail idéal. Sa rigueur et sa pédagogie sont un exemple à suivre. Je remercie tout particulièrement mon co-directeur de thèse le Professeur Christophe Desceliers pour son implication de tous les instants, qui m'ont guider tout au long de cette thèse. Sa présence, sa patience et son enseignement m'ont permis de bénéficier d'un encadrement exceptionnel. Je souhaite également remercier Laurent Gagliardini pour son aide et ses conseils qui m'ont aidé à m'intégrer dans le monde industriel.

Je me dois également de remercier l'ensemble des membres du laboratoire MSME pour leur gentillesse et sympathie. Plus particulièrement, mes collègues et amis des bureaux 113 et 118, Anthony, Brian, Picou, Quentin et Vincent. A tous ces moments de partage, dans les bureaux ou les congrès, et tous les repas ensemble qui ont permis de créer une ambiance anti-stress.

Je remercie ensuite le groupe PSA pour sa participation au financement de mes travaux de thèse.

Enfin, je remercie ma famille, mes amis ainsi que ma copine pour leur soutien sans faille durant ces trois années de thèse.

Résumé

Cette thèse traite de systèmes vibroacoustiques complexes sur une large bande de fréquences d'analyse et a été faite dans le cadre de la vibroacoustique des automobiles. Le système considéré est composé d'une structure complexe couplée à une cavité acoustique interne. La structure complexe est définie par une géométrie complexe, constituée de matériaux hétérogènes et de deux types de niveaux structurels : une partie principale rigide et de nombreuses sous-parties flexibles. Dans une telle structure, le modèle vibroacoustique est représenté par les modes élastiques habituels de déplacements globaux associés à la partie principale, et par de nombreux modes élastiques locaux, qui correspondent aux vibrations prépondérantes des sous-parties flexibles. Cependant, dans le cadre de la modélisation vibroacoustique automobile, la principale difficulté est l'imbrication des déplacements globaux avec les nombreux déplacements locaux, qui introduisent un chevauchement des trois domaines de fréquence habituels (basse (LF), moyenne (MF) et haute (HF)). Dans l'industrie automobile, des modèles numériques vibroacoustiques sont utilisés pour prédire les niveaux de bruit interne induits par des excitations solidiennes. Cependant, la dimension des modèles numériques vibroacoustiques est très élevée. Dans ce travail, le modèle numérique a 19 millions de degrés de liberté (DOF) pour la partie structurelle et 1 million de DOF pour la cavité acoustique couplée. Une dimension aussi élevée pose des problèmes de calcul qui sont pour la plupart surmontés par l'introduction d'un modèle numérique d'ordre réduit (ROM) construit avec une analyse modale classique. Néanmoins, la dimension d'un tel ROM est toujours très importante lorsque la bande de fréquence de l'analyse chevauche les domaines LF, MF et HF. Par conséquent, un modèle d'ordre réduit à plusieurs niveaux - pour la structure - est construit sur les bandes de fréquences LF, MF et HF. La stratégie est basée sur une projection multi-niveaux consistant à introduire trois bases d'ordre réduit (ROB) qui sont obtenues en utilisant une méthodologie de filtrage spatial des déplacements locaux. La méthode de filtrage nécessite l'introduction d'un ensemble de fonctions de forme globale qui définissent un sous-espace pour la projection de la matrice de masse de la structure, ce qui donne une matrice dont l'espace nul est constitué de déplacements locaux qui doivent être filtrés. En outre, un ROM classique utilisant des modes acoustiques est réalisée pour la cavité acoustique. Ensuite, le couplage entre le modèle d'ordre réduit multi-niveaux et le modèle d'ordre réduit acoustique est présenté. La modélisation probabiliste non paramétrique est ensuite proposée afin de prendre en compte les incertitudes du modèle induites par les erreurs de modélisation, erreurs dont les effets augmentent avec la fréquence. Ce nouveau modèle stochastique d'ordre réduit multi-niveaux permet d'adapter le niveau d'incertitudes de la structure à chaque partie de la large bande de fréquences, c'est-à-dire aux sous-bandes LF, MF et HF. Une des grandes difficultés de ce travail a été de développer une méthodologie et des algorithmes qui permettent d'analyser des modèles vibroacoustiques de très grande dimension avec des temps de calcul (CPU) qui restent relativement faibles et qui, de plus,

ne conduisent pas à des problèmes de mémoire (RAM) requérant l'utilisation de disques durs externes, ce qui rendrait impossible l'utilisation de la méthode développée. L'application présentée consiste en un modèle vibroacoustique numérique de très grande dimension d'une voiture (structure couplée à une cavité acoustique interne). Les résultats numériques obtenus sont ceux qui étaient espérés concernant leurs qualités et la faisabilité des calculs.

Abstract

This thesis deals with the vibroacoustics of complex systems over a broad frequency band of analysis and has been made as part of the vibroacoustics of automobiles. The system under consideration is composed of a complex structure coupled with an internal acoustic cavity. The complex structure is defined by a complex geometry, constituted of heterogeneous materials and of two types of structural levels: a stiff main part and numerous flexible sub-parts. In such a structure, the vibroacoustics model is represented by the usual global-displacements elastic modes associated with the main part, and by numerous local elastic modes, which correspond to the preponderant vibrations of the flexible sub-parts. However, in the framework of automobile vibroacoustic modeling, the main difficulty is the interweaving of the global displacements with the numerous local displacements, which introduce an overlap of the usual three frequency domains (low- (LF), medium- (MF), and high frequency (HF)). In the automotive industry, computational vibroacoustic models are used for predicting the internal noise levels due to structural excitations. However, the dimension of computational vibroacoustic models is very high. In this work, the computational model has 19 million of degrees-of-freedom (DOFs) for the structural part and 1 million of DOFs for the coupled acoustic cavity. Such a high dimension brings some computational challenges that are mostly overpassed by introducing a reduced-order computational model (ROM) constructed with a classical modal analysis. Nevertheless, the dimension of such ROM is still very important when the frequency band of analysis overlaps the LF, MF and HF domains. Consequently, a multi-level reduced-order model - for the structure is constructed over the LF, MF, and HF frequency bands. The strategy is based on a multi-level projection consisting in introducing three reduced-order bases (ROBs) that are obtained by using a spatial filtering methodology of local displacements. The filtering method requires the introduction of a set of global shape functions that define a subspace for projecting the mass matrix of the structure yielding a matrix for which the null space is made up of local displacements that need to be filtered out. In addition, a classical ROM using acoustic modes is carried out for the acoustic cavity. Then, the coupling between the multi-level reduced order model and the acoustic reduced-order model is presented. The nonparametric probabilistic modeling is then proposed in order to take into account the model uncertainties induced by modeling errors, errors whose effects increase with frequency. This novel stochastic multilevel ROM allows for adapting the level of uncertainties of the structure to each part of the broad frequency band, that is to the LF, MF, and HF sub-bands. One of the great difficulties of this work has been to develop a methodology and algorithms, which make it possible to analyze very large vibroacoustic computational models with computing times (CPU) which remain relatively low and which, moreover,

do not lead to memory (RAM) problems requiring the use of external hard disks, which would make it impossible to use the developed method. The application presented consists of a very large digital vibroacoustic model of a car (structure coupled to an internal acoustic cavity). The numerical results obtained are those which were hoped for concerning their qualities and the feasibility of the calculations.

Contents

| | | |
|----------|--|-----------|
| 1 | Introduction | 1 |
| 1.1 | Context | 1 |
| 1.2 | Position of the research | 3 |
| 1.3 | Objectives | 7 |
| 1.4 | Strategy | 7 |
| 1.5 | Organization of the manuscript | 9 |
| 2 | Construction of the reduced-order computational vibroacoustic model | 11 |
| 2.1 | Description of the vibroacoustic problem | 11 |
| 2.2 | Boundary value problem for the vibroacoustic system in the frequency domain . . | 12 |
| 2.3 | Weak formulation of the boundary value problem in the frequency domain | 15 |
| 2.4 | Reduced-order computational vibroacoustic model | 16 |
| 3 | Multilevel basis | 21 |
| 3.1 | Spatial filtering functions and finite-element projection | 22 |
| 3.2 | Low and high complexity level displacement bases | 25 |
| 4 | Multilevel reduced-order computational model | 31 |
| 4.1 | Construction of the multilevel displacements basis for the LF and MF domains . | 32 |
| 4.2 | Construction of the multilevel reduced-order model in the LF and MF domains . | 35 |
| 5 | Numerical applications for the multilevel reduced-order computational model | 37 |
| 5.1 | Description of the full-order computational model | 37 |
| 5.2 | Frequency domain limits ω_L , ω_M and ω_H | 38 |
| 5.3 | Complexity level for the HF domain | 38 |
| 5.4 | Case 1: Multilevel reduced-order model with $\omega_L/2\pi = 30$ Hz | 39 |
| 5.5 | Case 2: Multilevel reduced-order model with $\omega_L/2\pi = 200$ Hz | 41 |
| 6 | Stochastic multilevel reduced-order computational model in vibroacoustics | 51 |
| 6.1 | Random matrix theory | 52 |
| 6.2 | Classical nonparametric stochastic reduced-order computational model | 53 |
| 6.3 | Nonparametric stochastic multilevel reduced-order computational model | 54 |

| | | |
|---|--|-----------|
| 6.4 | Numerical applications for the classical nonparametric stochastic reduced-order computational vibroacoustic model | 55 |
| 6.5 | Numerical applications for the nonparametric stochastic multilevel reduced-order computational vibroacoustic model | 56 |
| 6.6 | Case 1: Stochastic multilevel reduced-order model with $\omega_L/2\pi = 30$ Hz | 56 |
| 6.7 | Case 2: Stochastic multilevel reduced-order model with $\omega_L/2\pi = 200$ Hz | 57 |
| 6.8 | Discussions | 59 |
| Conclusion and Perspectives | | 79 |
| A Independent Component Analysis using Nastran | | 81 |
| A.1 | Introduction | 81 |
| A.2 | Statistical reduction using ICA | 82 |
| A.3 | Calculation of the likelihood | 86 |
| A.4 | Discussion | 87 |
| A Bibliography | | 89 |

Chapter 1

Introduction

Contents

| | | |
|------------|---------------------------------------|----------|
| 1.1 | Context | 1 |
| 1.2 | Position of the research | 3 |
| 1.3 | Objectives | 7 |
| 1.4 | Strategy | 7 |
| 1.5 | Organization of the manuscript | 9 |

1.1 Context

In the context of the use of large scale computational models, the developments of methodologies for analyzing the vibroacoustics of automobiles and for identifying the models have been and are the subject of a lot of works over the past 20 years (see for example, by being very far from exhaustiveness, [1, 2, 3, 4, 5, 6, 7, 8, 9, 10, 11, 12, 13, 14, 15, 16, 17]).

This work deals with the linear vibroacoustic analysis framework of complex structures such as automobiles. An extension of the multilevel model reduction for complex structures with uncertainties is proposed by taking into account the vibroacoustic coupling. The application is made for automotive structures, but the methods are applicable for other complex structures. We call complex structures, mechanical structures resulting from the assembly of numerous, heterogeneous and geometrically irregular components.

The classical construction of reduced-order models (ROMs) are obtained through modal analysis in computational linear structural dynamics. The multilevel reduction that is proposed in this work will be constructed for a vibroacoustic computational model composed of a complex structure coupled with an internal acoustic cavity.

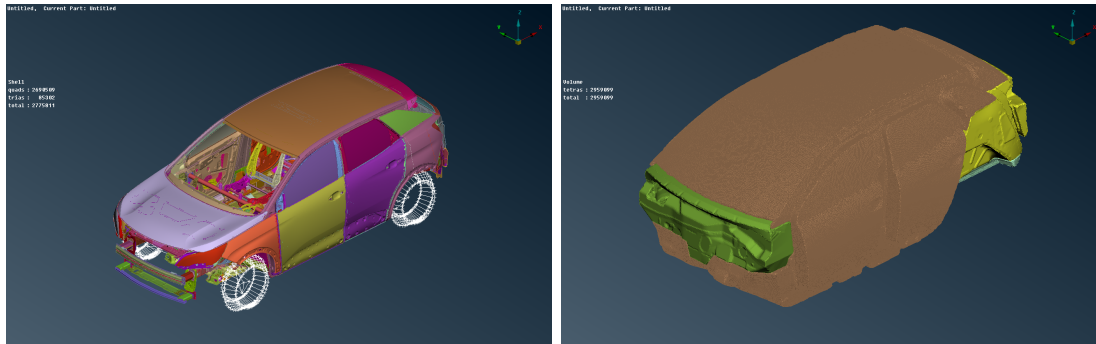


Figure 1.1 – Finite element model of the structure (on the left) and the coupled internal acoustic cavity (on the right).

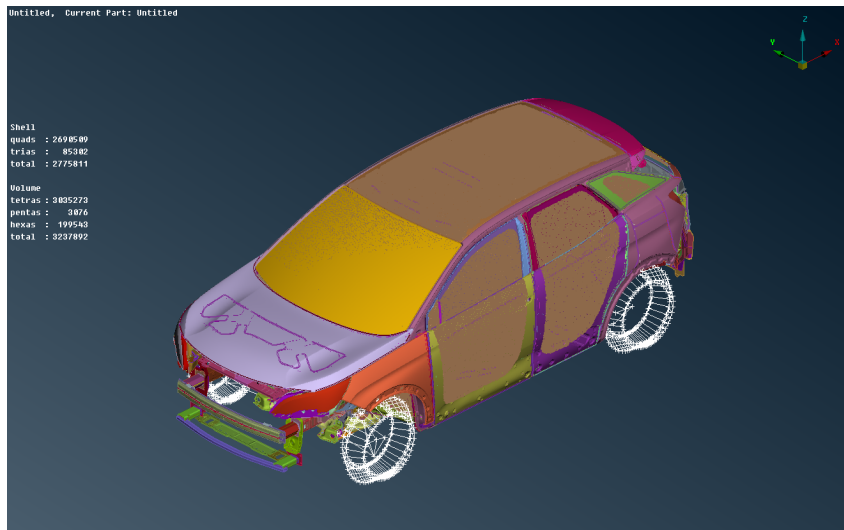


Figure 1.2 – Finite element model of a coupled vibroacoustic automobile.

The model is shown in Fig. 1.1, which is composed of 3 216 050 nodes for the structure and 688 015 nodes for the acoustic cavity. Acoustic specifications in the acoustic cavity of an automobile has become an important criterion for client. Constructors are paying heed more and more on this criterion. Conception criteria, like decreasing the level consumption or the total mass, are added to the criteria of vibroacoustic vehicle dimensioning.

These days, it is well known that the predictions in structural vibration and vibroacoustics over a broad frequency band, using a large scale computational model based on a finite element model [18, 19, 20], must be improved by taking into account the model uncertainties caused by modeling errors. The role of those modeling errors increases with the frequency. Consequently, any model of uncertainties should take into account the frequency evolution. Furthermore, the parametric probabilistic approach of uncertainties is known to be unable to reproduce efficiently the effects of modeling errors.

In such a framework, the nonparametric probabilistic approach of uncertainties will be used. For that, a ROM needs to be introduced in order to implement the nonparametric approach. Accordingly, these two conditions, frequency-evolution of the uncertainties and the reduced-order model, prompt us to propose the development of a multilevel ROM in computational structural dynamics and vibroacoustics. This new multilevel ROM will allow us to adapt the level of uncertainties of the structure to each part of the broad frequency band, that is to the LF (Low-Frequency), MF (Medium-Frequency), and HF (High-Frequency) sub-bands (see below). It is well known that the acoustic cavity can be considered as homogeneous. Consequently, the multilevel ROM will be not necessary for the acoustic cavity.

In structural dynamics and vibroacoustics, the frequency response function (FRF) is typically divided in three sub-bands. The LF band is characterized by a low modal density and by FRFs displaying isolated resonances. These are due to the presence of long-wavelength displacements of the main stiff part of the structure. Those displacements will be called « global displacements » and will be explained later. In contrast, the HF band is characterized by a high modal density and by smoother FRFs caused by the presence of numerous « local displacements ». The middle band, defined as the MF band, displays a non-uniform modal density. The shape of the FRFs exhibit strong variations due to a succession of strong overlapping and small overlapping of resonances [21]. The well-known effective and efficient method used for the LF band is the modal analysis [22, 23, 24, 25, 26, 27, 28, 29, 30, 31, 32], which gives a ROM whose reduced-order basis (ROB) is composed of the first elastic modes that are the first structural elastic modes. For the HF band, energy methods are commonly used like the statistical energy analysis [33, 34, 35, 36, 37, 38, 39, 40, 41, 42, 43]. To analyze the MF band, several methods has been proposed such as deterministic approaches dedicated to the deterministic linear dynamical equations [21, 44, 45, 26, 46, 47, 48, 49, 50]. Other methods are based on stochastic linear dynamical equations to take into account the uncertainties in the computational models [21, 51, 52, 53, 54, 55, 56, 4, 32, 14]. It should be noted that the uncertainties in the MF band plays an important role. To point up the earlier definitions of the different frequency bands, a typical FRF of a structure is shown in Fig. 1.3.

1.2 Position of the research

In this work, we examine the dynamical analysis of complex vibroacoustic system in a broad frequency band. The complex system can be separated in two parts, a complex structure (the car) coupled with an internal acoustic cavity (the cockpit). The complex structure is defined by a complex geometry, made up of heterogeneous materials and more specifically, characterized by the presence of numerous structural levels. For example, the structure is made up of a stiff main part embedding various flexible sub-parts. For such structures, there appears, in addition to the usual global-displacements elastic modes linked with the stiff skeleton, several local elastic modes that are associated with the predominant vibrations of the flexible sub-parts.

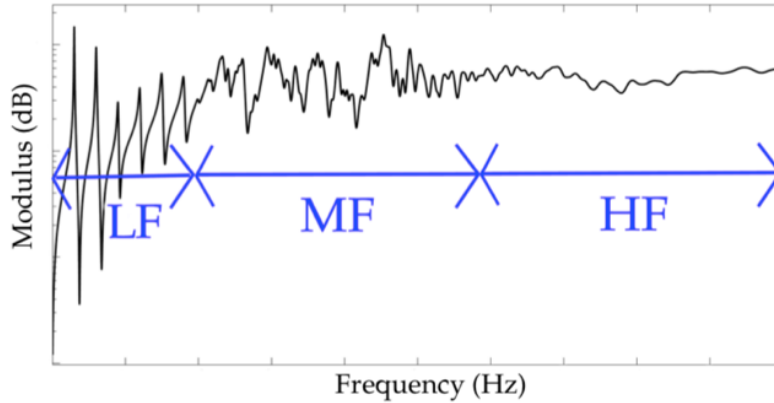


Figure 1.3 – Typical FRF behavior in LF, MF and HF bands. Modulus in dB scale with respect to the frequency.

Such complex structures can be found, for instance in aeronautics and aerospace, but above all in the automotive industry [2, 7, 6, 57]. There appears two main difficulties caused by the presence of the local displacements in the structure. Firstly, the modal density may increase abruptly from low frequencies, causing a high dimension ROM within modal analysis. Secondly, such ROMs may not be robust enough with respect to uncertainties caused by the presence of the numerous local displacements, which are known to be very sensitive to uncertainties. The engineering objectives for such complex structures are to obtain a computational model with a robust prediction for the global displacements at observation points that belong to the main stiff part.

For a vibroacoustic system composed of a complex elastic structure coupled with an internal acoustic cavity, characterized by the presence of numerous local elastic modes entangled with global elastic modes, the research are not plentiful. Nonetheless for the structural part, researches have been performed. In the experimental modal analysis framework, spatial filtering method of the local displacements [58], based on regularization schemes, has been proposed [59]. For computational models, the Guyan condensation technique [60] has also been used, consisting in introducing master structural nodes in which the mass is condensed. It allows the filtering of the local displacements. The downside is the complexity of the choice of the master nodes [61]. Filtering using the lumped mass matrix approximations have also been introduced by [62, 63, 64] but it depends on the mesh and cannot be adjust. The construction [34] of a global displacement basis using a coarse mesh yields important errors for the elastic energy. Other methods for extracting the long-wavelength elastic modes of the main structure, like the interface substructuring, has also been proposed [50]. Moreover, computational approaches based on the use of image processing [65] have been proposed for identifying the global elastic modes, in which the global displacements are considered as the eigenvectors of the frequency mobility matrix [66]. The extrapolation of the dynamical response using a sparse representation constructed using a few elastic modes has also been proposed in [67]. In the LF band, for slender structures ex-

hibiting a high modal density, simplified equivalent models have been proposed in [68, 69] and homogenization has been suggested in [70]. Though, using these approaches, the simplification of the model is not automatic and requires an expertise and validation continues to be necessary.

For complex structures for which the elastic modes are neither purely global nor purely local displacements, the increasing of the dimension of the ROM based on the classical modal analysis proves to be inconvenient. The methodology to sort the elastic modes depending to whether they are global displacements or local displacements is not relevant because the elastic modes are an association of both types of displacements. It is well known that large amplitudes of the local displacements are difficult to distinguish from the global ones using the modal shapes. The difficulty increases with the frequency.

Generally, in the case of a complex structure, an elastic mode is constituted of global displacements (long wavelength deformations) assorted with local displacements (short wavelength deformations) of differentiated structural level. One important observation is that as the frequency increases, the global displacements in the elastic modes are less and less perceptible. The fact is that they are covered by the high amplitudes local displacements.

Nevertheless, substructuring techniques have been used for trying to solve this separation problem. The substructuring techniques have deeply been studied [71, 72, 73]. As written in [74]: "historically, the concept of substructuring was first introduced by Argyris and Kelsey in 1959 [75] and by Przemieniecki in 1963 [76] and was extended by Guyan and Irons [60, 77]. Hurty [78, 79] considered the case of two substructures coupled through a geometrical interface. Finally, Craig and Bampton [80] has adapted the Hurty method. Many variants has been proposed for improving substructuring techniques [81, 82, 83, 84, 85], notably for the complex dynamical systems with many auxiliaries considered as substructures from Benfield and Hruda [86]. A new group of methods has been introduced for two coupled substructures with fixed geometrical interface (elastic modes) using structural modes with free geometry interface used in the Craig and Bampton and by MacNeal [87] and Rubin [88]. Then the Lagrange multipliers have been applied to write the coupling on the geometrical interface [89, 90, 91, 92]". The substructuring needs discarding the component modes associated with flexible sub-parts, to eliminate their associated local displacements. In the model considered, there is no clear boundary between the skeleton and the substructures, that is to say, between the main stiff part and the flexible sub-parts. This property can be explained by the complex geometry of the structure that is constructed in order to have a continuous series of structural levels, instead of clear separation, in addition to the various embedded equipments. In this type of setup, the notion of local displacements is relative. It is worth mentioning that, in comparison to the usual global displacements that are present in the LF band, the local displacements associated with the structural sub-levels (which can also appear in the LF band) are characterized by high complexity level, similarly to those in the HF band. Therefore, for the complex structure studied, there is an overlap of the three vibration

regimes (LF, MF and HF band).

Regarding the uncertainties in the computational model, the probabilistic framework is well suited to construct the stochastic models and to solve the inverse problems for the identification of the probabilistic models of uncertainties. Thereafter, we present the framework limited to the probabilistic approaches for uncertainty quantification. To take into account model parameter uncertainties, model uncertainties induced by modeling errors and the variabilities in the real dynamical system, different probabilistic approaches can be used (see [14]).

The *parametric probabilistic approach* is fairly well designed for model-parameter uncertainties, at least for a sufficient small number of parameters. It involves the construction of a prior and a posterior stochastic models of uncertain model parameters linked, for instance, to materials properties [93, 94, 95, 96, 97, 98, 99, 100, 101, 102, 103, 104, 105, 14], to geometry, to boundary conditions, etc. This method proved to be computationally efficient for both the computational model and its resulting ROM [106, 107] and for large-scale statistical inverse problems [108, 109, 110, 111, 112, 113]. The main limit of this approach is that it does not take into account neither the model uncertainties induced by modeling errors introduced during the construction of the computational model nor the uncertainties caused by the use of a ROM.

The *nonparametric probabilistic approach* [114, 14] allows model uncertainties induced by general modeling errors to be taken into account in the framework of linear dynamical systems. The modus operandi is done in two stages. Firstly, the construction of a linear ROM of dimension n using the linear computational model with m degrees of freedom (DOFs) and a reduced-order basis (ROB) of dimension n . Then, a linear stochastic ROM is built by replacing the deterministic matrices of the linear ROM by random matrices for which the probability distributions are constructed [14] using the Maximum Entropy (MaxEnt) [115, 116] principle of Information Theory. The construction of the linear stochastic ROM is fulfilled under the constraint generated from the available information such as algebraic positiveness, integrability of the inverse, and some statistical information. This approach enlarged for different family of random matrices and for linear boundary value problems [117, 118, 14]. Experimental validations and applications to statistical inverse problems can be found for linear problems in composites [119], viscoelasticity [120], dynamic substructuring [121, 122, 123], vibroacoustics [32, 2], robust design and optimization [124], etc, and for the identification and sampling the Bayesian posteriors of high-dimensional symmetric positive-definite random matrices for data-driven updating of computational models [125]. An extension to the nonlinear geometrical effects in structural analysis has also been made [126, 127, 128].

It is well known that the real systems exhibit variabilities. As such, for a given design of a structure, the manufactured objects differ from one to another one, which results in a dispersion in the FRFs. Those variabilities are caused by the small differences with respect to the unique

design that is used for constructing the computational model. It should be noted that the variability increases with the frequency.

Recently, a method has been proposed by Ezvan [129] to separate the local displacements and the global displacements using a spatial filtering (on wavelength). Moreover, the multilevel stochastic approach for structural dynamics has been introduced in [12] to adapt the level of the uncertainties in each frequency band: LF, MF, and HF. In this work, we present an extension to the case of vibroacoustic systems based on a reformulation of the construction of the multilevel ROM for the structural part.

1.3 Objectives

For complex structures, such as automobiles, numerous high complexity level types elastic modes are intertwined with the long wavelength types elastic modes. This provokes a high modal density and an overlap of the three vibration regimes (LF, MF, and HF) and therefore, two hurdles related to uncertainty quantification and to computational efficiency. As a reminder, the overlap is explained by the presence of high complexity level HF-type displacements with the usual global displacements of the LF band. The objective of this work is multiple. The first one, is to propose a stochastic multilevel ROM for the structure that is able to take into account the variability induced by the overlap in the three vibration regimes, which is a reformulation of the method proposed in [129, 12], for which the presentation, the developments, and the formulated interpretations are different. Secondly, we consider not only the structure but also the vibroacoustic system constituted of the structure coupled with the acoustic cavity. An objective of this work is to propose a predictive stochastic multilevel ROM whose dimension is inferior to the usual ROM constructed by using the classical modal analysis. Another very important objective is that the algorithms developed can be used for very large computational models without encountering problems related to the limitation of RAM and with numerical costs which remain low. This last objective requires in-depth methodological and algorithmic reflection. The last objective is the need to develop a methodology and algorithms, which are not intrusive with respect to commercial software.

1.4 Strategy

A new methodology has been introduced in [130] for the construction of a stochastic ROM devoted to dynamical structures possessing numerous local elastic modes in the LF range. The stochastic model is obtained by using the nonparametric probabilistic approach of uncertainties within a new formulation of the ROM whose ROB is made up of two families: on one hand the global displacements and on the other hand the local displacements. The separation of those two families is done by the introduction of a projection operator for the kinetic energy associated with a subspace of piecewise polynomial functions. The spatial dimension of the subdomains of

the displacements projection is constant. This allows a partition of the domain of the structure, and a control parameter of the filtering between the global displacements and the local displacements. The subdomain allows for excluding the local displacements by using an approximation. The generation of such subdomains is called a *uniform domain partition*. The Fast Marching Method [131, 132] is used in order to carry out the uniform domain partition for a complex finite element mesh. The application for the case of automobile structure has been proposed in [7, 6]. Papers associated with this methodology are [130, 7, 6, 133, 134]. A former PhD thesis was defended with a subject related to these papers [135].

In a following thesis by Ezvan (see [129, 12, 136, 137, 138, 139]), instead of the piecewise constant approximation, another methodology is used through the introduction of a computational framework for any approximation subspace for the kinetic energy. For automobile framework, polynomial shape functions, with support equivalent to the whole domain of the structure, have been used for constructing a spatial filtering for long wavelength displacements ROM. This generalization allows for achieving an efficient convergence of the long wavelength displacements ROM with respect to the chosen spatial filtering. Furthermore, a multilevel ROM has been proposed, whose the reduced-order basis (ROB) is composed of numerous families of displacements, which coincide with the different structural levels of the complex structure. This ROB has been constructed to achieve three families such as LF-, MF-, and HF-wavelength types of displacements using successive spatial filterings. The multilevel ROM lets on implementing a probabilistic model of uncertainties that is adapted to each vibration regime (LF, MF, and HF). By constructing the multilevel stochastic ROM, the statistical fluctuations for each vibration regime can be controlled. In the literature [140, 141, 142], multilevel substructuring methodologies exist but do not have the same objective at all and have been proposed only to speed up the solution of large scale generalized eigenvalue problems.

This work follows on from these two theses, in particular the Ezvan's thesis. In the present work [143, 144, 145, 17], the computational vibroacoustic model is introduced. In addition, the spatial filtering methodology has been modified and automated. The presentation of the multilevel ROM is novel as well as the developments of the algorithms and the interpretations that are made of them. In particular, the strategy will be to use polynomial shape functions to represent the behavior of the elastic modes in order to construct a long wavelength-displacements ROM for a complex structure such as an automotive. Moreover, a multilevel reduced-order computational model in vibroacoustics will be constructed, whose reduced-order basis is formed from three families of wavelength displacements (LF, MF, and HF), which correspond to the three structural levels of the complex structure. This will allow for implementing a nonparametric probabilistic model of uncertainties that will be adapted for each vibration regime. The stochastic multilevel reduced-order computational model in vibroacoustics will allow for controlling the statistical fluctuations for each frequency band type of displacements.

1.5 Organization of the manuscript

Chapter 2 is devoted to the construction of the reduced-order computational vibroacoustic model. The boundary value problem of the vibroacoustic system is presented in the frequency domain for a linear viscoelastic solid medium coupled with a linear dissipative acoustic fluid medium. Its weak formulation is then constructed. Its discretization by the finite element method yields the full-order computational vibroacoustic model in the frequency domain. Finally, the classical reduced-order computational vibroacoustic model is deduced by projecting the full-order computational vibroacoustic model on the truncated modal expansions of the solution of the problem.

Chapter 3 presents the principle of the spatial filtering. The construction of a multilevel basis is given and the associated algorithms are detailed. The methodology is introduced to separate the elastic modes in two quantities "low complexity level" and "high complexity level" displacements with regard to a maximal polynomial degree. The importance of the data storage with respect to the RAM limitations is also explained.

Chapter 4 deals with the construction of the multilevel reduced-order computational model involving the construction of the multilevel displacements basis and the construction of the associated multilevel displacements model for the LF and MF domains. This chapter lays the foundation for the entire method for which the parameters involved are introduced.

In Chapter 5, a numerical application of the multilevel reduced-order computational model is performed. The method is applied to two different cases. The results are compared and commented.

Chapter 6 is devoted to the stochastic multilevel reduced-order computational model in vibroacoustics. The probabilistic model of random matrices is constructed in the framework of the nonparametric probabilistic approach of model uncertainties. Then the classical nonparametric stochastic reduced-order computational model is introduced followed by the construction of the nonparametric multilevel reduced-order computational model in vibroacoustics. Finally the numerical application devoted to a large scale computational vibroacoustic model of an automobile is presented and commented.

After the conclusion and the perspectives, the reader will find an appendix devoted to the Independent Component Analysis (ICA) using the Nastran (commercial software), which is a computational tool for estimating a log-likelihood indicator to compare computation and experimental FRF measurements for automobiles [143, 15]. As this work on ICA, which was carried out at the start of the thesis, has been carried out with an automobile computational model that is different from the one presented in all the chapters, we have preferred to present this work on ICA in an Appendix for avoiding any confusion.

Chapter 2

Construction of the reduced-order computational vibroacoustic model

Contents

| | | |
|------------|--|-----------|
| 2.1 | Description of the vibroacoustic problem | 11 |
| 2.2 | Boundary value problem for the vibroacoustic system in the frequency domain | 12 |
| 2.3 | Weak formulation of the boundary value problem in the frequency domain | 15 |
| 2.4 | Reduced-order computational vibroacoustic model | 16 |

The purpose of this chapter is to construct the reduced-order computational vibroacoustic model (ROM) for a vibroacoustic system (the car and the air in its cockpit). In the next chapter, a Global/Local ROM will be presented and constructed in using its matrices. In this chapter, the boundary value problem is presented in the frequency domain for a linear viscoelastic solid medium coupled with a linear dissipative acoustic fluid medium. Then the weak formulation of the problem in the frequency domain of the vibroacoustic system is constructed. A full-order computational vibroacoustic model is then obtained by using the Finite Element method for discretizing the weak formulation of the boundary value problem. Finally, the ROM is constructed by projecting the full-order computational vibroacoustic model on the truncated modal expansions of the solutions of the problem.

2.1 Description of the vibroacoustic problem

Let us consider a vibroacoustic system that is constituted of a three-dimensional structure (the car) coupled with an internal acoustic cavity (the gas in the cockpit). Figure 2.1 shows a simplified description of the vibroacoustic system. Despite the fact that the acoustic cavity is internal, it is nevertheless assumed the acoustic cavity is almost closed with a nonsealed wall. The vibroacoustic system can be modeled as a linear viscoelastic solid medium that occupies

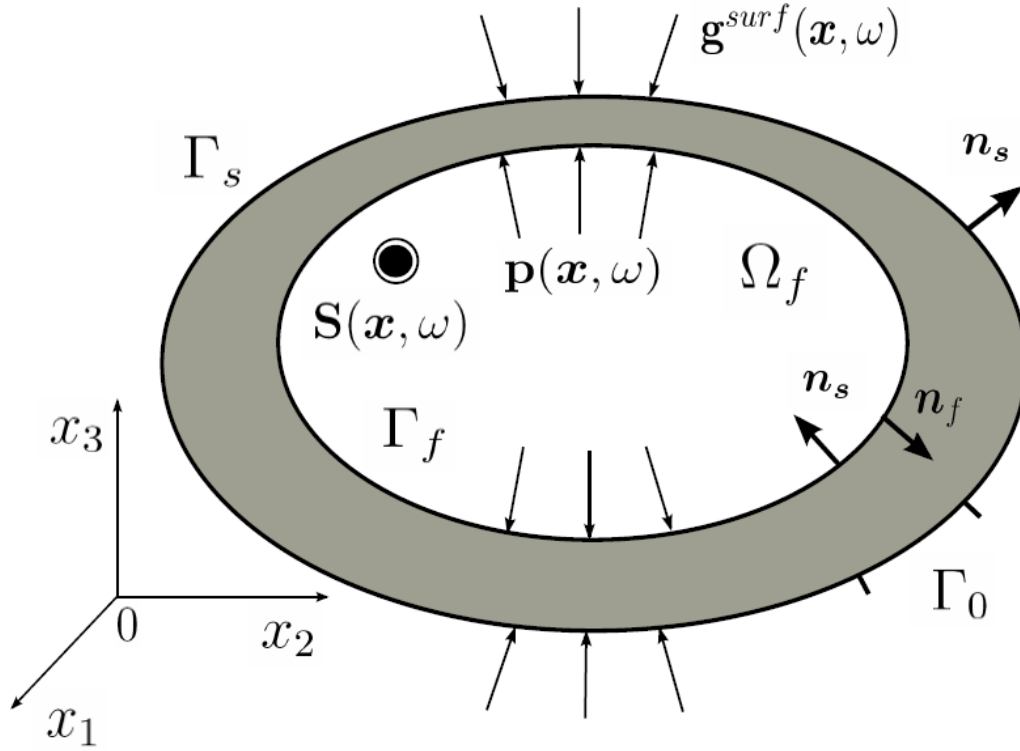


Figure 2.1 – Vibroacoustic system

the domain $\Omega_s \subset \mathbb{R}^3$. It is also assumed that the acoustic cavity can be modeled as a linear dissipative acoustic fluid medium that is homogeneous and occupying the domain $\Omega_f \subset \mathbb{R}^3$. The external boundary of domain Ω_s (see Fig. 2.1) is constituted of two parts Γ_s (on which are imposed external surface forces as Neumann boundary conditions) and Γ_0 (on which are imposed Dirichlet boundary conditions) while the boundary Γ_f of domain Ω_f is the coupling interface between the linear viscoelastic solid medium and the linear dissipative acoustic fluid medium. External loads are applied to the vibroacoustic system and they consist in the surface forces \mathbf{g}^{surf} on part Γ_s , the body forces \mathbf{g}^{vol} in Ω_s , and the acoustic source s in Ω_f . In addition, it is also assumed that the part Γ_0 is fixed. In a Cartesian reference frame $(\mathbf{e}_1, \mathbf{e}_2, \mathbf{e}_3)$, the dynamical response of the vibroacoustic system (under external loads) are the displacement field $\mathbf{u} = (u_1, u_2, u_3)$ in Ω_s of the linear viscoelastic solid medium and the pressure disturbance field p in Ω_f of the linear dissipative acoustic fluid medium. In the next section, the boundary value problem is presented for which the solutions are displacement field \mathbf{u} and pressure disturbance field p .

2.2 Boundary value problem for the vibroacoustic system in the frequency domain

In this section, we use the equations of the vibroacoustic system presented in [26].

2.2.1 Equations for the linear viscoelastic solid medium

In this section, the equations for the linear viscoelastic solid medium are established in the frequency domain. Note that hereinafter, the summation convention on repeated indices is used.

2.2.1.1 Balance equations and boundary conditions

In case there are no external body forces $\mathbf{g}^{\text{vol}} = 0$, then the balance equations for the linear viscoelastic solid medium in the frequency domain are written, for $i = 1, \dots, 3$, as

$$\rho_s u_i(\mathbf{x}; \omega) - \partial_j \sigma_{ij}(\mathbf{x}; \omega) = 0 \quad \text{in } \Omega_s, \quad (2.1)$$

in which $\mathbf{x} = (x_1, x_2, x_3)$ is the position vector of any point in \mathbb{R}^3 , where ω is the angular frequency belonging to the frequency band of analysis $\mathbb{B} = [\omega_{\min}, \omega_{\max}]$, where ρ_s is the mass density of the linear viscoelastic solid medium at rest, $\partial_j \sigma_{ij}$ is the divergence of the Cauchy stress tensor, and ∂_j is the partial derivative with respect to x_j . We assume that there are two Neumann boundary conditions on parts Γ_f and Γ_s , which, respectively, correspond to pressure field $p(\mathbf{x}; t)$ applied by the acoustic cavity on Γ_f and by surface forces $\mathbf{g}^{\text{surf}} = (g_1^{\text{surf}}, g_2^{\text{surf}}, g_3^{\text{surf}})$ on Γ_s . In addition, we also assume that a Dirichlet boundary condition is applied to Γ_0 . We then have, for all $i = 1, 2, 3$,

$$\begin{aligned} \sigma_{ij}(\mathbf{y}; \omega) n_j(\mathbf{y}) &= -p(\mathbf{y}; \omega) n_i(\mathbf{y}) \quad \text{on } \Gamma_f, \\ \sigma_{ij}(\mathbf{y}; \omega) n_j(\mathbf{y}) &= g_i^{\text{surf}}(\mathbf{y}; \omega) \quad \text{on } \Gamma_s, \\ u_i(\mathbf{y}; \omega) &= 0 \quad \text{on } \Gamma_0. \end{aligned}$$

where $\mathbf{n} = (n_1, n_2, n_3)$ is the outward unit vector of domain Ω_s and $\mathbf{y} = (y_1, y_2, y_3)$ is the vector of coordinates of a point located on the boundary of domain Ω_s .

2.2.1.2 Constitutive equations for the linear viscoelastic solid medium

In the frequency domain and for a linear viscoelastic solid medium, the constitutive equations are written as

$$\sigma_{ij}(\mathbf{x}, \omega) = (a_{ijkh}(\mathbf{x}, \omega) + i\omega b_{ijkh}(\mathbf{x}, \omega)) \varepsilon_{kh}(\mathbf{x}, \omega), \quad (2.2)$$

where $\varepsilon_{kh} = 1/2(\partial_k u_h + \partial_h u_k)$ is the linear strain tensor and where the viscoelastic coefficients $a_{ijkh}(\mathbf{x}, \omega)$ and $b_{ijkh}(\mathbf{x}, \omega)$ are frequency dependent and such that

1. $a_{ijkh}(\mathbf{x}, -\omega) = a_{ijkh}(\mathbf{x}, \omega)$,
2. $b_{ijkh}(\mathbf{x}, -\omega) = b_{ijkh}(\mathbf{x}, \omega)$,
3. $\lim_{\omega \rightarrow +\infty} a_{ijkh}(\mathbf{x}, \omega) < +\infty$,
4. $\lim_{\omega \rightarrow +\infty} b_{ijkh}(\mathbf{x}, \omega) = 0$,
5. $a_{ijkh}(\mathbf{x}, \omega) = a_{jikh}(\mathbf{x}, \omega) = a_{ijhk}(\mathbf{x}, \omega) = a_{khij}(\mathbf{x}, \omega)$,

$$6. \quad b_{ijkh}(\mathbf{x}, \omega) = b_{jikh}(\mathbf{x}, \omega) = b_{ijhk}(\mathbf{x}, \omega) = b_{khij}(\mathbf{x}, \omega) \quad ,$$

$$7. \quad a_{ijkh}(\mathbf{x}, \omega)X_{ij}X_{kh} \geq c_1X_{ij}X_{ij} \quad , \quad b_{ijkh}(\mathbf{x}, \omega)X_{ij}X_{ij} \geq c_2X_{ij}X_{kh} \quad ,$$

for all symmetric second-order tensor $\{X_{ij}\}_{ij}$ and where c_1 and c_2 are two positive real scalars that are independent of ω .

2.2.2 Equations for the linear dissipative acoustic fluid medium

The equations of the linear dissipative acoustic fluid medium are established in this section. These equations are presented in [26]. Let p and \mathbf{v} be the disturbances of the pressure and of the velocity in the linear dissipative acoustic fluid medium for which the undisturbed values (when the linear dissipative acoustic fluid medium is at rest) are p_f and \mathbf{v}_f . In the case for which the thermal conduction can be neglected in the acoustic fluid and if there is no acoustic source $s = 0$, then the equations of the linear dissipative acoustic fluid medium can be written in terms of pressure disturbance field p and velocity field \mathbf{v} . We then have

$$i\omega p(\mathbf{x}, \omega) = -\rho_f c_f^2 \nabla \cdot \mathbf{v}(\mathbf{x}, \omega) \quad , \quad (2.3)$$

$$i\omega \rho_f \mathbf{v}(\mathbf{x}, \omega) + \nabla p = -i\omega \tau \nabla p(\mathbf{x}, \omega) \quad , \quad (2.4)$$

in which the dot operator is the usual inner product in \mathbb{R}^3 , ρ_f and c_f are the mass density and sound velocity respectively in the linear dissipative acoustic fluid medium at rest and where τ , which can be frequency dependent, is given by

$$\tau = \frac{1}{\rho_f c_f^2} \left(\frac{4}{3} \eta + \zeta \right) \quad , \quad (2.5)$$

in which η is the dynamic viscosity and ζ is the second viscosity. Combining these two equations yields

$$-\omega^2 \frac{1}{\rho_f c_f^2} p(\mathbf{x}, \omega) - i\omega \frac{\tau}{\rho_f} \nabla^2 p(\mathbf{x}, \omega) - \frac{1}{\rho_f} \nabla^2 p(\mathbf{x}, \omega) = 0 \quad \text{in } \Omega_f \quad . \quad (2.6)$$

In addition, the following Neumann boundary condition on Γ_f can be straightforwardly deduced from Eq. (2.4),

$$\frac{(1 + i\omega\tau)}{\rho_f} \nabla p(\mathbf{y}, \omega) \cdot \mathbf{n}(\mathbf{y}) = \omega^2 \mathbf{u}(\mathbf{y}, \omega) \cdot \mathbf{n}(\mathbf{y}) \quad \text{on } \Gamma_f \quad , \quad (2.7)$$

where the displacement field $\mathbf{x} \mapsto \mathbf{u}(\mathbf{x}, \omega)$ is such that $\mathbf{v}(\mathbf{x}, \omega) = i\omega \mathbf{u}(\mathbf{x}, \omega)$ for all $\mathbf{x} \in \Omega_f \cup \Gamma_f$.

2.2.3 Boundary value problem in the frequency domain for the vibroacoustic system

The equations of the boundary value problem in the frequency domain for the vibroacoustic system consists in finding $\mathbf{x} \mapsto \mathbf{u}(\mathbf{x}, \omega)$ and $\mathbf{x} \mapsto p(\mathbf{x}, \omega)$ such that, for $i = 1, \dots, 3$,

$$\rho_s u_i(\mathbf{x}; \omega) - \partial_j \sigma_{ij}(\mathbf{x}; \omega) = 0 \quad \text{in } \Omega_s \quad , \quad (2.8)$$

$$\sigma_{ij}(\mathbf{x}, \omega) = (a_{ijkh}(\mathbf{x}, \omega) + i \omega b_{ijkh}(\mathbf{x}, \omega)) \varepsilon_{kh}(\mathbf{x}, \omega) \quad \text{in } \Omega_s \quad , \quad (2.9)$$

$$\varepsilon_{kh}(\mathbf{x}, \omega) = \frac{1}{2} (\partial_h u_k(\mathbf{x}, \omega) + \partial_k u_h(\mathbf{x}, \omega)) \quad \text{in } \Omega_s \quad , \quad (2.10)$$

$$\sigma_{ij}(\mathbf{y}; \omega) n_j(\mathbf{y}) = -p(\mathbf{y}; \omega) n_i(\mathbf{y}) \quad \text{on } \Gamma_f \quad , \quad (2.11)$$

$$\sigma_{ij}(\mathbf{y}; \omega) n_j(\mathbf{y}) = g_i^{\text{surf}}(\mathbf{y}; \omega) \quad \text{on } \Gamma_s \quad , \quad (2.12)$$

$$u_i(\mathbf{y}; \omega) = 0 \quad \text{on } \Gamma_0 \quad , \quad (2.13)$$

$$-\omega^2 \frac{1}{\rho_f c_f^2} p(\mathbf{x}, \omega) - i \omega \frac{\tau}{\rho_f} \nabla^2 p(\mathbf{w}, \omega) - \frac{1}{\rho_f} \nabla^2 p(\mathbf{x}, \omega) = 0 \quad \text{in } \Omega_f \quad , \quad (2.14)$$

$$\frac{(1 + i \omega \tau)}{\rho_f} \nabla p(\mathbf{y}, \omega) \cdot \mathbf{n}(\mathbf{y}) = \omega^2 \mathbf{u}(\mathbf{y}, \omega) \cdot \mathbf{n}(\mathbf{y}) \quad \text{on } \Gamma_f \quad . \quad (2.15)$$

2.3 Weak formulation of the boundary value problem in the frequency domain

The solution $\mathbf{x} \mapsto \mathbf{u}(\mathbf{x}, \omega)$ belongs to the set \mathcal{C}_s of all the admissible displacement fields and the solution $\mathbf{x} \mapsto p(\mathbf{x}, \omega)$ belongs to the set \mathcal{C}_f of all the admissible sound pressure fields. Let us introduce the sesquilinear forms of mass $m^s(\cdot, \cdot)$, damping $d^s(\cdot, \cdot)$, and stiffness $k^s(\cdot, \cdot)$, which are positive-definite hermitian on $\mathcal{C}_s \times \mathcal{C}_s$ and the antilinear form $\ell^s(\cdot)$ defined on \mathcal{C}_s that are defined, for all \mathbf{u} and $\delta \mathbf{u} = (\delta u_1, \delta u_2, \delta u_3)$ in \mathcal{C}_s , as

$$m^s(\mathbf{u}, \delta \mathbf{u}) = \int_{\Omega_s} \rho(\mathbf{x}) u_j(\mathbf{x}) \overline{\delta u_j(\mathbf{x})} d\mathbf{x} \quad , \quad (2.16)$$

$$d^s(\mathbf{u}, \delta \mathbf{u}) = \int_{\Omega_s} b_{ijkh}(\mathbf{x}) \partial_h u_k(\mathbf{x}) \overline{\partial_j \delta u_i(\mathbf{x})} d\mathbf{x} \quad , \quad (2.17)$$

$$k^s(\mathbf{u}, \delta \mathbf{u}) = \int_{\Omega_s} a_{ijkh}(\mathbf{x}) \partial_h u_k(\mathbf{x}) \overline{\partial_j \delta u_i(\mathbf{x})} d\mathbf{x} \quad , \quad (2.18)$$

$$\ell^s(\delta \mathbf{u}) = \int_{\Gamma_s} g_i^{\text{surf}}(\mathbf{y}) \overline{\delta u_i(\mathbf{y})} dS(\mathbf{y}) \quad , \quad (2.19)$$

in which $d\mathbf{x} = dx_1 dx_2 dx_3$ is the volume element and $dS(\mathbf{y})$ is the surface element. Let us introduce the sesquilinear form $m^f(\cdot, \cdot)$, which is positive-definite hermitian on $\mathcal{C}_f \times \mathcal{C}_f$, and the sesquilinear forms $d^f(\cdot, \cdot)$ and $k^f(\cdot, \cdot)$ that are positive hermitian on $\mathcal{C}_f \times \mathcal{C}_f$ such that for all p

and δp in \mathcal{C}_f , we have

$$m^f(p, \delta p) = \frac{1}{\rho_f c_f^2} \int_{\Omega_f} p(\mathbf{x}) \overline{\delta p(\mathbf{x})} d\mathbf{x} \quad , \quad (2.20)$$

$$d^f(p, \delta p) = \frac{\tau}{\rho_f} \int_{\Omega_f} \nabla p(\mathbf{x}) \cdot \overline{\nabla \delta p(\mathbf{x})} d\mathbf{x} \quad , \quad (2.21)$$

$$k^f(p, \delta p) = \frac{1}{\rho_f} \int_{\Omega_f} \nabla p(\mathbf{x}) \cdot \overline{\nabla \delta p(\mathbf{x})} d\mathbf{x} \quad . \quad (2.22)$$

Let $c(\cdot, \cdot)$ be the sesquilinear form of vibroacoustic coupling defined on $\mathcal{C}_f \times \mathcal{C}_s$ such that for all p and δp in \mathcal{C}_f and for all \mathbf{u} in \mathcal{C}_s , we have

$$c(p, \mathbf{u}) = \int_{\Gamma_f} p(\mathbf{y}) \overline{u_i(\mathbf{y})} n_i(\mathbf{y}) dS(\mathbf{y}) \quad . \quad (2.23)$$

The weak formulation of the boundary value problem in the frequency domain for the vibroacoustic system is then constructed by using the method of the test functions and is then defined as follows: find $\mathbf{u}(\cdot, \omega)$ in \mathcal{C}_s and $p(\cdot, \omega)$ in \mathcal{C}_f such that, for all $\delta \mathbf{u}$ in \mathcal{C}_s and δp in \mathcal{C}_f ,

$$-\omega^2 m^s(\mathbf{u}, \delta \mathbf{u}) + i\omega d^s(\mathbf{u}, \delta \mathbf{u}) + k^s(\mathbf{u}, \delta \mathbf{u}) + c(p, \delta \mathbf{u}) = \ell^s(\delta \mathbf{u}) \quad , \quad (2.24)$$

$$-\omega^2 m^f(p, \delta p) + i\omega d^f(p, \delta p) + k^f(p, \delta p) + \omega^2 \overline{c(\delta p, \mathbf{u})} = 0 \quad . \quad (2.25)$$

2.4 Reduced-order computational vibroacoustic model

2.4.1 Full-order computational vibroacoustic model

Let $\mathbf{u}(\omega)$ (resp. $\mathfrak{p}(\omega)$) be the finite element vectors of all the degrees of freedom corresponding to the nodal values on the finite element mesh of domain Ω_s (resp. Ω_f) for displacement field $\mathbf{u}(\cdot, \omega)$ (resp. disturbance of pressure field $p(\cdot, \omega)$). Let n_{dof}^s (resp. n_{dof}^f) be the dimension of vector $\mathbf{u}(\omega)$ (res. $\mathfrak{p}(\omega)$). The full-order computational vibroacoustic model is then constructed by discretizing the sesquilinear forms in Eqs. (2.24) and (2.25) by the finite-element method. Equations (2.24) and (2.25) are then replaced by

$$(-\omega^2 [\mathbb{M}^s] + i\omega [\mathbb{D}^s] + [\mathbb{K}^s]) \mathbf{u}(\omega) + [\mathbb{C}] \mathfrak{p}(\omega) = \mathbb{F}^s(\omega) \quad , \quad (2.26)$$

$$(-\omega^2 [\mathbb{M}^f] + i\omega [\mathbb{D}^f] + [\mathbb{K}^f]) \mathfrak{p}(\omega) + \omega^2 [\mathbb{C}]^T \mathbf{u}(\omega) = \mathbf{0} \quad , \quad (2.27)$$

in which $[\mathbb{M}^s]$, $[\mathbb{D}^s]$, and $[\mathbb{K}^s]$ are the $n_{\text{dof}}^s \times n_{\text{dof}}^s$ positive-definite symmetric matrices constructed by discretizing sesquilinear forms $m^s(\cdot, \cdot)$, $d^s(\cdot, \cdot)$, and $k^s(\cdot, \cdot)$, where $[\mathbb{M}^f]$ (resp. $[\mathbb{D}^f]$ and $[\mathbb{K}^f]$) is the $n_{\text{dof}}^f \times n_{\text{dof}}^f$ positive-definite (resp. positive) symmetric matrix constructed by discretizing sesquilinear form $m^f(\cdot, \cdot)$ (resp. $d^f(\cdot, \cdot)$ and $k^f(\cdot, \cdot)$), where $[\mathbb{C}]$ is the $n_{\text{dof}}^s \times n_{\text{dof}}^f$ matrix constructed by discretizing the sesquilinear form $c(\cdot, \cdot)$, and where \mathbb{F}^s is the finite-element vector constructed by discretizing the antilinear form ℓ^s . In low-frequency structural dynamics, mass matrix $[\mathbb{M}^s]$ is often approximated by a $n_{\text{dof}}^s \times n_{\text{dof}}^s$ positive-definite diagonal matrix $[\mathbb{M}^{\text{lump}}]$ constructed by lumped mass techniques. Such a lumped mass matrix will be used in Chapter 3 as

a metric for defining a new set of interpolating polynomial functions. The two Eqs. (2.26) and (2.27) can be rewritten as a single matrix equation,

$$\begin{pmatrix} -\omega^2[\mathbb{M}^s] + i\omega[\mathbb{D}^s] + [\mathbb{K}^s] & [\mathbb{C}] \\ \omega^2[\mathbb{C}]^T & -\omega^2[\mathbb{M}^f] + i\omega[\mathbb{D}^f] + [\mathbb{K}^f] \end{pmatrix} \begin{pmatrix} \mathfrak{u}(\omega) \\ \mathfrak{p}(\omega) \end{pmatrix} = \begin{pmatrix} \mathbb{F}^s(\omega) \\ \mathbf{0} \end{pmatrix}. \quad (2.28)$$

Note that the full-order computational vibroacoustic model is used for calculating $\mathfrak{u}(\omega)$ and $\mathfrak{p}(\omega)$ only for nonzero ω belonging to the frequency band of analysis $\mathbb{B} = [\omega_{\min}, \omega_{\max}]$ with $\omega_{\min} > 0$. Consequently, the solutions of the full-order computational vibroacoustic model are unique (see [26]).

2.4.2 Elastic eigenmodes

Let $0 < \lambda_1^s \leq \dots \leq \lambda_{n^s}^s$ be the $n^s \ll n_{\text{dof}}^s$ smallest eigenvalues that are solutions of the following generalized eigenvalue problem: find $\lambda_\alpha^s > 0$ and $\boldsymbol{\varphi}_\alpha^s$ in $\mathbb{R}^{n_{\text{dof}}^s}$ such that

$$[\mathbb{K}^s]\boldsymbol{\varphi}_\alpha^s = \lambda_\alpha^s[\mathbb{M}^s]\boldsymbol{\varphi}_\alpha^s. \quad (2.29)$$

The eigenvectors $\boldsymbol{\varphi}_1^s, \dots, \boldsymbol{\varphi}_{n^s}^s$ associated with the eigenvalues $0 < \lambda_1^s \leq \dots \leq \lambda_{n^s}^s$ verify the usual orthogonality properties and normalization,

$$(\boldsymbol{\varphi}_\beta^s)^T[\mathbb{M}^s]\boldsymbol{\varphi}_\alpha^s = \delta_{\alpha\beta}, \quad (\boldsymbol{\varphi}_\beta^s)^T[\mathbb{K}^s]\boldsymbol{\varphi}_\alpha^s = \lambda_\alpha^s \delta_{\alpha\beta}. \quad (2.30)$$

For the LF, MF, and HF domains, let $[\Phi^s] = (\boldsymbol{\varphi}_1^s \dots \boldsymbol{\varphi}_{n^s}^s)$ be the $n_{\text{dof}}^s \times n^s$ modal matrix.

2.4.3 Acoustic eigenmodes

Let $0 \leq \lambda_0^f \leq \dots \leq \lambda_{n^f}^f$ be the $n^f + 1 \ll n_{\text{dof}}^f$ smallest eigenvalues that are solutions of the following generalized eigenvalue problem: find $\lambda_\alpha^f \geq 0$ and $\boldsymbol{\varphi}_\alpha^f$ in $\mathbb{R}^{n_{\text{dof}}^f}$ such that

$$[\mathbb{K}^f]\boldsymbol{\varphi}_\alpha^f = \lambda_\alpha^f[\mathbb{M}^f]\boldsymbol{\varphi}_\alpha^f. \quad (2.31)$$

It should be noted that there is a zero eigenvalue λ_0^f because matrix $[\mathbb{K}^f]$ is not invertible. The eigenvectors $\boldsymbol{\varphi}_0^f, \dots, \boldsymbol{\varphi}_{n^f}^f$ associated with the eigenvalues $0 \leq \lambda_0^f \leq \dots \leq \lambda_{n^f}^f$ verify the usual orthogonality properties and normalization, for all $\alpha, \beta = 1, \dots, n^f$,

$$(\boldsymbol{\varphi}_\beta^f)^T[\mathbb{M}^f]\boldsymbol{\varphi}_\alpha^f = \delta_{\alpha\beta}, \quad (\boldsymbol{\varphi}_\beta^f)^T[\mathbb{K}^f]\boldsymbol{\varphi}_\alpha^f = \lambda_\alpha^f \delta_{\alpha\beta}. \quad (2.32)$$

For the LF, MF, and HF domains, the $n_{\text{dof}}^f \times n^f$ modal matrix is defined as $[\Phi^f] = (\boldsymbol{\varphi}_1^f \dots \boldsymbol{\varphi}_{n^f}^f)$ in which the eigenvector $\boldsymbol{\varphi}_0^f$, which is associated with the null eigenvalue λ_0^f , has been omitted from its columns.

2.4.4 Reduced-order computational vibroacoustic model in LF, MF, and HF domains

In the LF, MF, and HF domains, the ROM is constructed by using a truncated modal expansion of vectors $\mathbf{u}(\omega)$ and $\mathbf{p}(\omega)$ that are written as

$$\mathbf{u}(\omega) = [\Phi^s] \mathbf{q}^s \quad , \quad \mathbf{p}(\omega) = [\Phi^f] \mathbf{q}^f \quad , \quad (2.33)$$

in which modal matrices $[\Phi^s]$ and $[\Phi^f]$ have been defined in Sections 2.4.2 and 2.4.3. It should be noted that since eigenvector $\boldsymbol{\varphi}_0^f$ has been omitted from columns of modal matrix $[\Phi^f]$, then it is also excluded from the truncated modal expansion of $\mathbf{p}(\omega)$. This eigenvector is associated with the zero eigenvalue λ_0^f . Indeed, in the case of a car cockpit, the acoustic wall surrounding domain Ω_f is assumed to be nonsealed and consequently, the quasi-static pressure, which corresponds to the generalized coordinate q_0^f associated with eigenvector $\boldsymbol{\varphi}_0^f$, is balanced at any time t between the internal cavity and the outside and is not an unknown of the problem. Consequently, the equations of the full-order computational vibroacoustic model have been projected on the eigensubspace that is orthogonal to $\boldsymbol{\varphi}_0^f$ and that is spanned by eigenvectors $\boldsymbol{\varphi}_1^f, \dots, \boldsymbol{\varphi}_{n^f}^f$. In the LF, MF, and HF domains, the ROM is then deduced from Eq. (2.28) by using the truncated modal expansion in Eq. (2.33). We then have

$$\begin{pmatrix} -\omega^2[\mathcal{M}^s] + i\omega[\mathcal{D}^s] + [\mathcal{K}^s] & [\mathcal{C}] \\ \omega^2[\mathcal{C}]^T & -\omega^2[\mathcal{M}^f] + i\omega[\mathcal{D}^f] + [\mathcal{K}^f] \end{pmatrix} \begin{pmatrix} \mathbf{q}^s(\omega) \\ \mathbf{q}^f(\omega) \end{pmatrix} = \begin{pmatrix} \mathbf{f}^s(\omega) \\ \mathbf{0} \end{pmatrix} \quad , \quad (2.34)$$

where the generalized mass matrix $[\mathcal{M}^s]$, the generalized damping matrix $[\mathcal{D}^s]$, and the generalized stiffness matrix $[\mathcal{K}^s]$ are the $n^s \times n^s$ positive-definite matrices such that

$$[\mathcal{M}^s] = [\Phi^s]^T [\mathcal{M}^s] [\Phi^s] \quad , \quad [\mathcal{K}^s] = [\Phi^s]^T [\mathcal{K}^s] [\Phi^s] \quad , \quad [\mathcal{D}^s] = [\Phi^s]^T [\mathcal{D}^s] [\Phi^s] \quad , \quad (2.35)$$

and where the generalized matrices $[\mathcal{M}^f]$, $[\mathcal{D}^f]$, and $[\mathcal{K}^f]$ are the $n^f \times n^f$ positive-definite matrices such that

$$[\mathcal{M}^f] = [\Phi^f]^T [\mathcal{M}^f] [\Phi^f] \quad , \quad [\mathcal{K}^f] = [\Phi^f]^T [\mathcal{K}^f] [\Phi^f] \quad , \quad [\mathcal{D}^f] = [\Phi^f]^T [\mathcal{D}^f] [\Phi^f] \quad , \quad (2.36)$$

and finally, where

$$[\mathcal{C}] = [\Phi^s]^T [\mathcal{C}] [\Phi^f] \quad , \quad \mathbf{f}^s(\omega) = [\Phi^s]^T \mathbf{F}^s(\omega) \quad . \quad (2.37)$$

Using the orthogonality properties and normalization defined by Eqs. (2.30) and (2.32), matrices $[\mathcal{M}^s]$, $[\mathcal{K}^s]$, $[\mathcal{M}^f]$ and $[\mathcal{K}^f]$ can be rewritten as

$$[\mathcal{M}^s] = [I_{n^s}] \quad , \quad [\mathcal{K}^s] = [\Lambda^s] \quad , \quad (2.38)$$

$$[\mathcal{M}^f] = [I_{n^f}] \quad , \quad [\mathcal{K}^f] = [\Lambda^f] \quad , \quad (2.39)$$

in which $[I_{n^s}]$ and $[I_{n^f}]$ are the identity matrices with dimensions $n^s \times n^s$ and $n^f \times n^f$, and where $[\Lambda^s]_{\alpha\beta} = \lambda_\alpha^s \delta_{\alpha\beta}$ and $[\Lambda^f]_{\alpha\beta} = \lambda_\alpha^f \delta_{\alpha\beta}$ are diagonal $n^s \times n^s$ and $n^f \times n^f$ matrices.

2.4.5 Reduced-order computational vibroacoustic model in LF and MF

The LF, MF, and HF domains correspond to the frequency bands $[0, \omega_L]$, $[\omega_L, \omega_M]$, and $[\omega_M, \omega_H]$ (in rad.s^{-1}) where the three bounds ω_L , ω_M , and ω_H are assumed to be already known. Their respective value can be estimated by analyzing the graphs of the Frequency Response Functions (FRF) for some "important" degrees of freedom in the whole frequency domain by using the reduced-order computational model presented in Section 2.4.4. Furthermore, let n_L , n_M , and n_H be the number of structural elastic modes in the LF, MF, and HF domains, and let $n_{LM} = n_L + n_M$. Let $[\Phi_L^s]$, $[\Phi_M^s]$, and $[\Phi_H^s]$ be the matrices with dimensions $n_{\text{dof}}^s \times n_L$, $n_{\text{dof}}^s \times n_M$, and $n_{\text{dof}}^s \times n_H$ whose columns are the elastic eigenvectors belonging to frequency domains LF, MF, and HF respectively and such that

$$[\Phi^s] = \left([\Phi_L^s] \ [\Phi_M^s] \ [\Phi_H^s] \right) . \quad (2.40)$$

We also introduce the matrix $[\Phi_{LM}^s]$ that is defined by

$$[\Phi_{LM}^s] = \left([\Phi_L^s] \ [\Phi_M^s] \right) . \quad (2.41)$$

In the LF, MF, and HF domains, the ROM is constructed by using a truncated modal expansion of vectors $\mathfrak{u}(\omega)$ and $\mathfrak{p}(\omega)$ written as

$$\mathfrak{u}(\omega) = [\Phi_{LM}^s] \mathbf{q}^s \quad , \quad \mathfrak{p}(\omega) = [\Phi^f] \mathbf{q}^f \quad , \quad (2.42)$$

in which modal matrix $[\Phi^f]$ has been defined in Section 2.4.3. In the LF and MF domains, the ROM is then deduced from Eq. (2.28) by using the truncated modal expansion in Eq. (2.42). We then have

$$\begin{pmatrix} -\omega^2 [\mathcal{M}_{LM}^s] + i\omega [\mathcal{D}_{LM}^s] + [\mathcal{K}_{LM}^s] & [\mathcal{C}_{LM}] \\ \omega^2 [\mathcal{C}_{LM}]^T & -\omega^2 [\mathcal{M}^f] + i\omega [\mathcal{D}^f] + [\mathcal{K}^f] \end{pmatrix} \begin{pmatrix} \mathbf{q}^s(\omega) \\ \mathbf{q}^f(\omega) \end{pmatrix} = \begin{pmatrix} \mathbf{f}_{LM}^s(\omega) \\ \mathbf{0} \end{pmatrix} , \quad (2.43)$$

where the generalized mass matrix $[\mathcal{M}_{LM}^s]$, the generalized damping matrix $[\mathcal{D}_{LM}^s]$, and the generalized stiffness matrix $[\mathcal{K}_{LM}^s]$ are the $n_{LM} \times n_{LM}$ positive-definite matrices such that

$$[\mathcal{M}_{LM}^s] = [\Phi_{LM}^s]^T [\mathcal{M}_{LM}^s] [\Phi_{LM}^s] \quad , \quad [\mathcal{K}_{LM}^s] = [\Phi_{LM}^s]^T [\mathcal{K}_{LM}^s] [\Phi_{LM}^s] \quad , \quad [\mathcal{D}_{LM}^s] = [\Phi_{LM}^s]^T [\mathcal{D}_{LM}^s] [\Phi_{LM}^s] \quad , \quad (2.44)$$

and where

$$[\mathcal{C}_{LM}] = [\Phi_{LM}^s]^T [\mathcal{C}] [\Phi^f] \quad , \quad \mathbf{f}_{LM}^s(\omega) = [\Phi_{LM}^s]^T \mathbf{F}_{LM}^s(\omega) . \quad (2.45)$$

Using the orthogonality properties and normalization defined by Eqs. (2.30) and (2.32), matrices $[\mathcal{M}_{LM}^s]$ and $[\mathcal{K}_{LM}^s]$ can be rewritten as

$$[\mathcal{M}_{LM}^s] = [I_{n_{LM}}] \quad , \quad [\mathcal{K}_{LM}^s] = [\Lambda_{LM}^s] \quad , \quad (2.46)$$

$$[\mathcal{M}^f] = [I_{n^f}] \quad , \quad [\mathcal{K}^f] = [\Lambda^f] \quad , \quad (2.47)$$

in which $[I_{n_{LM}}]$ is the identity matrix with dimensions $n_{LM} \times n_{LM}$ and where the diagonal $n_{LM} \times n_{LM}$ matrix $[\Lambda_{LM}^s]$ is such that $[\Lambda_{LM}^s]_{\alpha\beta} = \lambda_\alpha^s \delta_{\alpha\beta}$.

Chapter 3

Multilevel basis

Contents

| | |
|--|-----------|
| 3.1 Spatial filtering functions and finite-element projection | 22 |
| 3.2 Low and high complexity level displacement bases | 25 |

In this chapter, we present a methodology to construct a new basis for $u(\omega)$, different from elastic eigenvectors. For constructing such a basis, the approach relies on a spatial filtering to decompose the set of the elastic eigenvectors into two sets of linearly independent displacement vectors that are no longer elastic modes. The two sets of displacement vectors are characterized by a polynomial degree. First, a set of « spatial filtering functions » is constructed as a set of mutually orthogonal multivariate polynomials, with respect to a given metric related to the sesquilinear form of mass, defined on Ω_s . Consequently, the shape of each « spatial filtering function » is weighted by the spatial mass distribution of the structure. Such set of « spatial filtering function » can then represent the displacements of separate components or assembled components of the structure as an automobile. A large wavelength elastic eigenvector, that is generally representative of the LF domain, would then be written as a sum of « spatial filtering functions » with a small polynomial degree. It should be noted that a spatially localized elastic eigenvector, that is generally representative of the HF domain, could also be written as a sum of « spatial filtering functions » with a small polynomial degree. Consequently, a low polynomial degree used of the « spatial filtering functions » cannot be used to characterize the eigenvectors in the LF, MF or HF domains. Nevertheless, the more the polynomial degree of the « spatial filtering functions » is high, the more it can represent coupling of displacements of different components of the structure. Hence, the polynomial degree of the « spatial filtering functions » can be used to characterize the level of complexity for the vector space spanned by a set of elastic eigenvectors. The more the polynomial degree of the « spatial filtering functions » is high, the more the complexity level is important. Hereinafter, the construction of a set of displacement vectors defined on Ω_s and referred as the « Low complexity level displacements basis » is presented in this chapter. The construction of its complementary counterpart into the set of the elastic eigenvectors is also presented and yields the construction of the « High

complexity level displacements basis ». Gathering the two bases together yields the « Multi-complexity-level displacements basis » that we will shorten into « Multilevel basis ». Such an approach has been already introduced in [129, 12], but the presentation, the developments, and the formulated interpretations are different. Note that such an approach will be applied in this manuscript only for the elastic eigenvectors of the structure and not for the fluid in the cockpit of the automobile because the acoustic cavity is homogeneous with regards to such a complexity characterization. It should be noted that, for simpler mechanical systems (with homogeneously distributed mass), there might be coincidence between the « low complexity level displacement basis » and the set of elastic eigenvectors in the LF domain.

3.1 Spatial filtering functions and finite-element projection

3.1.1 Set of mutually orthonormal polynomials as spatial filtering functions

Let m_1, m_2, \dots be real-valued multivariate monomials defined on Ω_s . We then have, for all $\mathbf{x} = (x_1, x_2, x_3)$ in Ω_s

$$m_k(\mathbf{x}) = (x_1)^{\alpha_k^1 - \alpha_k^2} (x_2)^{\alpha_k^2 - \alpha_k^3} (x_3)^{\alpha_k^3} \quad , \quad (3.1)$$

in which $\boldsymbol{\alpha}_k = (\alpha_k^1, \alpha_k^2, \alpha_k^3)$ is the k -th three-dimensional multi-index such that $0 < |\boldsymbol{\alpha}_1| \leq |\boldsymbol{\alpha}_2| \dots$ with $|\boldsymbol{\alpha}_k| = \alpha_k^1 + \alpha_k^2 + \alpha_k^3$ and such that $0 \leq \alpha_k^3 \leq \alpha_k^2 \leq \alpha_k^1 \leq d$. The number of such monomials with degree less or equal to d is $n_{\text{mon}} = (d+1)(d+2)(d+3)/6$. Let $p_1, p_2, \dots, p_{n_{\text{mon}}}$ be a set of multivariate three-dimensional polynomials defined on Ω_s and written as

$$p_\ell(\mathbf{x}) = \sum_{k=1}^{n_{\text{mon}}} m_k(\mathbf{x}) s_{k\ell} \quad , \quad (3.2)$$

in which $s_{k\ell}$ is the ℓ -th coefficient associated with the k -th monomial m_k involved into the monomial expansion of p_ℓ . By construction of the lumped mass matrix $[\mathbb{M}^{\text{lump}}]$ introduced in Chapter 2, for each node of the finite-element mesh of domain Ω_s , it is possible to associate a discrete mass $M_\gamma = [\mathbb{M}^{\text{lump}}]_{J_\gamma, J_\gamma}$ in which the J_γ -th degree of freedom corresponds to one of the three translational displacement located at the γ -th node of the finite element mesh and located at position \mathbf{x}^γ . The polynomials $p_1, p_2, \dots, p_{n_{\text{mon}}}$ can also be chosen such that they are orthogonal with respect to a metric defined by the lumped mass matrix $[\mathbb{M}^{\text{lump}}]$, such that, for all ℓ_1 and ℓ_2 in $\{1, \dots, n_{\text{mon}}\}$,

$$\sum_{\gamma=1}^{n_{\text{nodes}}} M_\gamma p_{\ell_1}(\mathbf{x}^\gamma) p_{\ell_2}(\mathbf{x}^\gamma) = \delta_{\ell_1 \ell_2} \quad , \quad (3.3)$$

in which n_{nodes} is the number of nodes in the finite-element mesh of Ω_s and where \mathbf{x}^γ is the γ -th node. For the sake of brevity, let us assume that there are 6 degrees of freedom at each node of the finite element mesh of Ω_s . In this case, we have $n_{\text{dof}}^s = 6 n_{\text{nodes}}$. Hereinafter, the polynomials $p_1, p_2, \dots, p_{n_{\text{mon}}}$ will be referred as the « spatial filtering functions ».

3.1.2 Computation of the filtering functions values at the finite-element nodes

Let us introduce the $n_{\text{nodes}} \times n_{\text{nodes}}$ real-valued matrix $[m^{\text{lump}}]_{\gamma\tilde{\gamma}} = M_{\gamma} \delta_{\gamma\tilde{\gamma}}$ of the lumped mass at the nodes mesh and the $n_{\text{nodes}} \times n_{\text{mon}}$ matrix $[p]_{\gamma\ell} = p_{\ell}(\mathbf{x}^{\gamma})$ of the polynomial values at the nodes of the mesh. Note that for complex vibroacoustic model in high dimension and when $n_{\text{mon}} \ll n_{\text{nodes}}$, the kernel space of $[p]^T$ is not reduced to the null space. Then, Eq. (3.3) can be rewritten as

$$[p]^T [m^{\text{lump}}] [p] = [I_{n_{\text{mon}}}] \quad , \quad (3.4)$$

in which $[I_{n_{\text{mon}}}]$ is the $n_{\text{mon}} \times n_{\text{mon}}$ identity matrix. Let $[s]_{k\ell} = s_{k\ell}$ be the real $n_{\text{mon}} \times n_{\text{mon}}$ matrix of the monomial decomposition coefficients of polynomials p_{ℓ} and let $[m]_{\gamma k} = m_k(\mathbf{x}^{\gamma})$ be the real $n_{\text{nodes}} \times n_{\text{mon}}$ matrix of the monomial values at the nodes of the mesh. Then, Eq. (3.2) can be rewritten as

$$[p] = [m] [s] \quad . \quad (3.5)$$

Substituting Eq. (3.5) into Eq. (3.4) yields

$$[q]^T [q] = [I_{n_{\text{mon}}}] \quad , \quad (3.6)$$

where $[q] = [m^{\text{lump}}]^{1/2} [m] [s]$ is a $n_{\text{nodes}} \times n_{\text{mon}}$ matrix. We then have

$$[q] = [m^{\text{lump}}]^{1/2} [p] \quad . \quad (3.7)$$

From Eq. (3.6), it can be deduced that $[q]$ is an orthogonal matrix that can directly be computed as the economy-size QR decomposition $[q] [r]$ of matrix $[m^{\text{lump}}]^{1/2} [m]$ in which $[r]$ is a $n_{\text{mon}} \times n_{\text{mon}}$ upper triangular matrix. Then, $[s] = [r]^{-1}$ is also an upper triangular matrix if $[r]$ is an invertible matrix. Then, the nodal values of polynomials $p_1, \dots, p_{n_{\text{mon}}}$ can be calculated by $[p] = [m^{\text{lump}}]^{-1/2} [q] [r]^{-1}$. Nevertheless, the computation of $[p]$ is not required for efficiently carrying out the filtering approach, which avoids the numerical cost to compute inverse matrix $[r]^{-1}$ and also avoids to store $[r]$. Only the computation of $[q]$ is required.

3.1.3 Finite-element projection matrix associated with the filtering functions

Let $\mathfrak{u}^1, \mathfrak{u}^2$, and \mathfrak{u}^3 be the $\mathbb{R}^{n_{\text{nodes}}}$ vectors of all the degrees of freedom that correspond to translational displacement into directions $\mathbf{e}_1, \mathbf{e}_2$, and \mathbf{e}_3 for the nodes of the finite element mesh. Let \mathfrak{w} be the vector of all the degrees of freedom that are not translational displacements. Let \mathfrak{u} be the vector of all the degrees of freedom that, consequently, gathers all values of $\mathfrak{u}^1, \mathfrak{u}^2, \mathfrak{u}^3$, and \mathfrak{w} . Assembling $\mathfrak{u}^1, \mathfrak{u}^2, \mathfrak{u}^3$, and \mathfrak{w} into \mathfrak{u} yields

$$\mathfrak{u} = [R] \mathfrak{w} + \sum_{j=1}^3 [T_j] \mathfrak{u}^j \quad , \quad (3.8)$$

in which, for all $j = 1, 2, 3$, the entries of the $n_{\text{dof}}^s \times n_{\text{nodes}}$ matrix $[T_j]$ are 0 or 1 only and such that, for all $j, j' = 1, 2, 3$, i

$$[T_j]^T [T_{j'}] = \delta_{jj'} [I_{n_{\text{nodes}}}] \quad , \quad (3.9)$$

$$[T_j]^T [R] = [0] \quad . \quad (3.10)$$

For all $j = 1, 2, 3$, it can then be deduced that

$$\mathbf{u}^j = [T_j]^T \mathbf{u} \quad . \quad (3.11)$$

In addition, since $[M^{\text{lump}}]$ is diagonal then, for all $j, j' = 1, 2, 3$, we also have

$$[T_j]^T [M^{\text{lump}}] [T_{j'}] = \delta_{jj'} [m^{\text{lump}}] \quad . \quad (3.12)$$

For $j = 1, 2, 3$, let $\mathbf{u}^j = [p] \mathbf{c}^j$ be the polynomial approximation of vector \mathbf{u}^j such that \mathbf{c}^j in $\mathbb{R}^{n_{\text{mon}}}$ minimizes $\mathbf{c} \mapsto \|[p] \mathbf{c} - \mathbf{u}^j\|^2$. The solution of this least square minimization problem is well known and can be written, using the pseudo-inverse, as

$$\mathbf{c}^j = \left([p]^T [m^{\text{lump}}] [p] \right)^{-1} [p]^T [m^{\text{lump}}] \mathbf{u}^j \quad , \quad (3.13)$$

which can be rewritten, using Eqs. (3.4) and (3.11), as

$$\mathbf{c}^j = [p]^T [m^{\text{lump}}] [T_j]^T \mathbf{u} \quad . \quad (3.14)$$

Consequently, for all $j = 1, 2, 3$, the polynomial approximation \mathbf{u}^j of vector \mathbf{u}^j is such that

$$\mathbf{u}^j = [p] [p]^T [m^{\text{lump}}] [T_j]^T \mathbf{u} \quad . \quad (3.15)$$

Let us introduce the polynomial approximation \mathbf{u} of the vector of the degrees of freedom \mathbf{u} constructed by replacing \mathbf{u}^j by its polynomial approximation \mathbf{u}^j and by replacing the non-translational degrees of freedom \mathbf{w} by the null vector. We then have

$$\mathbf{u} = [P] \mathbf{u} \quad , \quad (3.16)$$

in which we have introduced the $n_{\text{dof}}^s \times n_{\text{dof}}^s$ matrix $[P]$ defined by

$$[P] = \sum_{j=1}^3 [T_j] [p] [p]^T [m^{\text{lump}}] [T_j]^T \quad . \quad (3.17)$$

Consequently, $[P]$ can be computed by the usual assembling algorithm of the finite-element method for the element matrix $[p] [p]^T [m^{\text{lump}}]$. In addition, the kernel of $[P]$ is not reduced to the null space since $[P] \mathbf{u}_0 = 0$ for any non-zero vector \mathbf{u}_0 written, for any vector \mathbf{w} , as

$$\mathbf{u}_0 = [R] \mathbf{w} + \sum_{j=1}^3 [T_j] \mathbf{u}_0^j \quad \text{with} \quad [p]^T [m^{\text{lump}}] \mathbf{u}_0^j = \mathbf{0} \quad . \quad (3.18)$$

Indeed, left multiplying \mathbf{u}_0 by $[P]$ and using Eqs. (3.9) and (3.10) yield

$$[P] \mathbf{u}_0 = [P] [R] \mathbf{w} + \sum_{j=1}^3 [P] [T_j] \mathbf{u}_0^j \quad , \quad (3.19)$$

$$= \sum_{j=1}^3 [T_j] [p] [p]^T [m^{\text{lump}}] \overbrace{[T_j]^T [R]}^{[0]} \mathbf{w} + \sum_{j=1}^3 \sum_{j'=1}^3 [T_{j'}] [p] [p]^T [m^{\text{lump}}] \overbrace{[T_{j'}]^T [T_j]}^{\delta_{jj'} [I_{n_{\text{mon}}}] } \mathbf{u}_0^j \quad , \quad (3.20)$$

$$= \sum_{j=1}^3 [T_j] [p] \underbrace{[p]^T [m^{\text{lump}}] \mathbf{u}_0^j}_{\mathbf{0}} \quad , \quad (3.21)$$

$$= \mathbf{0} \quad . \quad (3.22)$$

Note that for such vector it is always possible to find a vector v_0^j such that $[p]^T [m^{\text{lump}}] v_0^j = \mathbf{0}$ since in high dimension, the kernel of $[p]^T$ is not reduced to the null space (see Section 3.1.2). Consequently, in all the rest of this work, matrix $[\mathbb{P}]$ will be referred as the matrix of the finite-element projection associated with the spatial filtering. Note that n_{dof}^s can be equal to several millions and consequently, it is not possible to store the full matrix $[\mathbb{P}]$ in the random access memory (RAM) or even on a hard disk.

3.2 Low and high complexity level displacement bases

3.2.1 Projected mass matrix

An unusual mass matrix is introduced and defined as the finite-element projection on the filtering functions $[\mathbb{P}]^T [M^s] [\mathbb{P}]$ of mass matrix $[M^s]$ defined in Chapter 2. It will be used for setting up an unusual eigenvalue problem from which the both low and high complex level displacement bases will be constructed. Nevertheless, the computation of $[\mathbb{P}]^T [M^s] [\mathbb{P}]$ requires the computation of matrix $[\mathbb{P}]$ (which cannot be stored) and consequently of matrix $[p]$. Hence, computation of $[\mathbb{P}]^T [M^s] [\mathbb{P}]$ is replaced by the computation of $[M^{\text{proj}}] = [\mathbb{P}]^T [m^{\text{lump}}] [\mathbb{P}]$ in order to take advantage of orthogonality relations of polynomials $[p]$. By using Eqs. (3.4), (3.7), and (3.12), and by introducing matrix $[b] = [m^{\text{lump}}]^{1/2} [q]$, we then have

$$[M^{\text{proj}}] = \left(\sum_{j=1}^3 [T_j] [m^{\text{lump}}] [p] [p]^T [T_j]^T \right) [m^{\text{lump}}] \left(\sum_{j'=1}^3 [T_{j'}] [p] [p]^T [m^{\text{lump}}] [T_{j'}]^T \right) , \quad (3.23)$$

$$= \sum_{j,j'=1}^3 [T_j] [m^{\text{lump}}] [p] [p]^T \overbrace{[T_j]^T [m^{\text{lump}}] [T_{j'}]}^{[m^{\text{lump}}] \delta_{jj'}} [T_{j'}] [p] [p]^T [m^{\text{lump}}] [T_{j'}]^T , \quad (3.24)$$

$$= \sum_{j=1}^3 [T_j] [m^{\text{lump}}] [p] \overbrace{[p]^T [m^{\text{lump}}] [p]}^{I_{n_{\text{mon}}}} [p] [p]^T [m^{\text{lump}}] [T_j]^T , \quad (3.25)$$

$$= \sum_{j=1}^3 [T_j] [m^{\text{lump}}]^{1/2} [q] [q]^T [m^{\text{lump}}]^{1/2} [T_j]^T , \quad (3.26)$$

$$= \sum_{j=1}^3 [T_j] [b] [b]^T [T_j]^T . \quad (3.27)$$

Consequently, the projected matrix $[M^{\text{proj}}]$ can be constructed by using the usual finite-element assembling algorithm applied to the $n_{\text{nodes}} \times n_{\text{nodes}}$ matrix $[b] [b]^T$. As announced in Section 3.1.2, it requires only the computation of matrix $[q]$ and avoids both the computation and the storage of matrices $[p]$ and $[s]$. Furthermore, Eq. (3.27) can be rewritten as

$$[M^{\text{proj}}] = [N] [N]^T , \quad (3.28)$$

where the $n_{\text{dof}}^s \times n_{\text{mon}}$ matrix $[\mathbb{N}]$ is defined by

$$[\mathbb{N}] = ([T_1] [b] \quad [T_2] [b] \quad [T_3] [b]) \quad . \quad (3.29)$$

3.2.2 Conditions on the reduced-order basis for the filtering

Let N be a given positive integer such that $N \leq n_{\text{dof}}^s$ and let $[\mathbb{U}]$ be a given $n_{\text{dof}}^s \times N$ matrix for which the columns is a set of linearly independent finite-element displacements that are mutually orthogonal with respect to the metric defined by the mass matrix $[\mathbb{M}^s]$ and the stiffness matrix $[\mathbb{K}^s]$, such that

$$[\mathbb{U}]^T [\mathbb{K}^s] [\mathbb{U}] = [\Lambda] \quad , \quad [\mathbb{U}]^T [\mathbb{M}^s] [\mathbb{U}] = [I_N] \quad , \quad (3.30)$$

where $[\Lambda]$ is a $N \times N$ positive-definite diagonal matrix and where $[I_N]$ is the $N \times N$ unit matrix. It should be noted that such orthogonality relations are also verified by matrix $[\Phi^s]$ defined in Chapter 2. Nevertheless, they do not imply

$$[\mathbb{K}^s] [\mathbb{U}] = [\mathbb{M}^s] [\mathbb{U}] [\Lambda] \quad . \quad (3.31)$$

The spatial filtering method that is presented in this chapter can be applied to any reduced-order basis represented by such a matrix $[\mathbb{U}]$ that fulfills relations in Eq. (3.30), such as $[\Phi^s]$ for instance. Applying the following method with $[\mathbb{U}] = [\Phi^s]$ will be carried out for defining the first spatial filtering in Chapter 4.

3.2.3 Reduced-order projected mass matrix

The reduced-order projected mass matrix $[\mathcal{M}^{\text{proj}}]$ is then introduced as the $N \times N$ matrix defined as

$$[\mathcal{M}^{\text{proj}}] = [\mathbb{U}]^T [\mathbb{M}^{\text{proj}}] [\mathbb{U}] \quad . \quad (3.32)$$

Note that since $[\mathbb{M}^{\text{proj}}]$ is positive but not definite, then $[\mathcal{M}^{\text{proj}}]$ is also positive but not definite. Using Eq. (3.27) yields

$$[\mathcal{M}^{\text{proj}}] = [\mathcal{N}] [\mathcal{N}]^T \quad , \quad (3.33)$$

in which the $N \times n_{\text{mon}}$ matrix $[\mathcal{N}]$ is written as

$$[\mathcal{N}] = [\mathbb{U}]^T [\mathbb{N}] \quad , \quad (3.34)$$

$$= ([\mathbb{U}]^T [T_1] [b] \quad [\mathbb{U}]^T [T_2] [b] \quad [\mathbb{U}]^T [T_3] [b]) \quad , \quad (3.35)$$

$$= (([T_1]^T [\mathbb{U}])^T [b] \quad ([T_2]^T [\mathbb{U}])^T [b] \quad ([T_3]^T [\mathbb{U}])^T [b]) \quad , \quad (3.36)$$

$$= ([\Phi_1^s]^T [b] \quad [\Phi_2^s]^T [b] \quad [\Phi_3^s]^T [b]) \quad , \quad (3.37)$$

in which we have introduced the $n_{\text{nodes}} \times N$ matrices $[\mathbb{U}_j] = [T_j]^T [\mathbb{U}]$ for all $j = 1, 2, 3$. From a numerical programming aspect, matrix $[\mathbb{U}_j]$ is constructed by removing all the rows in $[\mathbb{U}]$ that do not correspond to the degree of freedom of translational displacement into direction \mathbf{e}_j .

3.2.4 Construction of the low complexity level displacements basis

Let \mathcal{S} be the vector space that is spanned by columns of $[\mathcal{U}]$. Let \mathcal{S}^{low} be the subspace of \mathcal{S} that is defined as the vector space of all the vectors of finite element displacements \mathbf{v} in \mathcal{S} with non-zero kinetic energy $\frac{1}{2} \mathbf{v}^T [\mathcal{M}^{\text{proj}}] \mathbf{v}$. Let n^{low} be the dimension of \mathcal{S}^{low} , which is assumed to be spanned by a set of n^{low} linearly independent vectors $\mathbf{u}_1^{\text{low}} \dots \mathbf{u}_{n^{\text{low}}}^{\text{low}}$ of dimension $n_{\text{dof}}^{\text{s}}$. Since \mathcal{S}^{low} is a subspace of \mathcal{S} by construction, then $\mathbf{u}_\alpha^{\text{low}}$ can be written, for all $\alpha = 1, \dots, n^{\text{low}}$, as

$$\mathbf{u}_\alpha^{\text{low}} = [\mathcal{U}] [\Phi^{\text{proj}}] \boldsymbol{\varphi}_\alpha^{\text{low}} \quad , \quad (3.38)$$

where $\boldsymbol{\varphi}_1^{\text{low}}, \dots, \boldsymbol{\varphi}_{n^{\text{low}}}^{\text{low}}$ are linearly independent vectors of dimension n^{low} and $[\Phi^{\text{proj}}]$ is a $N \times n^{\text{low}}$ rectangular matrix such that $[\Phi^{\text{proj}}]^T$ corresponds to the orthogonal projection operator from \mathcal{S} into \mathcal{S}^{low} for a given metric that is defined hereinafter. The objective of this section is to construct matrix $[\Phi^{\text{proj}}]$ and the set of linearly independent vectors $\mathbf{u}_1^{\text{low}} \dots \mathbf{u}_{n^{\text{low}}}^{\text{low}}$. Let us first consider the following generalized eigenvalue problem: find $\boldsymbol{\varphi}_\alpha^{\text{proj}}$ in \mathbb{R}^N and $\lambda_\alpha^{\text{proj}} > 0$ such that

$$[\Lambda] \boldsymbol{\varphi}_\alpha^{\text{proj}} = \lambda_\alpha^{\text{proj}} [\mathcal{M}^{\text{proj}}] \boldsymbol{\varphi}_\alpha^{\text{proj}} \quad . \quad (3.39)$$

Since matrix $[\mathcal{M}^{\text{proj}}]$ is positive but not definite, then the eigenvalues are sorted in ascending order $0 < \lambda_1^{\text{proj}} \leq \dots \leq \lambda_{n^{\text{low}}}^{\text{proj}} < \dots \leq \lambda_n^{\text{proj}}$ in which rank n^{low} is such that $\lambda_\alpha^{\text{proj}}$ is not finite for any $\alpha > n^{\text{low}}$. Note that computing matrix $[\mathcal{M}^{\text{proj}}]$ is not required. Indeed, by using Eq. (3.33), the economy size Singular Value Decomposition (SVD) of matrix $[\Lambda]^{-1/2} [\mathcal{N}]$ is written as $[\Lambda]^{-1/2} [\mathcal{N}] = [U^{\text{proj}}] [\Sigma^{\text{proj}}] [V^{\text{proj}}]^T$ in which $[U^{\text{proj}}]$ is a rectangular $N \times n^{\text{low}}$ matrix with $[U^{\text{proj}}]^T [U^{\text{proj}}] = [I_{n^{\text{low}}}]$, and $[V^{\text{proj}}]$ is a rectangular $n_{\text{mon}} \times n^{\text{low}}$ matrix with $[V^{\text{proj}}]^T [V^{\text{proj}}] = [I_{n^{\text{low}}}]$ that does not need to be computed and in which $[\Sigma^{\text{proj}}]$ is a diagonal positive-definite $n^{\text{low}} \times n^{\text{low}}$ matrix. For all $\alpha = 1, \dots, n^{\text{low}}$, we have $\lambda_\alpha^{\text{proj}} = ([\Sigma^{\text{proj}}]_{\alpha\alpha})^{-2}$ and $[\Phi^{\text{proj}}] = [\Lambda]^{-1/2} [U^{\text{proj}}] [\Sigma^{\text{proj}}]$ where $[\Phi^{\text{proj}}]$ is the $N \times n^{\text{low}}$ modal matrix $[\Phi^{\text{proj}}] = [\boldsymbol{\varphi}_1^{\text{proj}} \dots \boldsymbol{\varphi}_{n^{\text{low}}}^{\text{proj}}]$. Furthermore, we also have the two orthogonality and normalization relations,

$$[\Phi^{\text{proj}}]^T [\Lambda] [\Phi^{\text{proj}}] = [\Sigma^{\text{proj}}] \quad , \quad [\Phi^{\text{proj}}]^T [\mathcal{M}^{\text{proj}}] [\Phi^{\text{proj}}] = [I_{n^{\text{low}}}] \quad . \quad (3.40)$$

A second eigenvalue problem is then solved for eventually constructing the low complexity level displacements basis. It consists in finding $\boldsymbol{\varphi}_\alpha^{\text{low}}$ in $\mathbb{R}^{n^{\text{low}}}$ and $\lambda_\alpha^{\text{low}} > 0$ such that

$$[\Phi^{\text{proj}}]^T [\Lambda] [\Phi^{\text{proj}}] \boldsymbol{\varphi}_\alpha^{\text{low}} = \lambda_\alpha^{\text{low}} [\Phi^{\text{proj}}]^T [I_N] [\Phi^{\text{proj}}] \boldsymbol{\varphi}_\alpha^{\text{low}} \quad , \quad (3.41)$$

which can be rewritten as

$$[\Sigma^{\text{proj}}] \boldsymbol{\varphi}_\alpha^{\text{low}} = \lambda_\alpha^{\text{low}} [\Phi^{\text{proj}}]^T [\Phi^{\text{proj}}] \boldsymbol{\varphi}_\alpha^{\text{low}} \quad . \quad (3.42)$$

The n^{low} eigenvalues $0 < \lambda_1^{\text{low}} \leq \dots \leq \dots \leq \lambda_{n^{\text{low}}}^{\text{low}}$ of the generalized eigenvalue problem defined in Eq. (3.41) are finite and positive and the associated eigenvectors $\boldsymbol{\varphi}_1^{\text{low}}, \dots, \boldsymbol{\varphi}_{n^{\text{low}}}^{\text{low}}$ are assumed to be normalized with respect to matrix $[\Phi^{\text{proj}}]^T [\Phi^{\text{proj}}]$. Once again, computing matrix $[\Phi^{\text{proj}}]^T [\Phi^{\text{proj}}]$ is not required when n^{low} is large. Indeed, the SVD of matrix $[\Sigma^{\text{proj}}]^{-1/2} [\Phi^{\text{proj}}]^T$ is

written as $[\Sigma^{\text{proj}}]^{-1/2} [\Phi^{\text{proj}}]^T = [U^{\text{low}}] [\Sigma^{\text{low}}] [V^{\text{low}}]^T$ in which $[U^{\text{low}}]$ and $[V^{\text{low}}]$ are two $n^{\text{low}} \times n^{\text{low}}$ unit matrices and $[\Sigma^{\text{low}}]$ is a diagonal positive-definite $n^{\text{low}} \times n^{\text{low}}$ matrix. We then have $\lambda_\alpha^{\text{low}} = ([\Sigma^{\text{low}}]_{\alpha\alpha})^{-2}$ for all $\alpha = 1, \dots, n^{\text{low}}$ and $[\Phi^{\text{low}}] = [\Sigma^{\text{proj}}]^{-1/2} [U^{\text{low}}] [\Sigma^{\text{low}}]$ where $[\Phi^{\text{low}}]$ is the $n^{\text{low}} \times n^{\text{low}}$ modal matrix $[\Phi^{\text{low}}] = (\varphi_1^{\text{low}} \dots \varphi_{n^{\text{low}}}^{\text{low}})$. Furthermore, we also have the two orthogonality and normalization relations

$$[\Phi^{\text{low}}]^T [\Phi^{\text{proj}}]^T [\Lambda] [\Phi^{\text{proj}}] [\Phi^{\text{low}}] = [\Lambda^{\text{low}}] \quad , \quad (3.43)$$

$$[\Phi^{\text{low}}]^T [\Phi^{\text{proj}}]^T [\Phi^{\text{proj}}] [\Phi^{\text{low}}] = [I_{n^{\text{low}}}] \quad , \quad (3.44)$$

where $[\Lambda^{\text{low}}] = [\Sigma^{\text{low}}]^{-2}$ is a diagonal matrix. The low level complexity displacements basis is then introduced as the set of n^{low} algebraically independent finite element vectors $[U^{\text{low}}] = [u_1^{\text{low}} \dots u_{n^{\text{low}}}^{\text{low}}]$ defined, for all $\alpha = 1, \dots, n^{\text{low}}$, by

$$u_\alpha^{\text{low}} = [U] [\Phi^{\text{proj}}] \varphi_\alpha^{\text{low}} \quad . \quad (3.45)$$

Note that such low level complexity displacements basis spans the same vector space \mathcal{S}^{low} as the set of the n^{low} linearly independent finite element vectors $[U^{\text{proj}}] = (u_1^{\text{proj}} \dots u_{n^{\text{low}}}^{\text{proj}})$ defined, for all $\alpha = 1, \dots, n^{\text{low}}$, by

$$u_\alpha^{\text{proj}} = [U] \varphi_\alpha^{\text{proj}} \quad . \quad (3.46)$$

It should be noted that

$$[U^{\text{low}}]^T [K^s] [U^{\text{low}}] = [\Lambda^{\text{low}}] \quad , \quad [U^{\text{low}}]^T [M^s] [U^{\text{low}}] = [I_{n^{\text{low}}}] \quad , \quad (3.47)$$

while there is only one orthogonality relation that can be built for $[U^{\text{proj}}]$,

$$[U^{\text{proj}}]^T [K^s] [U^{\text{proj}}] = [\Lambda^{\text{proj}}] \quad . \quad (3.48)$$

Consequently, $[U^{\text{low}}]$ fulfills orthogonality relations in Eq. (3.47) and then the spatial filtering method can also be recurrently applied to $[U^{\text{low}}]$ by replacing $[U]$ with $[U^{\text{low}}]$ in the previous developments, which is not possible for U^{proj} . Such a recurrence will be used in Chapter 4 for introducing the second spatial filtering. Despite relations in Eq. (3.47) seem to be very similar to the relations in Eq.(2.30), it should be noted that, in general, $\lambda_\alpha^{\text{low}} \neq \lambda_\alpha^s$ and $u_\alpha^{\text{low}} \neq \varphi_\alpha^s$ for all $\alpha = 1, \dots, n^{\text{low}}$. Consequently, in general, the low complexity level displacements basis $[U^{\text{proj}}]$ does not correspond to elastic modes. Furthermore, it will be more convenient for the next chapters to introduce matrix $[Q^{\text{low}}] = [\Phi^{\text{proj}}] [\Phi^{\text{low}}]$. By using Eq. (3.44), we then have

$$[Q^{\text{low}}]^T [Q^{\text{low}}] = [I_{n^{\text{low}}}] \quad . \quad (3.49)$$

We then have

$$[U^{\text{low}}] = [U] [Q^{\text{low}}] \quad . \quad (3.50)$$

3.2.5 Construction of the high complexity level displacements basis

Since n^{low} is usually very small with respect to N , then vector space \mathcal{S}^{low} might not allow an accurate representation of any finite element solution $u(\omega)$ that is represented by the basis made up of the columns of $[\mathbb{U}]$. It is the reason why a second displacement basis is introduced and that is such that it spans the vector space $\mathcal{S}^{\text{high}}$ defined as the complement vector space of \mathcal{S}^{low} into \mathcal{S} with respect to the metric associated with the mass finite element matrix $[\mathbb{M}^s]$. Let $n^{\text{high}} = N - n^{\text{low}}$ and let $[\mathbb{U}^{\text{high}}] = (u_1^{\text{high}} \dots u_{n^{\text{high}}}^{\text{high}})$ be the $n_{\text{dof}}^s \times n^{\text{high}}$ matrix whose columns form a set of mutually linearly independent vectors $u_1^{\text{high}}, \dots, u_{n^{\text{high}}}^{\text{high}}$ that span $\mathcal{S}^{\text{high}}$. Hereinafter, $[\mathbb{U}^{\text{high}}]$ will be referred as the high complexity level displacements basis. As $\mathcal{S}^{\text{high}}$ is a subspace of \mathcal{S}^s (by construction), then for all $\alpha = 1, \dots, n^{\text{high}}$, u_α^{high} can be written as

$$u_\alpha^{\text{high}} = [\mathbb{U}] [\Phi^{\text{comp}}] \varphi_\alpha^{\text{high}} \quad , \quad (3.51)$$

where $\varphi_1^{\text{high}}, \dots, \varphi_{n^{\text{high}}}^{\text{high}}$ are linearly independent vectors belonging to $\mathbb{R}^{n^{\text{high}}}$ and $[\Phi^{\text{comp}}]$ is any $N \times n^{\text{high}}$ rectangular matrix such that

$$[\Phi^{\text{comp}}]^T [\Phi^{\text{comp}}] = [I_{n^{\text{high}}}] \quad . \quad (3.52)$$

Since by construction, u_α^{high} is normal (for the metric defined by matrix $[\mathbb{M}^s]$) to subspace $\mathcal{S}^{\text{proj}}$, for all $\alpha = 1, \dots, n^{\text{high}}$, we have

$$[\mathbb{U}^{\text{proj}}]^T [\mathbb{M}^s] u_\alpha^{\text{high}} = \mathbf{0} \quad . \quad (3.53)$$

Since $[\mathbb{U}]^T [\mathbb{M}^s] [\mathbb{U}] = [I_N]$ then Eq. (3.53) is rewritten as

$$[\Phi^{\text{proj}}]^T [\Phi^{\text{comp}}] \varphi_\alpha^{\text{high}} = \mathbf{0} \quad . \quad (3.54)$$

Since Eq. (3.54) is verified for the vectors $\varphi_1^{\text{high}}, \dots, \varphi_{n^{\text{high}}}^{\text{high}}$ in $\mathbb{R}^{n^{\text{high}}}$, which are linearly independent, we have

$$[\Phi^{\text{proj}}]^T [\Phi^{\text{comp}}] = [0_{n^{\text{low}} \times n^{\text{high}}}] \quad , \quad (3.55)$$

where $[0_{n^{\text{low}} \times n^{\text{high}}}]$ is the $n^{\text{low}} \times n^{\text{high}}$ zero matrix. Taking into account Eqs. (3.52) and (3.55), then matrix $[\Phi^{\text{comp}}]$ can be defined as the real matrix whose columns are the right-singular vectors associated with the n^{high} zero singular values of the SVD of matrix $[\Phi^{\text{proj}}]^T$. The linearly independent vectors $\varphi_1^{\text{high}}, \dots, \varphi_{n^{\text{high}}}^{\text{high}}$ in $\mathbb{R}^{n^{\text{high}}}$ can arbitrarily be defined as the solutions of the following generalized eigenvalue problem: find $\varphi_\alpha^{\text{high}}$ in $\mathbb{R}^{n^{\text{high}}}$ and $\lambda_\alpha^{\text{high}} > 0$ such that

$$\left([\Phi^{\text{comp}}]^T [\mathbb{U}]^T [\mathbb{K}^s] [\mathbb{U}] [\Phi^{\text{comp}}] \right) \varphi_\alpha^{\text{high}} = \lambda_\alpha^{\text{high}} \left([\Phi^{\text{comp}}]^T [\mathbb{U}]^T [\mathbb{M}^s] [\mathbb{U}] [\Phi^{\text{comp}}] \right) \varphi_\alpha^{\text{high}} \quad , \quad (3.56)$$

which can be rewritten as

$$[\Phi^{\text{comp}}]^T [\Lambda] [\Phi^{\text{comp}}] \varphi_\alpha^{\text{high}} = \lambda_\alpha^{\text{high}} \varphi_\alpha^{\text{high}} \quad . \quad (3.57)$$

Consequently, we have the following orthogonality relations

$$[\mathbb{U}^{\text{high}}]^T [\mathbb{K}^s] [\mathbb{U}^{\text{high}}] = [\Lambda^{\text{high}}] \quad , \quad [\mathbb{U}^{\text{high}}]^T [\mathbb{M}^s] [\mathbb{U}^{\text{high}}] = [I_{n^{\text{high}}}] \quad , \quad (3.58)$$

where $[\Lambda^{\text{high}}]$ is a positive-definite diagonal matrix whose non-zero entries are the eigenvalues $\lambda_1^{\text{high}}, \dots, n^{\text{high}}$ and where $[\Phi^{\text{high}}] = (\varphi_1^{\text{low}} \dots \varphi_{n^{\text{high}}}^{\text{low}})$ is such that

$$[\Phi^{\text{high}}]^T [\Phi^{\text{high}}] = [I_N] \quad , \quad (3.59)$$

in which $[I_N]$ is the identity matrix with dimensions $N \times N$. Furthermore, it will be more convenient for the next chapters to introduce matrix $[Q^{\text{high}}] = [\Phi^{\text{comp}}] [\Phi^{\text{high}}]$. We then have

$$[\mathbb{U}^{\text{high}}] = [\mathbb{U}] [Q^{\text{high}}] \quad . \quad (3.60)$$

Using Eqs. (3.52) and (3.59), it can be deduced that

$$[Q^{\text{high}}]^T [Q^{\text{high}}] = [I_{n^{\text{high}}}] \quad . \quad (3.61)$$

In addition, using Eq. (3.55) yields

$$[Q^{\text{low}}]^T [Q^{\text{high}}] = [0_{n^{\text{low}} \times n^{\text{high}}}] \quad . \quad (3.62)$$

Finally, it is important to note that, since $[\mathbb{U}^{\text{high}}]$ fulfills orthogonality relations in Eq. (3.58) then the spatial filtering method can be recurrently also applied to $[\mathbb{U}^{\text{high}}]$ by replacing $[\mathbb{U}]$ with $[\mathbb{U}^{\text{high}}]$ in the previous developments. Such a recurrence will be used in Chapter 4 for introducing the second spatial filtering.

Chapter 4

Multilevel reduced-order computational model

Contents

| | |
|---|-----------|
| 4.1 Construction of the multilevel displacements basis for the LF and MF domains | 32 |
| 4.2 Construction of the multilevel reduced-order model in the LF and MF domains | 35 |

In this chapter, the methodology presented in Chapter 3 is used to construct a multilevel reduced-order computational model. Such multilevel reduced-order computational model is constructed by carrying out recursively two successive spatial filterings to the elastic eigenvectors of the structure, which belong to the LF (Low Frequency) and MF (Medium Frequency) frequency domains. For such a construction, it is assumed that the upper and lower frequency bounds ω_L , ω_M , and ω_H of the LF, MF, and HF domains have already been defined and are known. The strategy and the principle for the recursive two successive spatial filterings are shown in Fig. 4.1. A first spatial filtering is carried out for $[\mathcal{U}] = [\Phi_{LM}^s]$ with a polynomial degree d (see Chapter 3) equal to d_M that characterizes the complexity level of the elastic eigenvectors in the MF domain in order to filter out any displacements contribution with complexity level higher than those in the MF domain. This first spatial filtering yields the two displacements bases denoted by $[\mathcal{U}_{LM}]$ and $[\mathcal{U}_H]$ that correspond to $[\mathcal{U}^{\text{low}}]$ and $[\mathcal{U}^{\text{high}}]$ introduced in Chapter 3. It should be noted that the subscript H is used to remind that those displacements vectors have the highest complexity level. Hence, the subscript H does not refer to the HF domain. The second spatial filtering is carried by replacing $[\mathcal{U}]$ introduced in Chapter 3 by $[\mathcal{U}_{LM}]$ and with a polynomial degree d equal to d_L that characterizes the complexity level of the elastic eigenvectors in the LF domain. This second spatial filtering yields two displacements bases denoted by $[\mathcal{U}_L]$ and $[\mathcal{U}_M]$ that correspond to $[\mathcal{U}^{\text{low}}]$ and $[\mathcal{U}^{\text{high}}]$ introduced in Chapter 3. Hereinafter, the complexity level of the set of elastic eigenvectors in a frequency domain (LF, MF or HF) will be shortened in « complexity level of the frequency domain (LF, MF or HF) ».

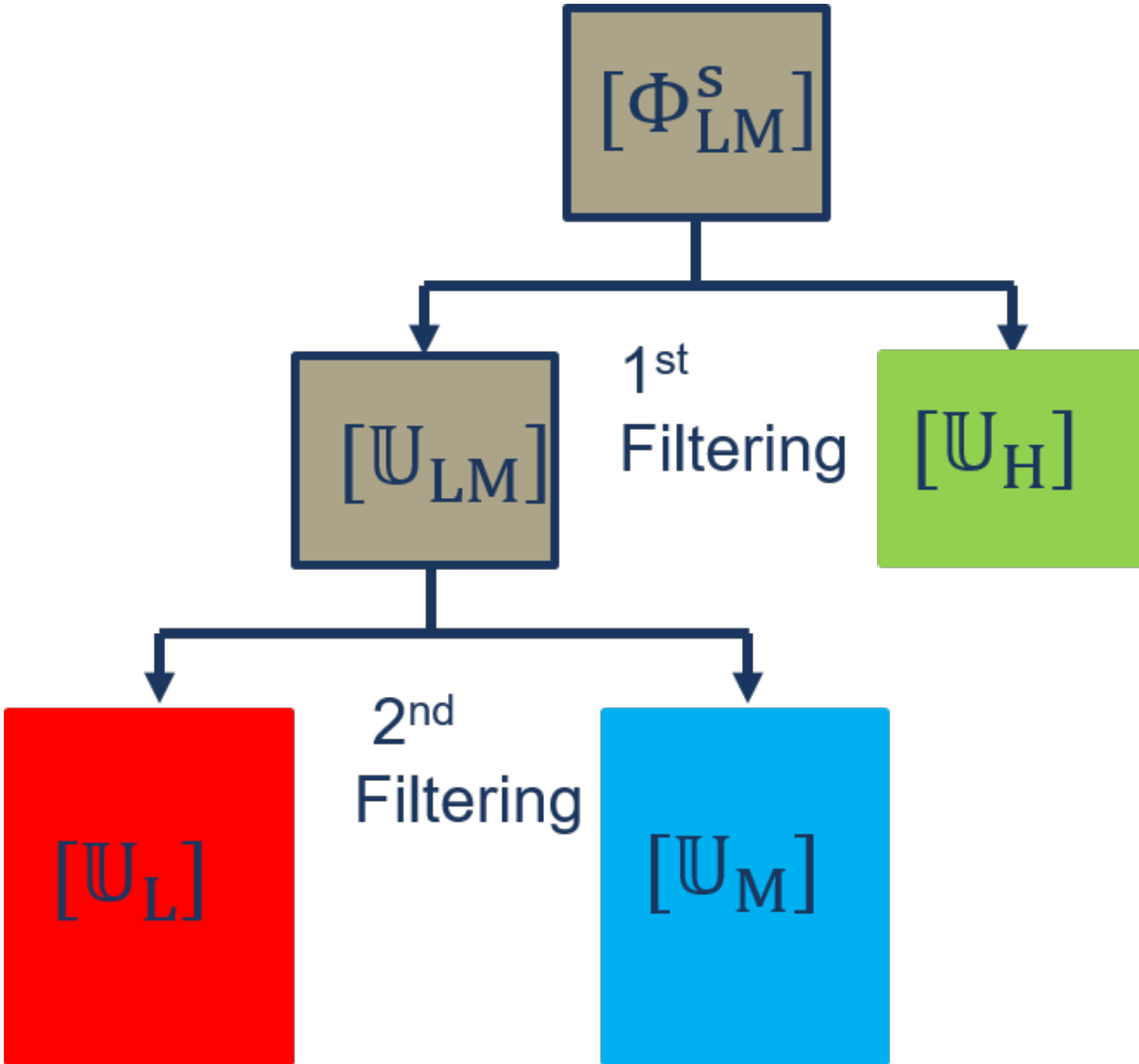


Figure 4.1 – Two spatial filterings to construct the multilevel displacement basis

4.1 Construction of the multilevel displacements basis for the LF and MF domains

As previously said, the upper and lower frequency bounds of the LF, MF, and HF domains are known. The spatial filtering method presented in Chapter 3 is then carried out for a polynomial degree parameter d equal to d_M (first spatial filtering) and then equal to d_L (second spatial filtering). The calculation of the values d_M and d_L is presented in Chapter 5.

4.1.1 Complexity level of LF, MF, and HF domains

In order to determine the value d_M of d for the first spatial filtering, we propose to study the graph of $d \mapsto \text{conv}_M(d)$ where, for all d that is positive, $\text{conv}_M(d)$ is equal to the number n^{low}

of non-zero eigenvalues introduced in Chapter 3 for $[\mathcal{U}] = [\Phi_M^s]$. Then, the value d_M is fixed as the smallest value of d such that $\text{conv}_M(d) > n_H(1 - \varepsilon_M)$ in which ε_M is a tolerance threshold close to zero. Such a method to determine the value d_M of d allows the characterization by polynomial parameter d of the complexity level of the MF domain. Then, using the spatial filtering with $d = d_M$ would allow separating every displacement contributions that have a complexity level higher than the complexity level of the MF domain. In order to determine the value d_L of d for the second spatial filtering, we propose to study the graph of $d \mapsto \text{conv}_L(d)$ where, for all d that is positive, $\text{conv}_L(d)$ is equal to the number n^{low} of non-zero eigenvalues introduced in Chapter 3 for $[\mathcal{U}] = [\Phi_L^s]$. Then, the value d_L is fixed as the smallest value of d such that $\text{conv}_L(d) > n_L(1 - \varepsilon_L)$ in which ε_L is a tolerance threshold close to zero. Such a method to determine the value d_L of d allows the characterization by polynomial parameter d of the complexity level of the LF domain. Then, using the spatial filtering with $d = d_L$ would allow for separating the displacement contributions that have a complexity level higher than the complexity level of the LF domain. Furthermore, due to the random access memory (RAM) limitation of the computers, there is a maximal value d_{max} for the polynomial parameter d that can be used in practice to compute matrix $[q]$ (see Section 3.1.2) when performing the QR decomposition of matrix $[m^{\text{lump}}]^{1/2}[m]$ as explained in Section 3.1.2. At the time this work has been carried out, we found out that $d_{\text{max}} = 40$ with Matlab on a 1500 Gigabytes RAM machine. Such a relatively high value for d_{max} makes it possible to estimate the complexity level of the HF domain by calculating a value d_H of d . It will be carried out by studying the graph of the function $d \mapsto \text{conv}_H(d)$ where, for all $d > 0$, $\text{conv}_H(d)$ is equal to the number n^{low} of non-zero eigenvalues introduced in Chapter 3 with $[\mathcal{U}] = [\Phi_H^s]$. Then, the value d_H is fixed as the smallest value of d such that $\text{conv}_H(d) > n_H(1 - \varepsilon_H)$ in which ε_H is a tolerance threshold much less than 1 (close to zero). Such a method to determine the value d_H of d allows the characterization by polynomial parameter d of the complexity level of the HF domain but it will not be used for constructing the multilevel reduced-order computational model.

4.1.2 First spatial filtering

For a given value d_M of d , the spatial filtering method presented in Chapter 3 is performed again with $[\mathcal{U}] = [\Phi_{LM}]$ in order to construct two matrices $[\mathcal{U}^{\text{low}}]$ and $[\mathcal{U}^{\text{high}}]$ that are renamed as $[\mathcal{U}_{LM}]$ and $[\mathcal{U}_H]$ to avoid any confusion with the previous spatial filtering. Let $n_{\mathcal{U}_{LM}}$ and $n_{\mathcal{U}_H}$ be the number of columns of matrices $[\mathcal{U}_{LM}]$ and $[\mathcal{U}_H]$. From Eq. (3.50), matrix $[\mathcal{U}_{LM}]$ can be rewritten as

$$[\mathcal{U}_{LM}] = [\Phi_{LM}^s][Q_{LM}] \quad , \quad (4.1)$$

where the matrix $[Q_{LM}]$ is the matrix $[Q^{\text{low}}]$ in Eq. (3.50) with $[\mathcal{U}] = [\Phi^s]$ and $d = d_M$. Consequently, Eq. (3.49) yields

$$[Q_{LM}]^T [Q_{LM}] = [I_{n_{\mathcal{U}_{LM}}}] \quad , \quad (4.2)$$

in which $[I_{n_{\mathcal{U}_{LM}}}]$ is the identity matrix of dimensions $n_{\mathcal{U}_{LM}} \times n_{\mathcal{U}_{LM}}$. In addition, by using Eq. (3.60), the matrix $[\mathcal{U}_H]$ can be rewritten as

$$[\mathcal{U}_H] = [\mathcal{U}] [Q_H] \quad , \quad (4.3)$$

where the matrix $[Q_H]$ is the matrix $[Q^{\text{high}}]$ in Eq. (3.60) with $[\mathcal{U}] = [\mathcal{U}_{LM}]$ and $d = d_L$. Consequently, Eq. (3.61) yields

$$[Q_H]^T [Q_H] = [I_{n_{\mathcal{U}_H}}] \quad , \quad (4.4)$$

in which $[I_{n_{\mathcal{U}_H}}]$ is the identity matrix of dimensions $n_{\mathcal{U}_H} \times n_{\mathcal{U}_H}$. In addition, from Eq. (3.62), it can be deduced that

$$[Q_{LM}]^T [Q_H] = [0_{n_{\mathcal{U}_{LM}} \times n_{\mathcal{U}_H}}] \quad , \quad (4.5)$$

where $[0_{n_{\mathcal{U}_{LM}} \times n_{\mathcal{U}_H}}]$ is the $n_{\mathcal{U}_{LM}} \times n_{\mathcal{U}_H}$ zero matrix. Each column of matrix $[\mathcal{U}_H]$ is a displacement vector with a complexity level higher than the complexity level of the MF domain. In the case of simple structures, matrix $[\mathcal{U}_H]$ is « empty ». Nevertheless, in the case of complex structures as automobiles, it can be expected that matrix $[\mathcal{U}_H]$ is almost never « empty » because very local displacements are observed even in the LF domain.

4.1.3 Second spatial filtering

For a given value d_L of d , the spatial filtering method presented in Chapter 3 is carried again with $[\mathcal{U}] = [\mathcal{U}_{LM}]$ to construct two matrices $[\mathcal{U}^{\text{low}}]$ and $[\mathcal{U}^{\text{high}}]$ respectively that are renamed as $[\mathcal{U}_L]$ and $[\mathcal{U}_M]$ respectively to avoid any confusion with the previous spatial filtering. Let $n_{\mathcal{U}_L}$ and $n_{\mathcal{U}_M}$ respectively be the number of columns of matrices $[\mathcal{U}_L]$ and $[\mathcal{U}_M]$. From Eq. (3.50), matrix $[\mathcal{U}_{LM}]$ can be rewritten as

$$[\mathcal{U}_L] = [\mathcal{U}] [Q_L] \quad (4.6)$$

$$= [\mathcal{U}_{LM}] [Q_L] \quad (4.7)$$

$$= [\Phi_{LM}^s] [Q_{LM}] [Q_L] \quad , \quad (4.8)$$

where matrix $[Q_L]$ is the matrix $[Q^{\text{low}}]$ in Eq. (3.50) for $[\mathcal{U}] = [\mathcal{U}_{LM}]$ and $d = d_L$. Consequently, Eq. (3.61) yields

$$[Q_L]^T [Q_L] = [I_{n_{\mathcal{U}_L}}] \quad , \quad (4.9)$$

in which $[I_{n_{\mathcal{U}_L}}]$ is the identity matrix of dimensions $n_{\mathcal{U}_L} \times n_{\mathcal{U}_L}$. Each column of matrix $[\mathcal{U}_L]$ is a displacement vector with a complexity level of the same order than the complexity level of the LF domain. In case d_L is less than d_M , which is usually the case, then the subscript L reminds that the vectors in the columns of $[\mathcal{U}_L]$ gather the vectors with the lowest complexity level. Hence, the subscript L does not refer to the LF domain. In addition, from Eq. (3.60), matrix $[\mathcal{U}_M]$ can be rewritten as

$$[\mathcal{U}_M] = [\mathcal{U}] [Q_M] \quad (4.10)$$

$$= [\mathcal{U}_{LM}] [Q_M] \quad (4.11)$$

$$= [\Phi_{LM}^s] [Q_{LM}] [Q_M] \quad , \quad (4.12)$$

where the matrix $[Q_M]$ is the matrix $[Q^{\text{high}}]$ in Eq. (3.60) with $[U] = [U_{LM}]$ and $d = d_L$. Consequently, Eq. (3.61) yields

$$[Q_M]^T [Q_M] = [I_{n_{U_M}}] \quad , \quad (4.13)$$

in which $[I_{n_{U_M}}]$ is the identity matrix of dimensions $n_{U_M} \times n_{U_M}$. Each column of matrix $[U_M]$ is a displacement vector with a complexity level of higher order than the complexity level of the LF domain but less than the complexity level of the columns of $[U_H]$. The subscript M reminds that the vectors in the columns of $[U_M]$ gather the vectors with a medium complexity level. Hence, the subscript M does not refer to the MF domain.

4.2 Construction of the multilevel reduced-order model in the LF and MF domains

An approximation of the finite-element displacement vector $u(\omega)$ is then written with respect to its expansion on the bases represented by matrices $[U_L]$, $[U_M]$, and $[U_H]$,

$$u(\omega) = [U_L] \mathbf{q}_L^s(\omega) + [U_M] \mathbf{q}_M^s(\omega) + [U_H] \mathbf{q}_H^s(\omega) \quad . \quad (4.14)$$

This expansion can be rewritten as

$$u(\omega) = [U_{LMH}] \mathbf{q}_{LMH}^s(\omega) \quad , \quad (4.15)$$

where

$$[U_{LMH}] = \begin{pmatrix} [U_L] & [U_M] & [U_H] \end{pmatrix} \quad , \quad \mathbf{q}_{LMH}^s = \begin{pmatrix} \mathbf{q}_L^s(\omega) \\ \mathbf{q}_M^s(\omega) \\ \mathbf{q}_H^s(\omega) \end{pmatrix} \quad . \quad (4.16)$$

By using Eqs. (4.1), (4.6), and (4.10), the matrix $[U_{LMH}]$ can be rewritten as

$$[U_{LMH}] = [\Phi_{LM}^s] \begin{pmatrix} [Q_{LM}] [Q_L] & [Q_{LM}] [Q_M] & [Q_H] \end{pmatrix} \quad (4.17)$$

$$= [\Phi_{LM}^s] [Q_{LMH}] \quad , \quad (4.18)$$

in which

$$[Q_{LMH}] = \begin{pmatrix} [Q_{LM}] [Q_L] & [Q_{LM}] [Q_M] & [Q_H] \end{pmatrix} \quad . \quad (4.19)$$

We then obtain the multilevel reduced-order model

$$\begin{pmatrix} -\omega^2 [M_{LMH}^s] + i\omega [D_{LMH}^s] + [K_{LMH}^s] & [C_{LMH}] \\ \omega^2 [C_{LMH}]^T & -\omega^2 [M^f] + i\omega [D^f] + [K^f] \end{pmatrix} \begin{pmatrix} \mathbf{q}_{LMH}^s(\omega) \\ \mathbf{q}^f(\omega) \end{pmatrix} = \begin{pmatrix} \mathbf{f}_{LMH}^s(\omega) \\ \mathbf{0} \end{pmatrix} \quad , \quad (4.20)$$

where

$$[M_{LMH}^s] = [U_{LMH}]^T [M^s] [U_{LMH}] = [Q_{LMH}]^T [\mathcal{M}_{LM}^s] [Q_{LMH}] \quad , \quad (4.21)$$

$$[D_{LMH}^s] = [U_{LMH}]^T [D^s] [U_{LMH}] = [Q_{LMH}]^T [\mathcal{D}_{LM}^s] [Q_{LMH}] \quad , \quad (4.22)$$

$$[K_{LMH}^s] = [U_{LMH}]^T [K^s] [U_{LMH}] = [Q_{LMH}]^T [\mathcal{K}_{LM}^s] [Q_{LMH}] \quad , \quad (4.23)$$

$$[C_{\text{LMH}}] = [U_{\text{LMH}}]^T [C] [\Phi^f] = [Q_{\text{LMH}}]^T [\mathcal{C}_{\text{LM}}] \quad , \quad (4.24)$$

$$\mathfrak{f}_{\text{LMH}}^s(\omega) = [U_{\text{LMH}}]^T \mathbb{F}^s(\omega) = [Q_{\text{LMH}}]^T \mathbf{f}_{\text{LM}}^s(\omega) \quad , \quad (4.25)$$

and where the generalized matrices $[\mathcal{M}_{\text{LM}}^s]$, $[\mathcal{D}_{\text{LM}}^s]$, $[\mathcal{X}_{\text{LM}}^s]$, $[\mathcal{C}_{\text{LM}}]$, and the generalized vector \mathbf{f}_{LM}^s are introduced in Section 2.4.5. Using Eqs. (4.2), (4.4), (4.5), (4.9), and (4.13) yields

$$[Q_{\text{LMH}}]^T [Q_{\text{LMH}}] = [I_{n_{\text{LM}}}] \quad . \quad (4.26)$$

Consequently, $[M_{\text{LMH}}]$ is equal to the identity matrix $[I_{n_{\text{LM}}}]$ and therefore, it is a diagonal matrix, which is not the case, in general, for matrices $[D_{\text{LMH}}]$ and $[K_{\text{LMH}}]$.

Chapter 5

Numerical applications for the multilevel reduced-order computational model

Contents

| | | |
|------------|---|-----------|
| 5.1 | Description of the full-order computational model | 37 |
| 5.2 | Frequency domain limits ω_L, ω_M and ω_H | 38 |
| 5.3 | Complexity level for the HF domain | 38 |
| 5.4 | Case 1: Multilevel reduced-order model with $\omega_L/2\pi = 30$ Hz | 39 |
| 5.5 | Case 2: Multilevel reduced-order model with $\omega_L/2\pi = 200$ Hz | 41 |

In this chapter, a numerical application is presented for the methodology presented in Chapters 3 and 4. In the following section, the three frequency bounds ω_L , ω_M , and ω_H (see Section 2.4.5) are determined by analyzing the FRF for a given excitation (input) and for a set of observation points (outputs). Then the multilevel reduced-order computational model is constructed and validated by comparison with the classical reduced-order computational model in Section 2.4.5.

5.1 Description of the full-order computational model

This full-order computational model is a three-dimensional finite-element model of an automobile (see Fig. 5.1) The total number of degree of freedom is $n_{\text{dof}}^s + n_{\text{dof}}^f = 19\,984\,315$. An intensive computational effort has been carried out to calculate the $n^s = 25\,685$ elastic modes for the structure and the $n^f = 4\,427$ elastic modes for the acoustic cavity in the whole LF, MF and HF domains (0 to 2000 Hz) allowing the construction of matrices $[\Phi^s]$ and $[\Phi^f]$. The excitations are located in the structure at four points (clvd, clvg, clrd and clrg) as shown in Fig. 5.1. They have been chosen because they represent engine supports. Figure 5.1 also shows the location of the observation points for the structure and the cavity. For the structure, they correspond to the flooring points (ccvvg and ccurg) and again the points clvd and clvg. For the acoustic cavity, the observation points (avd, avg, ard and arg) are located at to the ear of the passengers.

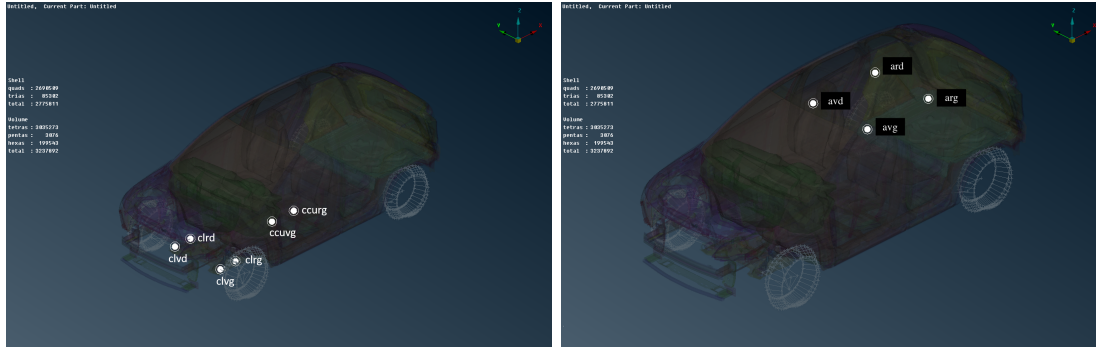


Figure 5.1 – Excitation (input) and observation (output) points for calculated FRF. On the right, observation points for the acoustic cavity which corresponds to the four hearing points (avd, avg, ard and arg) of the four passengers in the passengers. On the left, excitation points (clvd and clvg) and observation points (ccuvg, ccurg and again clvd, clvg) for the structure.

5.2 Frequency domain limits ω_L , ω_M and ω_H

The frequency limits each frequency domains (LF, MF and HF) have been determined by analyzing the FRF for a given input (excitation at point clvg and in X -direction) and 12 outputs (observations on ccuvg, ccurg, clvd and clvg in X -, Y -, and Z -directions). Figures 5.2 to 5.7 show the graph of the mean value of these 12 FRF with different frequency scaling. Comparing Figs. 5.2 and 5.3 does not allow a clear conclusion on the value of ω_L . Indeed, the upper limit of the LF domain is unclear for such a structure: it could be $\omega/2\pi = 30$ Hz as well as $\omega/2\pi = 200$ Hz. Comparing Figs. 5.2, 5.6, and 5.7 allows an estimation of the upper limit of the MF domain with $\omega_L/2\pi = 800$ Hz and of course, the upper limit of the validity domain of the reduced-order computational model is $\omega_H/2\pi = 2000$ Hz. The determination of the value d_M (resp. d_L) of polynomial parameter d for the first (resp. second) spatial filtering does depend on the eigenvectors belonging to the MF (resp. LF) domain, then it is clear that uncertainty on the values of ω_M (resp. ω_L) yields uncertainties on the value of d_M (resp. d_L) as well on the construction of the multilevel reduced-order computational model. It is the reason why two constructions of the multilevel displacement bases $[\mathbb{U}_L]$, $[\mathbb{U}_M]$ and $[\mathbb{U}_H]$ are presented in the following yielding to two construction of the multilevel reduced-order computational model. The first case will correspond to $\omega/2\pi = 30$ Hz and the second case will correspond to $\omega/2\pi = 200$ Hz. Note that in the frequency domain $[0, \omega_M]$, there are $n_{LM} = 7470$ structural modes and $n_{LM}^f = 419$ acoustic modes.

5.3 Complexity level for the HF domain

As presented in Section 4.1.1, the complexity level of the HF domain is quantified by the value d_H of polynomial degree parameter d in studying the graph of mapping $d \mapsto \text{conv}_H(d)$ (see Fig. 5.6). It can be seen that $d_H = 32$. Nevertheless, it can also be seen that the values of $\text{conv}_H(d)$ are not negligible for small values of d . A possible interpretation is that there is no cutoff value

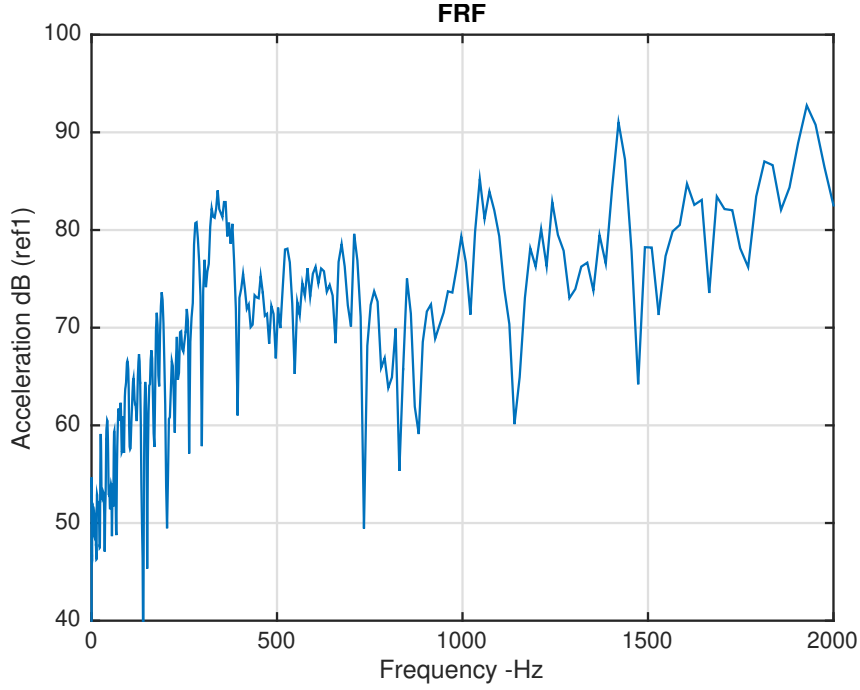


Figure 5.2 – Graph of the mean value of the 12 frequency response functions for a same excitation in X -direction at a point $clvg$ and observation in X -, Y -, and Z -directions at points $ccwvg$, $ccurg$, $clvd$ and $clvg$. Vertical axis: acceleration. Horizontal axis: frequency $f = \omega/2\pi$ in Hz for $f \in [0, 2000]$ Hz.

d_H^{cutoff} of d , which can filter out all the eigenvectors in the HF domain into the columns of matrix $[U^{\text{high}}]$. Consequently, it seems impossible to consider the HF domain as being only a purely high complexity level domain. We should observe a superposition of large structural component displacements on very local displacements. Note that it is not expected that the values d_L and d_M to be higher than d_H since it would mean that the complexity level of either the LF or MF domain is greater than the complexity level of the HF domain.

5.4 Case 1: Multilevel reduced-order model with $\omega_L/2\pi = 30$ Hz

In this section, the value ω_L is assumed to be equal to $30 \times 2\pi$ rad/s. As presented in Section 4.1.1, the complexity level of the LF (resp. MF) domain is quantified by the value d_L (resp. d_M) of polynomial degree parameter d in studying the graph of mapping $d \mapsto \text{conv}_L(d)$ (resp. $d \mapsto \text{conv}_M(d)$) that is shown in Fig. 5.7. It can be seen that $d_M = 29$ and $d_L = 3$ that are lesser than d_H is in accordance with the usual expertise in structural dynamics in which complexity level of the HF domain is higher than the complexity level of the MF, which is higher than the complexity level of the LF domain. Nevertheless, it also can be seen that the values of $d \mapsto \text{conv}_M(d)$ are not negligible for small values of d as it is the case for $d \mapsto \text{conv}_M(d)$. Once again, a possible interpretation is that there is no cutoff value d_M^{cutoff} of d , which can filter out all the eigenvectors in the MF domain into the columns of matrix $[U^{\text{high}}]$. Consequently, it seems impossible to consider the MF domain as being a purely (moderate) high complexity level domain only. Again, it can

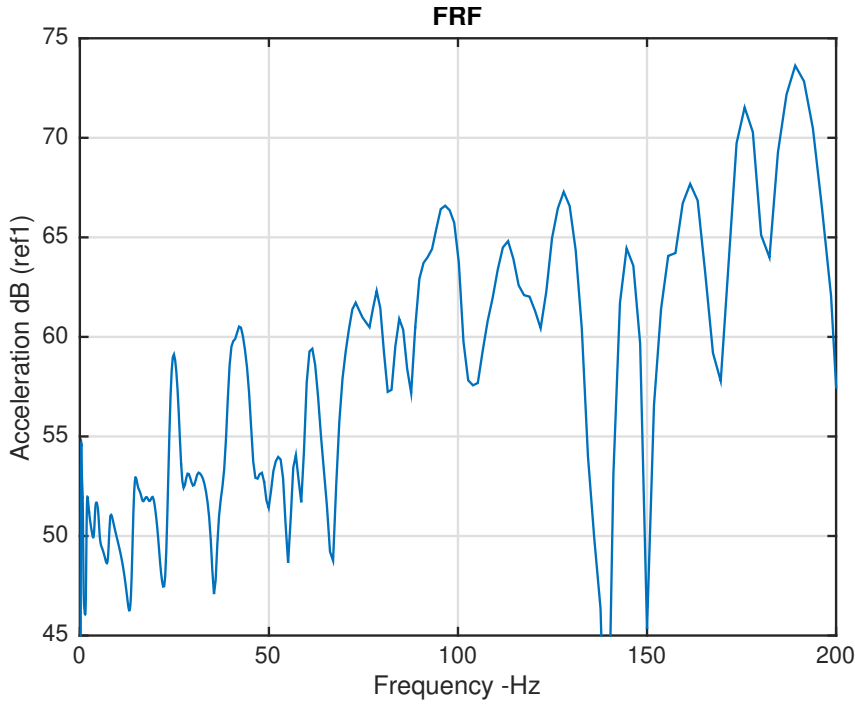


Figure 5.3 – Graph of the mean value of the 12 frequency response functions for a same excitation in X -direction at point $clvg$ and observation in X -, Y -, and Z -directions at points $ccvrg$, $ccvrg$, $clvd$ and $clvg$. Vertical axis: acceleration. Horizontal axis: frequency $f = \omega/2\pi$ in Hz for $f \in [0, 200]Hz$.

be expected to observe a superposition of large structural component displacements on more or less local displacements. In short, for constructing the multilevel reduced-order computational model, the parameters are $\omega_L = 30/2\pi$, $\omega_M = 800/2\pi$, $d_L = 3$ and $d_M = 29$. The number of columns of $[U_L]$ (resp. $[U_M]$ and $[U_H]$) is $n_{U_L} = 60$ (resp. $n_{U_M} = 7383$ and $n_{U_H} = 27$). Three multilevel reduced-order computational models have been used by removing some columns of $[U_{LMH}] = ([U_L][U_M][U_H])$. Figure 5.8 (resp. Fig. 5.9) presents the FRF for an excitation at point $clvg$ in X -direction and an observation at point $ccvrg$ (resp. $ccvrg$) in X -direction for $[U_{LMH}] = [U_M]$ (green lines), $[U_{LMH}] = [U_L]$ (red lines), $[U_{LMH}] = [U_H]$ (cyan lines, but out of range on the figure) and $[U_{LMH}] = ([U_L][U_M][U_H])$ (black lines). It has previously been checked that the FRF calculated with the multilevel reduced-order computational model with $[U_{LMH}] = ([U_L][U_M][U_H])$ perfectly fits the FRF calculated by the reduced-order computational model in Section 2.4.5. It can be seen that for $[U_{LMH}] = [U_M]$, the FRF is almost accurately well calculated into the whole MF domain and that for $[U_{LMH}] = [U_L]$, the FRF is almost accurately well calculated into the LF domain (up to 58.13 Hz for Fig. 5.8 and up to 77.11 Hz for Fig. 5.9). Such a result yields the conclusion that, at least for the chosen parameters ω_L and ω_M , $[U_M]$ spans almost the same vector space as the elastic eigenvectors in the MF domain (we have $n_{LM} \simeq n_{U_M}$). Figure 5.10 presents the FRF for an excitation at point $clvg$ in X -direction and four observations of the pressure (in dB) at points avg (top, left), arg (top, right), avd (bottom, left) and ard (bottom, right) for $[U_{LMH}] = [U_M]$ (green lines), $[U_{LMH}] = [U_L]$ (red lines),

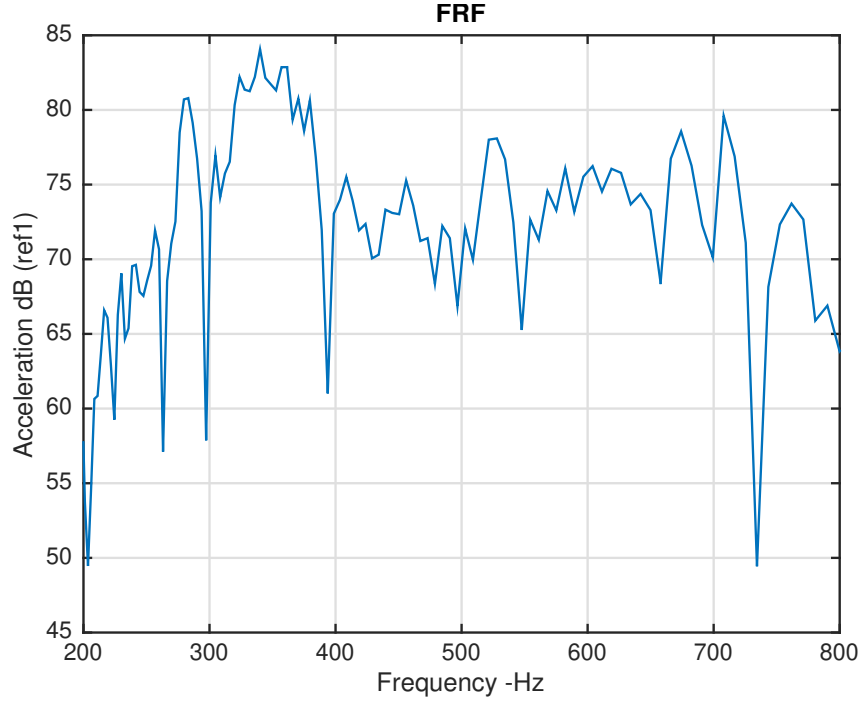


Figure 5.4 – Graph of the mean value of the 12 frequency response functions for a same excitation in X -direction at a point $clvg$ and observation in X -, Y -, and Z -directions at points $ccwvg$, $ccurg$, $clvd$ and $clvg$. Vertical axis: acceleration. Horizontal axis: frequency $f = \omega/2\pi$ in Hz for $f \in [200, 800]$ Hz.

$[u_{LMH}] = [u_H]$ (cyan lines) and $[u_{LMH}] = ([u_L] [u_M] [u_H])$ (black lines). It has previously been checked that this FRF calculated with the multilevel reduced-order computational model with $[u_{LMH}] = ([u_L] [u_M] [u_H])$ perfectly fits the FRF calculated by the reduced-order computational model in Section 2.4.5. Nevertheless, it can be seen in Fig. 5.10 that none of the basis $[u_L]$, $[u_M]$ and $[u_H]$ representing displacement vector $u(\omega)$ is able to account by itself only of the vibroacoustics for such a coupled fluid-structure system.

5.5 Case 2: Multilevel reduced-order model with $\omega_L/2\pi = 200$ Hz

In this section, the value ω_L is assumed to be equal to $200 \times 2\pi$ rad/s. The complexity level of the LF (resp. MF) domain is quantified by the value d_L (resp. d_M) of polynomial degree parameter d in studying the graph of mapping $d \mapsto \text{conv}_L(d)$ (resp. $d \mapsto \text{conv}_M(d)$) that is shown in Fig. 5.11. It can be seen that $d_M = 22$ and $d_L = 14$ that are still lesser than d_H is in accordance with the usual expertise in structural dynamics in which complexity level of the HF domain is higher than the complexity level of the MF, which is higher than the complexity level of the LF domain. As for case 1, it also can be seen that the values of $d \mapsto \text{conv}_M(d)$ are not negligible for small values of d as it is the case for $d \mapsto \text{conv}_M(d)$. Again, a possible interpretation is that there is no cutoff value d_M^{cutoff} of d , which can filter out all the eigenvectors in the MF domain into the columns of matrix $[u^{\text{high}}]$. Consequently, it seems impossible to consider the MF domain as being

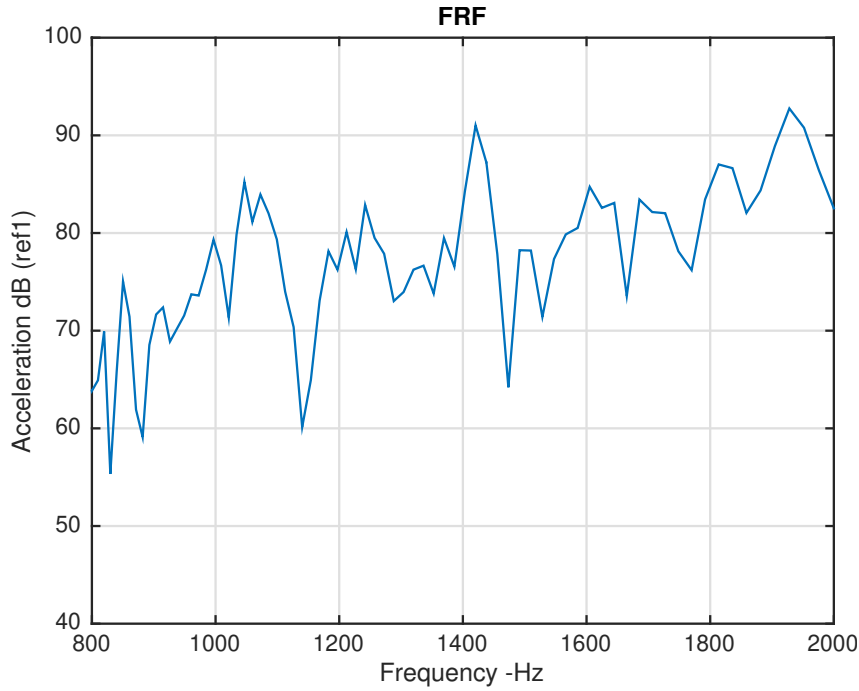


Figure 5.5 – Graph of the mean value of the 12 frequency response functions for a same excitation in X -direction at a point $clvg$ and observation in X -, Y -, and Z -directions at points $ccvrg$, $ccurg$, $clvd$ and $clvg$. Vertical axis: acceleration. Horizontal axis: frequency $f = \omega/2\pi$ in Hz for $f \in [800, 2000]Hz$.

a purely (moderate) high complexity level domain only. Again, it can be expected to observe a superposition of large structural component displacements on more or less local displacements. Again, for constructing the multilevel reduced-order computational model, the parameters are $\omega_L = 200/2\pi$, $\omega_M = 800/2\pi$, $d_L = 14$ and $d_M = 22$. The number of columns of $[U_L]$ (resp. $[U_M]$ and $[U_H]$) is $n_{U_L} = 2040$ (resp. $n_{U_M} = 4698$ and $n_{U_H} = 742$). It should be noted that the number of columns of $[U_L]$ and $[U_H]$ is higher than for case 1. Three multilevel reduced-order computational models have been used by removing some columns of $[U_{LMH}] = ([U_L] [U_M] [U_H])$.

Figure 5.12 (resp. Fig.5.13) presents the FRF for an excitation at point $clvg$ in X -direction and an observation at point $ccvg$ (resp. $ccurg$) in X -direction for $[U_{LMH}] = [U_M]$ (green lines), $[U_{LMH}] = [U_L]$ (red lines), $[U_{LMH}] = [U_H]$ (cyan lines) and $[U_{LMH}] = ([U_L] [U_M] [U_H])$ (black lines). It has previously been checked that the FRF calculated with the multilevel reduced-order computational model with $[U_{LMH}] = ([U_L] [U_M] [U_H])$ perfectly fits the FRF calculated by the reduced-order computational model in Section 2.4.5. At opposite of case 1, it can be seen that for $[U_{LMH}] = [U_M]$, the FRF is no longer accurately well calculated into the whole MF domain and that for $[U_{LMH}] = [U_L]$, the FRF is almost accurately well calculated into the LF domain up to 338.9 Hz. Such a result yields the conclusion that, in general and at opposite of case 1 that was a special case, $[U_M]$ does not span the same vector space as the elastic eigenvectors in the MF domain (note that we have $n_{LM} \neq n_{U_M}$). Figure 5.14 presents the FRF for an excitation at point $clvg$ in X -direction and four observations of the pressure (in dB) at points avg (top,

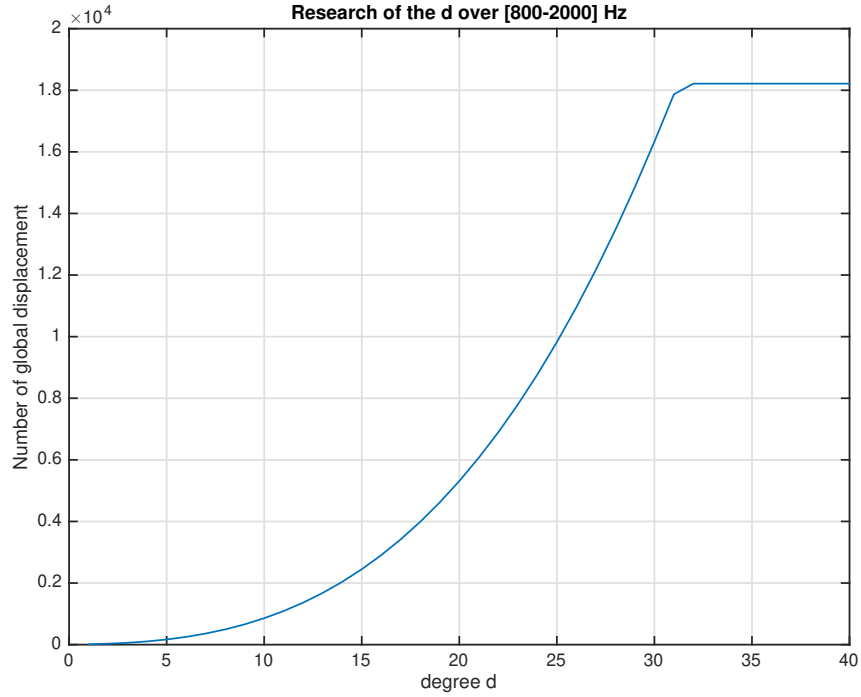


Figure 5.6 – Graph of mapping $d \mapsto \text{conv}_H(d)$. Horizontal axis: polynomial degree d . Vertical axis: Number of columns of matrix $[\mathcal{U}^{\text{low}}]$ for $[\mathcal{U}] = [\Phi_H]$.

left), arg (top, right), avd (bottom, left) and ard (bottom, right) for $[\mathcal{U}_{\text{LMH}}] = [\mathcal{U}_{\text{M}}]$ (green lines), $[\mathcal{U}_{\text{LMH}}] = [\mathcal{U}_{\text{L}}]$ (red lines), $[\mathcal{U}_{\text{LMH}}] = [\mathcal{U}_{\text{H}}]$ (cyan lines) and $[\mathcal{U}_{\text{LMH}}] = ([\mathcal{U}_{\text{L}}] [\mathcal{U}_{\text{M}}] [\mathcal{U}_{\text{H}}])$ (black lines). It has previously been checked that this FRF calculated with the multilevel reduced-order computational model with $[\mathcal{U}_{\text{LMH}}] = ([\mathcal{U}_{\text{L}}] [\mathcal{U}_{\text{M}}] [\mathcal{U}_{\text{H}}])$ perfectly fits the FRF calculated by the reduced-order computational model in Section 2.4.5. Nevertheless, as for case 1, it can be seen in Fig. 5.14 that none of the basis $[\mathcal{U}_{\text{L}}]$, $[\mathcal{U}_{\text{M}}]$ and $[\mathcal{U}_{\text{H}}]$ for representing displacement vector $\mathfrak{u}(\omega)$ is able to account by itself only of the vibroacoustics for such a coupled fluid-structure system.

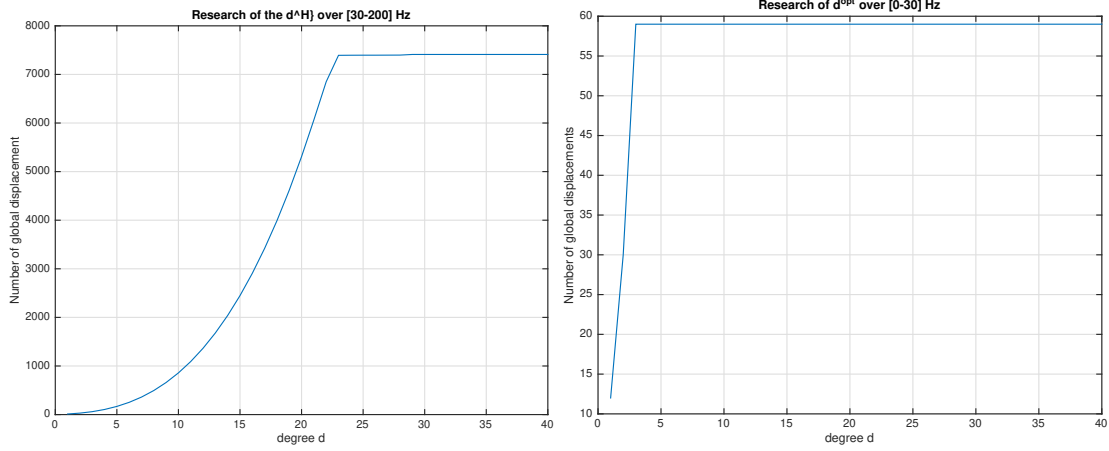


Figure 5.7 – Complexity levels for the case 1. On the left, graph of $d \mapsto \text{conv}_M(d)$. On the right, graph of $d \mapsto \text{conv}_L(d)$. Horizontal axis: polynomial degree d . Vertical axis: Number of columns of matrix $[\mathcal{U}^{\text{low}}]$ for $[\mathcal{U}] = [\Phi_M]$ (on the left) and for $[\mathcal{U}] = [\Phi_M]$ (on the right).

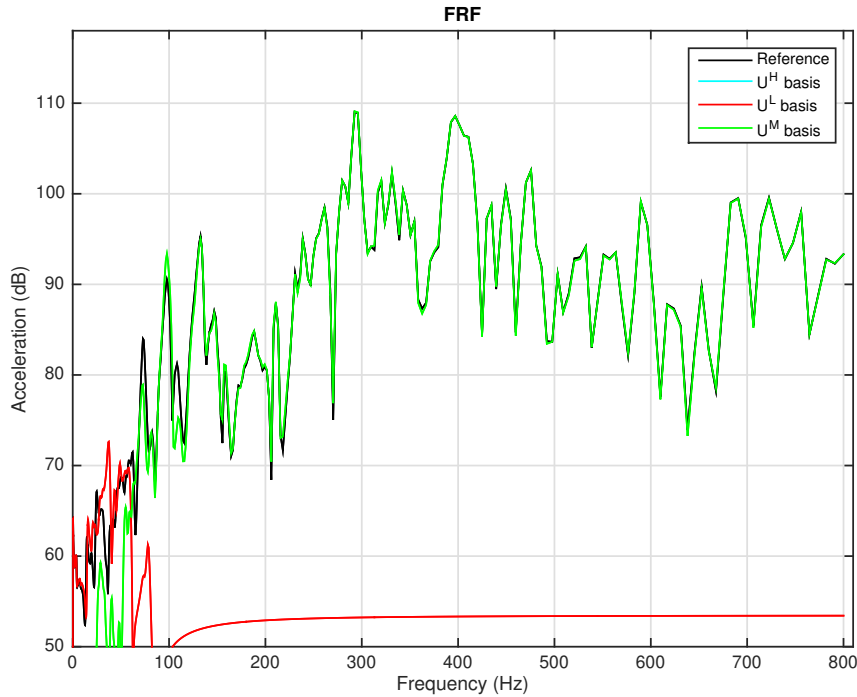


Figure 5.8 – Case 1: FRF for an excitation at point *clvg* in X -direction and an observation at point *ccvg* X -direction for $[\mathcal{U}_{\text{LMH}}] = [\mathcal{U}_M]$ (green lines), $[\mathcal{U}_{\text{LMH}}] = [\mathcal{U}_L]$ (red lines), $[\mathcal{U}_{\text{LMH}}] = [\mathcal{U}_H]$ (cyan lines, but out of range on the figure) and $[\mathcal{U}_{\text{LMH}}] = ([\mathcal{U}_L] [\mathcal{U}_M] [\mathcal{U}_H])$ (black lines). Horizontal axis: frequency $\omega/2\pi$ in Hz. Vertical axis: Acceleration in dB.

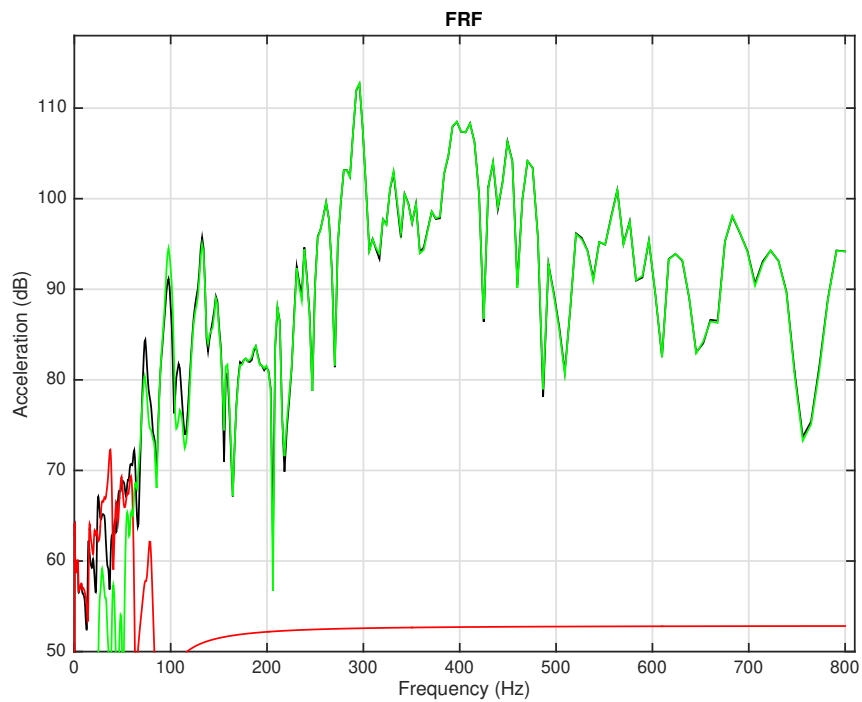


Figure 5.9 – Case 1: FRF for an excitation at point *clvg* in *X*-direction and an observation at point *ccurg* in *X*-direction for $[U_{LMH}] = [U_M]$ (green lines), $[U_{LMH}] = [U_L]$ (red lines), $[U_{LMH}] = [U_H]$ (cyan lines, but out of range on the figure) and $[U_{LMH}] = ([U_L] [U_M] [U_H])$ (black lines). Horizontal axis: frequency $\omega/2\pi$ in Hz. Vertical axis: Acceleration in dB.

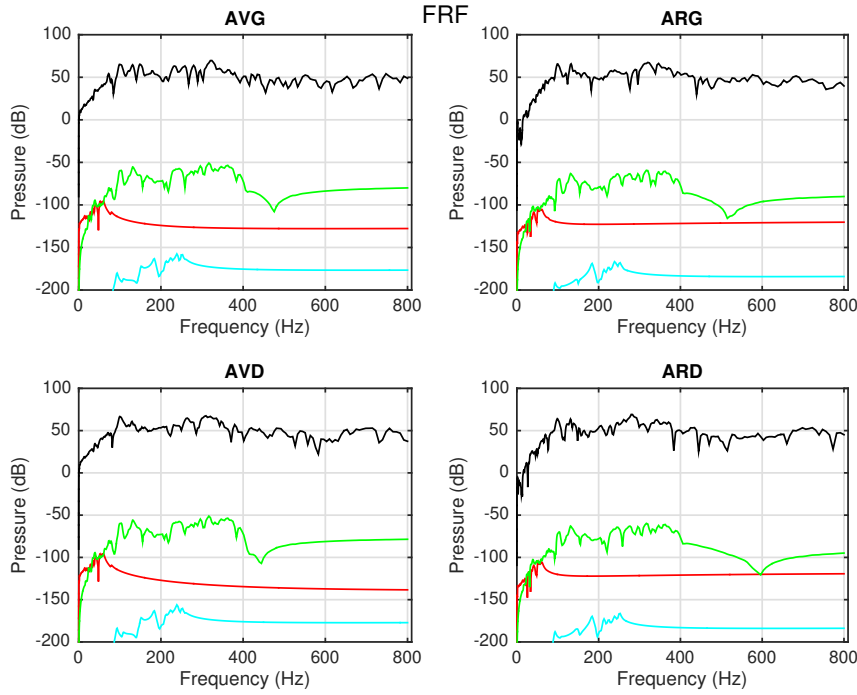


Figure 5.10 – Case 1: FRF for an excitation at point *clvg* in *X*-direction and the four observations of pressure (in dB) at points *avg* (top, left), *arg* (top, right), *avd* (bottom, left) and *ard* (bottom, right) for $[\mathcal{U}_{LMH}] = [\mathcal{U}_M]$ (green lines), $[\mathcal{U}_{LMH}] = [\mathcal{U}_L]$ (red lines), $[\mathcal{U}_{LMH}] = [\mathcal{U}_H]$ (cyan lines, but out of range on the figure) and $[\mathcal{U}_{LMH}] = ([\mathcal{U}_L] [\mathcal{U}_M] [\mathcal{U}_H])$ (black lines). Horizontal axis: frequency $\omega/2\pi$ in Hz. Vertical axis: Pressure in dB.

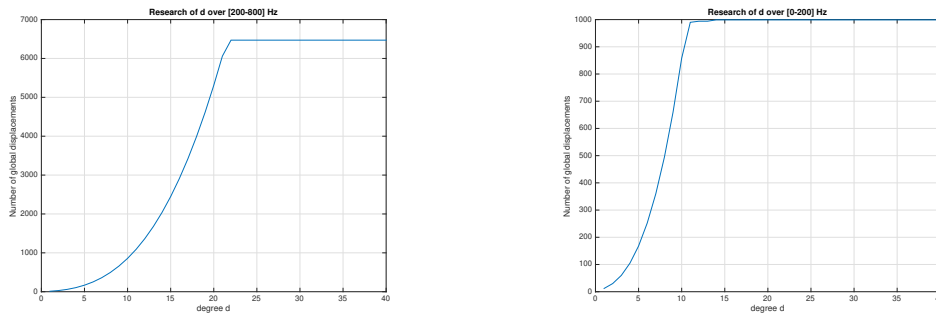


Figure 5.11 – Complexity levels for the case 2. On the left, graph of $d \mapsto \text{conv}_M(d)$. On the right, graph of $d \mapsto \text{conv}_L(d)$. Horizontal axis: polynomial degree d . Vertical axis: Number of columns of matrix $[\mathcal{U}^{\text{low}}]$ for $[\mathcal{U}] = [\Phi_M]$ (on the left) and for $[\mathcal{U}] = [\Phi_M]$ (on the right).

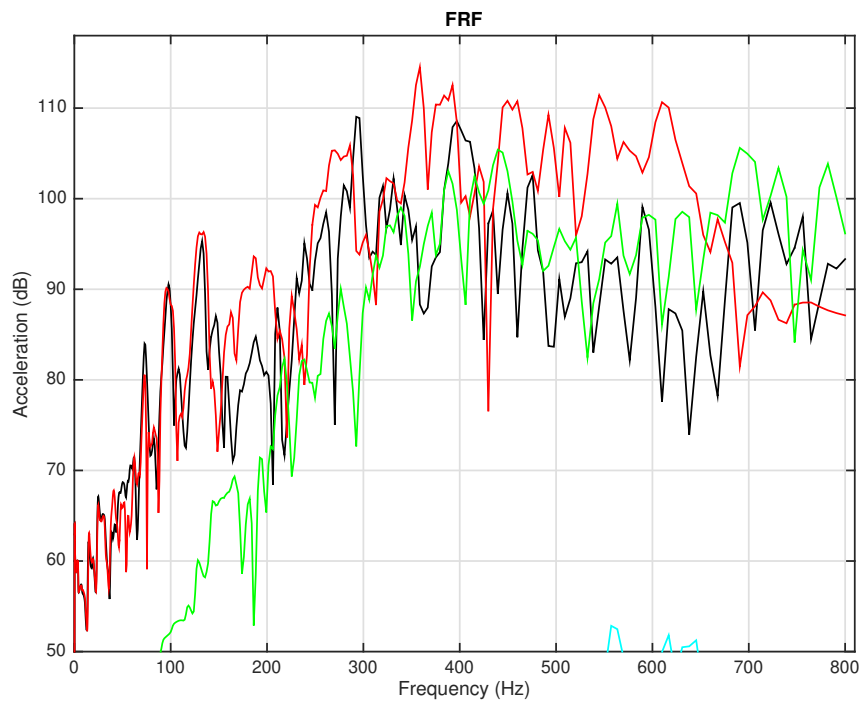


Figure 5.12 – Case 2: FRF for an excitation at point *clvg* in *X*-direction and an observation at point *ccvg* in *X*-direction for $[U_{LMH}] = [U_M]$ (green lines), $[U_{LMH}] = [U_L]$ (red lines), $[U_{LMH}] = [U_H]$ (cyan lines, but out of range on the figure) and $[U_{LMH}] = ([U_L][U_M][U_H])$ (black lines). Horizontal axis: frequency $\omega/2\pi$ in Hz. Vertical axis: Acceleration in dB.

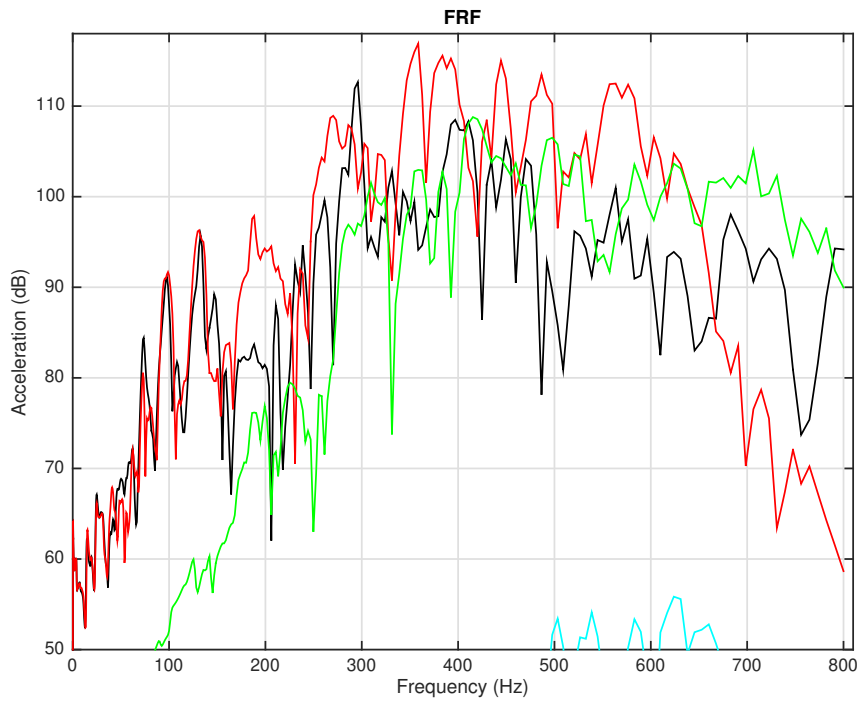


Figure 5.13 – Case 2: FRF for an excitation at point *clvg* in *X*-direction and an observation at point *ccurg* in *X*-direction for $[U_{LMH}] = [U_M]$ (green lines), $[U_{LMH}] = [U_L]$ (red lines), $[U_{LMH}] = [U_H]$ (cyan lines, but out of range on the figure) and $[U_{LMH}] = ([U_L] [U_M] [U_H])$ (black lines). Horizontal axis: frequency $\omega/2\pi$ in Hz. Vertical axis: Acceleration in dB.

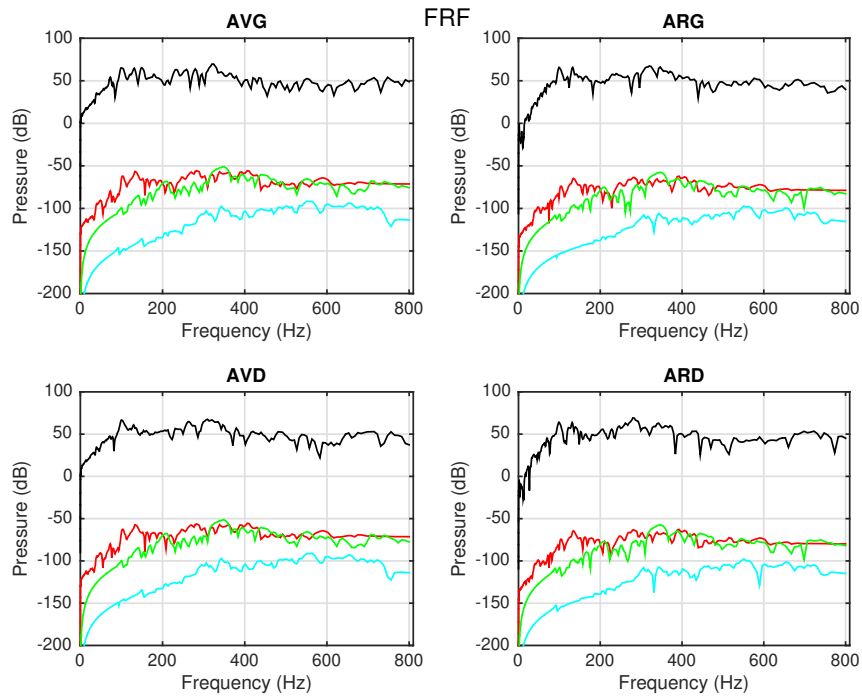


Figure 5.14 – Case 2: FRF for an excitation at point *clvg* in *X*-direction and four observations of pressure (in dB) at points *avg* (top, left), *arg* (top, right), *avd* (bottom, left) and *ard* (bottom, right) for $[\mathbf{U}_{LMH}] = [\mathbf{U}_M]$ (green lines), $[\mathbf{U}_{LMH}] = [\mathbf{U}_L]$ (red lines), $[\mathbf{U}_{LMH}] = [\mathbf{U}_H]$ (cyan lines, but out of range on the figure) and $[\mathbf{U}_{LMH}] = ([\mathbf{U}_L] [\mathbf{U}_M] [\mathbf{U}_H])$ (black lines). Horizontal axis: frequency $\omega/2\pi$ in Hz. Vertical axis: Pressure in dB.

Chapter 6

Stochastic multilevel reduced-order computational model in vibroacoustics

Contents

| | | |
|------------|---|-----------|
| 6.1 | Random matrix theory | 52 |
| 6.2 | Classical nonparametric stochastic reduced-order computational model | 53 |
| 6.3 | Nonparametric stochastic multilevel reduced-order computational model | 54 |
| 6.4 | Numerical applications for the classical nonparametric stochastic reduced-order computational vibroacoustic model | 55 |
| 6.5 | Numerical applications for the nonparametric stochastic multilevel reduced-order computational vibroacoustic model | 56 |
| 6.6 | Case 1: Stochastic multilevel reduced-order model with $\omega_L/2\pi = 30$ Hz | 56 |
| 6.7 | Case 2: Stochastic multilevel reduced-order model with $\omega_L/2\pi = 200$ Hz | 57 |
| 6.8 | Discussions | 59 |

The objective of this chapter is to take into account the model uncertainties induced by the modeling errors by using the nonparametric probabilistic approach and to construct the stochastic multilevel reduced-order computational model in vibroacoustics. The nonparametric probabilistic approach for the model uncertainties (see [114, 14]) consists in directly substituting the matrices of the multilevel reduced-order computational model presented in Chapter 4 by random matrices. The probabilistic model of these random matrices has been constructed by the use of the MaxEnt principle. The hyperparameters of the probabilistic model for each random matrix consist of the mean value of the random matrix and a dispersion coefficient that controls the level of statistical fluctuations, which reflect the level of uncertainties.

6.1 Random matrix theory

In this section, we briefly present important ensembles of random matrices. More details can be found in [114, 14].

6.1.1 Random Matrix Ensemble SG_0^+

This ensemble is the most fundamental set of random matrices that are used in the construction. Let n be any positive integer. A random matrix $[\mathbf{G}_0]$ in SG_0^+ with values in $\mathbb{M}_n^+(\mathbb{R})$ and such that

$$E\{[\mathbf{G}_0]\} = [I_n] \quad , \quad E\{\log(\det([\mathbf{G}_0]))\} = \nu_{\mathbf{G}_0} \quad , \quad |\nu_{\mathbf{G}_0}| < +\infty \quad , \quad (6.1)$$

in which $E\{\cdot\}$ is the mathematical expectation operator, $[I_n]$ is the identity matrix of dimension $n \times n$ and the condition $E\{\log(\det([\mathbf{G}_0]))\} = \nu_{\mathbf{G}_0}$ allows the invertibility and the integration of random inverse matrix $[\mathbf{G}_0]^{-1}$ to be satisfied. The probability density function of random matrix $[\mathbf{G}_0]$ defined on $\mathbb{S}_n = \mathbb{M}_n^+(\mathbb{R})$ is then written as

$$p_{[\mathbf{G}_0]}([G]) = \mathbf{1}_n([G]) \kappa (\det[G])^{(n+1)\frac{1-\delta^2}{2\delta^2}} e^{-\frac{n+1}{2\delta^2}\text{tr}[G]} \quad . \quad (6.2)$$

The normalisation constant κ is defined by

$$\kappa = (2\pi)^{-n(n-1)/4} \left(\frac{n+1}{2\delta^2}\right)^{\frac{n(n+1)}{2\delta^2}} \left(\prod_{j=1}^n \Gamma\left(\frac{n+1}{2\delta^2} + \frac{1-j}{2}\right)\right)^{-1} \quad , \quad (6.3)$$

where, for all $z > 0$, $\Gamma(z) = \int_0^{+\infty} t^{z-1} e^{-t} dt$. Hence, $[\mathbf{G}_0]$ is defined by an unique parameter δ that control the statistical dispersion and with values in $[0, \sqrt{\frac{n+1}{n+5}}]$. This dispersion coefficient is defined as

$$\delta = \left\{ \frac{E\{\|[\mathbf{G}_0] - E\{[\mathbf{G}_0]\}\|_F^2\}}{\|E\{[\mathbf{G}_0]\}\|_F^2} \right\}^{\frac{1}{2}} \quad . \quad (6.4)$$

Since random matrix $[\mathbf{G}_0]$ is almost surely positive definite, then there exists an unique random upper triangular matrix denoted as $[\mathbf{L}]$ that is such that the Cholesky factorization of random matrix $[\mathbf{G}_0]$ is written as

$$[\mathbf{G}_0] = [\mathbf{L}]^T [\mathbf{L}] \quad , \quad \text{almost surely} \quad . \quad (6.5)$$

It is proven that random entries $[\mathbf{L}]_{jj'}$ of random upper triangular matrix $[\mathbf{L}]$ are such that

$$[\mathbf{L}]_{j'j} = \xi V_{j'j} \quad , \quad \text{for } j' < j \leq n \quad , \quad (6.6)$$

$$[\mathbf{L}]_{jj} = \xi \sqrt{2h(\eta_j, V_{jj})} \quad \text{for } j \leq n \quad , \quad (6.7)$$

where $\{V_{j'j}, 1 \leq j' \leq j \leq n\}$ is a set of normalized Gaussian real-valued random variables that are mutually independent. The real-valued parameters ξ and η_j are such that $\xi = \delta(n+1)^{-\frac{1}{2}}$ and $\eta_j = \frac{n+1}{2\delta^2} + \frac{1-j}{2}$. The function h is written as $h(\eta, V) = F_{\Gamma_\eta}^{-1}(F_V(v))$ where F_V is the cumulative distribution function of a normalized Gaussian real-valued random variable V and where F_{Γ_η} is

the cumulative distribution function of the Gamma real-valued random variable Γ_η of parameter η . The independent realizations $[\mathbf{G}_0(\theta_1)], \dots, [\mathbf{G}_0(\theta_{n_R})]$ of random matrix $[\mathbf{G}_0]$ are constructed by using Eqs. (6.5), (6.6) and (6.7) and independent realisations $v_{j'j}(\theta_1), \dots, v_{j'j}(\theta_{n_R})$ of random variable $V_{j'j}$. Consequently, for all $1 \leq r \leq n_R$ and for all $j' < j \leq n$, we have

$$[\mathbf{G}_0(\theta_r)] = [\mathbf{L}(\theta_r)]^T [\mathbf{L}(\theta_r)] \quad , \quad [\mathbf{L}(\theta_r)]_{j'j} = \xi v_{j'j}(\theta_r) \quad , \quad [\mathbf{L}(\theta_r)]_{jj} = \xi \sqrt{2h(\eta_j, v_{jj}(\theta_r))} . \quad (6.8)$$

6.1.2 Ensemble SE^{rect}

Let n and m be any positive integer. Let SE^{rect} be the set of the $\mathbb{M}_{mn}(\mathbb{R})$ -valued second-order random matrix $[\mathbf{A}^{rect}]$. Let $[A^{rect}] = E\{[\mathbf{A}^{rect}]\}$ be the mean value of random matrix $[\mathbf{A}^{rect}]$ for which the null space is assumed to be only the zero vector in \mathbb{R}^n . We then have

$$[A^{rect}] = [U][A] \quad , \quad (6.9)$$

where $[A] \in \mathbb{M}_n^+(\mathbb{R})$ and $[U] \in \mathbb{M}_{mn}(\mathbb{R})$ such that $[U]^T[U] = [I_n]$. Such a factorization can directly be deduced from an SVD of matrix $[A^{rect}]$. The ensemble SE^{rect} is then constructed as the set of the random matrices $[\mathbf{A}^{rect}]$ that are written as

$$[\mathbf{A}^{rect}] = [U][\mathbf{A}] \quad , \quad (6.10)$$

where $[\mathbf{A}]$ is written as $[\mathbf{A}] = [L_A]^T [\mathbf{G}_0] [L_A]$ in which the deterministic upper triangular matrix $[L_A]$ is such that $[L_A]^T [L_A] = [A]$ and where $[\mathbf{G}_0]$ is a random matrix in ensemble SE_0^+ for which the dispersion coefficient is δ_A . The independent realizations $[\mathbf{A}^{rect}(\theta_1)], \dots, [\mathbf{A}^{rect}(\theta_{n_R})]$ of random matrix $[\mathbf{A}^{rect}]$ are constructed by using independent realizations $[\mathbf{G}_0(\theta_1)], \dots, [\mathbf{G}_0(\theta_{n_R})]$ of random matrix $[\mathbf{G}_0] \in \text{SG}_0^+$ and Eq. (6.10),

$$[\mathbf{A}^{rect}(\theta_r)] = [U] [L_A]^T [\mathbf{G}_0(\theta_r)] [L_A] \quad . \quad (6.11)$$

6.2 Classical nonparametric stochastic reduced-order computational model

The classical nonparametric stochastic reduced-order computational model is constructed by substituting the deterministic generalized matrices $[\mathcal{C}_{\text{LM}}]$, $[\mathcal{M}_{\text{LM}}^s]$, $[\mathcal{D}_{\text{LM}}^s]$, and $[\mathcal{K}_{\text{LM}}^s]$ of the reduced-order computational vibroacoustic model presented in Section 2.4.5 by the random matrices $[\mathbf{C}_{\text{LM}}]$, $[\mathbf{M}_{\text{LM}}^s]$, $[\mathbf{D}_{\text{LM}}^s]$, and $[\mathbf{K}_{\text{LM}}^s]$. Note that for such a stochastic computational model, it is assumed that there is no model uncertainties in the acoustic cavity but only on the structure and on its coupling with the acoustic cavity. The classical nonparametric stochastic reduced-order computational model is then written as

$$\begin{pmatrix} -\omega^2[\mathbf{M}_{\text{LM}}^s] + i\omega[\mathbf{D}_{\text{LM}}^s] + [\mathbf{K}_{\text{LM}}^s] & [\mathbf{C}_{\text{LM}}] \\ \omega^2[\mathbf{C}_{\text{LM}}]^T & -\omega^2[\mathcal{M}^f] + i\omega[\mathcal{D}^f] + [\mathcal{K}^f] \end{pmatrix} \begin{pmatrix} \mathbf{Q}^s(\omega) \\ \mathbf{Q}^f(\omega) \end{pmatrix} = \begin{pmatrix} \mathbf{f}_{\text{LM}}^s(\omega) \\ \mathbf{0} \end{pmatrix} \quad , \quad (6.12)$$

in which $\mathbf{Q}^s(\omega)$ is a \mathbb{C}^{n^s} -valued random vector and where $\mathbf{Q}^f(\omega)$ is a \mathbb{C}^{n^f} -valued random vector. The finite element displacement vector $\mathfrak{u}(\omega)$ (resp. the finite-element pressure vector $\mathfrak{p}(\omega)$) is

then replaced by the $\mathbb{C}^{n_{\text{dof}}^{\text{s}}}$ -valued random vector $\mathbf{U}(\omega)$ (resp. the $\mathbb{C}^{n_{\text{dof}}^{\text{f}}}$ -valued random vector $\mathbf{P}(\omega)$), which are such that

$$\mathbf{U}(\omega) = [\Phi_{\text{LM}}^{\text{s}}] \mathbf{Q}^{\text{s}}(\omega) \quad , \quad \mathbf{P}(\omega) = [\Phi^{\text{f}}] \mathbf{Q}^{\text{f}}(\omega) \quad , \quad (6.13)$$

The random matrix $[\mathbf{C}_{\text{LM}}]$ belongs to ensemble SE^{rect} (see Section 6.1.2) with a dispersion coefficient δ denoted by $\delta_{\mathbf{C}_{\text{LM}}}$. Let random matrix $[\mathbf{A}]$ be any of matrices $[\mathcal{M}_{\text{LM}}^{\text{s}}]$, $[\mathcal{D}_{\text{LM}}^{\text{s}}]$, and $[\mathcal{K}_{\text{LM}}^{\text{s}}]$. The Cholesky factorization of matrix $[A] = E\{[\mathbf{A}]\}$ is written as $[A] = [L_A]^T [L_A]$ in which $[L_A]$ is an upper triangular matrix. The probabilistic model of random matrix $[\mathbf{A}]$ is then written as

$$[\mathbf{A}] = [L_A]^T [\mathbf{G}_A] [L_A] \quad , \quad (6.14)$$

where the random matrix $[\mathbf{G}_A]$ is a random matrix belonging to SG_0^+ with a dispersion coefficient δ denoted by δ_A . Consequently, the construction of the stochastic model involves four dispersion coefficients, $\delta_{\mathbf{C}_{\text{LM}}}$, $\delta_{\mathcal{M}_{\text{LM}}^{\text{s}}}$, $\delta_{\mathcal{D}_{\text{LM}}^{\text{s}}}$, and $\delta_{\mathcal{K}_{\text{LM}}^{\text{s}}}$ associated with the probabilistic model of random matrices $[\mathbf{C}_{\text{LM}}]$, $[\mathcal{M}_{\text{LM}}^{\text{s}}]$, $[\mathcal{D}_{\text{LM}}^{\text{s}}]$, and $[\mathcal{K}_{\text{LM}}^{\text{s}}]$.

6.3 Nonparametric stochastic multilevel reduced-order computational model

The nonparametric stochastic multilevel reduced-order computational model is constructed by substituting the deterministic generalized matrices $[C_{\text{LMH}}]$, $[M_{\text{LMH}}^{\text{s}}]$, $[D_{\text{LMH}}^{\text{s}}]$, and $[K_{\text{LMH}}^{\text{s}}]$ of the reduced-order computational vibroacoustic model presented in Section 2.4.5 by random matrices $[\mathbf{C}_{\text{LMH}}]$, $[\mathbf{M}_{\text{LMH}}^{\text{s}}]$, $[\mathbf{D}_{\text{LMH}}^{\text{s}}]$, and $[\mathbf{K}_{\text{LMH}}^{\text{s}}]$. The classical nonparametric stochastic reduced-order computational model is then written as

$$\begin{pmatrix} -\omega^2 [\mathbf{M}_{\text{LMH}}^{\text{s}}] + i\omega [\mathbf{D}_{\text{LMH}}^{\text{s}}] + [\mathbf{K}_{\text{LMH}}^{\text{s}}] & [\mathbf{C}_{\text{LMH}}] \\ \omega^2 [\mathbf{C}_{\text{LMH}}]^T & -\omega^2 [\mathcal{M}^{\text{f}}] + i\omega [\mathcal{D}^{\text{f}}] + [\mathcal{K}^{\text{f}}] \end{pmatrix} \begin{pmatrix} \mathbf{Q}_{\text{LMH}}^{\text{s}}(\omega) \\ \mathbf{Q}^{\text{f}}(\omega) \end{pmatrix} = \begin{pmatrix} \mathbf{f}_{\text{LMH}}^{\text{s}}(\omega) \\ \mathbf{0} \end{pmatrix} \quad , \quad (6.15)$$

in which $\mathbf{Q}_{\text{LMH}}^{\text{s}}(\omega)$ is a $\mathbb{C}^{n_{\text{v}_L} + n_{\text{v}_M} + n_{\text{v}_H}}$ -valued random vector and where $\mathbf{Q}^{\text{f}}(\omega)$ is a $\mathbb{C}^{n^{\text{f}}}$ -valued random vector $\mathbf{Q}^{\text{f}}(\omega)$. Again, note that for such a stochastic computational model, it is assumed that there is no modeling uncertainties on the acoustic cavity but only on the structure and its coupling with the acoustic cavity. The finite element displacement vector $\mathbf{u}(\omega)$ (resp. the finite-element pressure vector $\mathbf{p}(\omega)$) is then replaced by the $\mathbb{C}^{n_{\text{dof}}^{\text{s}}}$ -valued random vector $\mathbf{U}(\omega)$ (resp. the $\mathbb{C}^{n_{\text{dof}}^{\text{f}}}$ -valued random vector $\mathbf{P}(\omega)$) written as

$$\mathbf{U}(\omega) = [\mathbf{U}_{\text{LMH}}] \mathbf{Q}_{\text{LMH}}^{\text{s}}(\omega) \quad , \quad \mathbf{P}(\omega) = [\Phi^{\text{f}}] \mathbf{Q}^{\text{f}}(\omega) \quad . \quad (6.16)$$

Concerning the probabilistic models of $[\mathbf{C}_{\text{LMH}}]$, $[\mathbf{M}_{\text{LMH}}^{\text{s}}]$, $[\mathbf{D}_{\text{LMH}}^{\text{s}}]$, and $[\mathbf{K}_{\text{LMH}}^{\text{s}}]$, a naive approach would consist in substituting matrices $[\mathcal{C}_{\text{LM}}]$, $[\mathcal{M}_{\text{LM}}^{\text{s}}]$, $[\mathcal{D}_{\text{LM}}^{\text{s}}]$, and $[\mathcal{K}_{\text{LM}}^{\text{s}}]$ in the expressions of matrices $[C_{\text{LMH}}]$, $[M_{\text{LMH}}^{\text{s}}]$, $[D_{\text{LMH}}^{\text{s}}]$, and $[K_{\text{LMH}}^{\text{s}}]$ given by Eqs. (4.21) to (4.24) by the random matrices $[\mathbf{C}_{\text{LM}}]$, $[\mathcal{M}_{\text{LM}}^{\text{s}}]$, $[\mathcal{D}_{\text{LM}}^{\text{s}}]$, and $[\mathcal{K}_{\text{LM}}^{\text{s}}]$ that have been introduced in Section 6.2. Nevertheless, such a probabilistic model would be exactly the same as for the probabilistic model in

Section 6.2 and consequently, it would not be interesting. Hereinafter, the probabilistic model for $[\mathbf{C}_{\text{LMH}}]$, $[\mathbf{M}_{\text{LMH}}^s]$, $[\mathbf{D}_{\text{LMH}}^s]$, and $[\mathbf{K}_{\text{LMH}}^s]$, which is different from the probabilistic model in Section 6.2 is presented. Concerning the random matrix $[\mathbf{C}_{\text{LMH}}]$, the probabilistic model is constructed by substituting matrix $[\mathcal{C}_{\text{LM}}]$ in Eq. (4.24) by random matrix $[\mathbf{C}_{\text{LM}}]$ that has been introduced in Section 6.2. We then have

$$[\mathbf{C}_{\text{LMH}}] = [\mathbf{Q}_{\text{LMH}}]^T [\mathbf{C}_{\text{LM}}] \quad . \quad (6.17)$$

Furthermore, let random matrix $[\mathbf{A}]$ be any of $[\mathbf{M}_{\text{LMH}}^s]$, $[\mathbf{D}_{\text{LMH}}^s]$, and $[\mathbf{K}_{\text{LMH}}^s]$. The Cholesky factorization of matrix $[A] = E\{[\mathbf{A}]\}$ is written as $[A] = [L_A]^T [L_A]$ in which $[L_A]$ is an upper triangular matrix. The probabilistic model of random matrix $[\mathbf{A}]$ is then written as

$$[\mathbf{A}] = [L_A]^T [\mathbf{G}_A] [L_A] \quad , \quad (6.18)$$

where the random matrix $[\mathbf{G}_A]$ is written as

$$[\mathbf{G}_A] = \begin{bmatrix} [\mathbf{G}_{\text{L},A}] & [0] & [0] \\ [0] & [\mathbf{G}_{\text{M},A}] & [0] \\ [0] & [0] & [\mathbf{G}_{\text{H},A}] \end{bmatrix} \quad , \quad (6.19)$$

in which the random matrices $[\mathbf{G}_{\text{L},A}]$, $[\mathbf{G}_{\text{M},A}]$, and $[\mathbf{G}_{\text{H},A}]$ belong to ensemble SG_0^+ with dimension $n_{\text{U}_L} \times n_{\text{U}_L}$, $n_{\text{U}_M} \times n_{\text{U}_M}$, and $n_{\text{U}_H} \times n_{\text{U}_H}$, and with dispersion coefficients $\delta_{\text{L},A}$, $\delta_{\text{M},A}$, and $\delta_{\text{H},A}$. Consequently, the construction of the nonparametric stochastic multilevel reduced-order computational model involves ten dispersion coefficients: $\delta_{\mathcal{C}_{\text{LMH}}}$ for $[\mathbf{C}_{\text{LMH}}]$; $\delta_{\text{L},\mathbf{M}_{\text{LMH}}^s}$, $\delta_{\text{M},\mathbf{M}_{\text{LMH}}^s}$, $\delta_{\text{H},\mathbf{M}_{\text{LMH}}^s}$ for $[\mathbf{M}_{\text{LMH}}^s]$; $\delta_{\text{L},\mathbf{D}_{\text{LMH}}^s}$, $\delta_{\text{M},\mathbf{D}_{\text{LMH}}^s}$, $\delta_{\text{H},\mathbf{D}_{\text{LMH}}^s}$ for $[\mathbf{D}_{\text{LMH}}^s]$; and $\delta_{\text{L},\mathbf{K}_{\text{LMH}}^s}$, $\delta_{\text{M},\mathbf{K}_{\text{LMH}}^s}$, $\delta_{\text{H},\mathbf{K}_{\text{LMH}}^s}$ for $[\mathbf{K}_{\text{LMH}}^s]$.

6.4 Numerical applications for the classical nonparametric stochastic reduced-order computational vibroacoustic model

We present an application of the classical nonparametric stochastic reduced-order computational vibroacoustic model to quantify the uncertainties related to the FRF due to mode uncertainties. The Monte Carlo numerical method is used as the stochastic solver of the stochastic computational model in order to quantify the model uncertainty on a random FRF for an excitation in X -direction at point clvd and for an observation in X -direction at point ccurg with $\delta_{\mathcal{C}_{\text{LM}}} = 0.4$, $\delta_{\mathcal{M}_{\text{LM}}^s} = \delta_{\mathcal{D}_{\text{LM}}^s} = \delta_{\mathcal{K}_{\text{LM}}^s} = 0.3$. The number of realizations is 46 and there are 200 frequency points distributed in \log_{10} -scale between 20 Hz and 200 Hz. The relatively low value of the number of realizations was chosen to minimize the CPU time. It allows to preserve qualitatively and quantitatively the stochastic results. The main influence is a relative poor approximation of the lower envelopes of the confidence domains, which would be smoother with a greater number of realizations. Figure 6.1 presents the results: the confidence region for a probability level of 95% is shown (yellow), the nominal FRF calculated by the deterministic computational model (blue), and the statistical mean value (red). Figure 6.2 presents the results of the vibroacoustic FRF: the confidence region for a probability level of 95% is shown (yellow), the nominal FRF calculated by the deterministic computational model (black), and the statistical mean value (red).

6.5 Numerical applications for the nonparametric stochastic multilevel reduced-order computational vibroacoustic model

We present the uncertainty quantification on some FRF for the structure and for the acoustic cavity, due to model uncertainties, by using the nonparametric stochastic multilevel reduced-order computational model. Since two cases have been considered into Chapter 5, for $\omega_L/2\pi = 30$ Hz and for $\omega_L/2\pi = 200$ Hz, then two cases will be presented again. Similarly to the classical nonparametric stochastic ROM, all the results presented in this section have been obtained by using 46 realizations and 200 frequency points distributed in \log_{10} -scale between 20 Hz and 200 Hz. We recall that this relatively low value of the number of realizations was chosen to minimize the CPU time and allows us to preserve qualitatively and quantitatively the stochastic results (the main influence is a relative poor approximation of the lower envelopes of the confidence domains, which would be smoother with a greater number of realizations).

6.6 Case 1: Stochastic multilevel reduced-order model with $\omega_L/2\pi = 30$ Hz

Case 1 corresponds to $\omega_L/2\pi = 30$ Hz. We consider several random FRFs for an excitation in X -direction at points clvd and clvg, for observations in X -direction at points ccurg and ccuvrg, with $\delta_{\mathcal{C}_{\text{LMH}}} = 0.4$ for all the calculations performed in this case 1, and for several set of values of $\delta_{\mathcal{M}_{\text{LMH}}^s}$, $\delta_{\mathcal{D}_{\text{LMH}}^s}$, $\delta_{\mathcal{K}_{\text{LMH}}^s}$. The first set of values for the dispersion coefficients corresponds to higher statistical fluctuations on the block matrix that corresponds to $[\mathcal{U}_L]$ and smaller statistical fluctuations on the block matrices that correspond to $[\mathcal{U}_M]$ and $[\mathcal{U}_H]$. Figure 6.3 presents the confidence region for a probability level of 95% (yellow), the nominal FRF calculated by the deterministic computational model (blue), and the statistical mean value (red) for $\delta_{L,\mathcal{K}_{\text{LMH}}^s} = 0.25$, $\delta_{L,\mathcal{D}_{\text{LMH}}^s} = \delta_{L,\mathcal{M}_{\text{LMH}}^s} = 0.3$, and $\delta_{M,\mathcal{K}_{\text{LMH}}^s} = \delta_{H,\mathcal{K}_{\text{LMH}}^s} = \delta_{M,\mathcal{D}_{\text{LMH}}^s} = \delta_{H,\mathcal{D}_{\text{LMH}}^s} = \delta_{M,\mathcal{M}_{\text{LMH}}^s} = \delta_{H,\mathcal{M}_{\text{LMH}}^s} = 0.05$ for several FRFs. Figure 6.7 presents the confidence region for a probability level of 95% (yellow), the nominal FRF calculated by the deterministic vibroacoustic computational model (black), and the statistical mean value (red) for $\delta_{L,\mathcal{K}_{\text{LMH}}^s} = 0.25$, $\delta_{L,\mathcal{D}_{\text{LMH}}^s} = \delta_{L,\mathcal{M}_{\text{LMH}}^s} = 0.3$, and $\delta_{M,\mathcal{K}_{\text{LMH}}^s} = \delta_{H,\mathcal{K}_{\text{LMH}}^s} = \delta_{M,\mathcal{D}_{\text{LMH}}^s} = \delta_{H,\mathcal{D}_{\text{LMH}}^s} = \delta_{M,\mathcal{M}_{\text{LMH}}^s} = \delta_{H,\mathcal{M}_{\text{LMH}}^s} = 0.05$ for the excitation point clvg and the observation points (AVG, AVD, ARG and ARD). The excitation is in X -direction at point clvd (upper figures) and at point clrg (bottom figures). The observation is in X -direction at point ccuvrg (figures on the left) and at point ccurg (figures).

The next set of values for the dispersion coefficients corresponds to higher statistical fluctuations on the block matrix that corresponds to $[\mathcal{U}_M]$ and smaller statistical fluctuations on the block matrices that correspond to $[\mathcal{U}_L]$ and $[\mathcal{U}_H]$. Fig. 6.4 presents the confidence region for a probability level of 95% (yellow), the nominal FRF calculated by the deterministic computational model (blue), and the statistical mean value (red) for $\delta_{M,\mathcal{K}_{\text{LMH}}^s} = 0.25$, $\delta_{M,\mathcal{D}_{\text{LMH}}^s} = 0.3$,

$\delta_{M,\mathcal{M}_{LMH}^s} = 0.3$, and $\delta_{L,\mathcal{K}_{LMH}^s} = \delta_{H,\mathcal{K}_{LMH}^s} = \delta_{L,\mathcal{D}_{LMH}^s} = \delta_{H,\mathcal{D}_{LMH}^s} = \delta_{L,\mathcal{M}_{LMH}^s} = \delta_{H,\mathcal{M}_{LMH}^s} = 0.05$ for several FRFs. Figure 6.8 presents the confidence region for a probability level of 95% (yellow), the nominal FRF calculated by the deterministic vibroracoustic computational model (black), and the statistical mean value (red) for $\delta_{M,\mathcal{K}_{LMH}^s} = 0.25$, $\delta_{M,\mathcal{D}_{LMH}^s} = 0.3$, $\delta_{M,\mathcal{M}_{LMH}^s} = 0.3$, and $\delta_{L,\mathcal{K}_{LMH}^s} = \delta_{H,\mathcal{K}_{LMH}^s} = \delta_{L,\mathcal{D}_{LMH}^s} = \delta_{H,\mathcal{D}_{LMH}^s} = \delta_{L,\mathcal{M}_{LMH}^s} = \delta_{H,\mathcal{M}_{LMH}^s} = 0.05$ for the excitation point clvg and the observation points (AVG, AVD, ARG and ARD). The excitation is in X -direction at point clvd (upper figures) and at point clrg (bottom figures). The observation is in X -direction at point ccvug (figures on the left) and at point ccurg (figures on the right).

The next set of values for the dispersion coefficients correspond to higher statistical fluctuations on the block matrix that corresponds to $[U_H]$ and smaller statistical fluctuations on the block matrices that correspond to $[U_L]$ and $[U_M]$. Fig. 6.5 presents the confidence region for a probability level of 95% (yellow), the nominal FRF calculated by the deterministic computational model (blue), and the statistical mean value (red) for $\delta_{H,\mathcal{K}_{LMH}^s} = 0.25$, $\delta_{H,\mathcal{D}_{LMH}^s} = 0.3$, $\delta_{H,\mathcal{M}_{LMH}^s} = 0.3$, and $\delta_{L,\mathcal{K}_{LMH}^s} = \delta_{H,\mathcal{K}_{LMH}^s} = \delta_{L,\mathcal{D}_{LMH}^s} = \delta_{M,\mathcal{D}_{LMH}^s} = \delta_{L,\mathcal{M}_{LMH}^s} = \delta_{M,\mathcal{M}_{LMH}^s} = 0.05$ for several FRFs. Figure 6.9 presents the confidence region for a probability level of 95% (yellow), the nominal FRF calculated by the deterministic vibroracoustic computational model (black), and the statistical mean value (red) for $\delta_{H,\mathcal{K}_{LMH}^s} = 0.25$, $\delta_{H,\mathcal{D}_{LMH}^s} = 0.3$, $\delta_{H,\mathcal{M}_{LMH}^s} = 0.3$, and $\delta_{L,\mathcal{K}_{LMH}^s} = \delta_{H,\mathcal{K}_{LMH}^s} = \delta_{L,\mathcal{D}_{LMH}^s} = \delta_{M,\mathcal{D}_{LMH}^s} = \delta_{L,\mathcal{M}_{LMH}^s} = \delta_{M,\mathcal{M}_{LMH}^s} = 0.05$ for the excitation point clvg and the observation points (AVG, AVD, ARG and ARD). The excitation is in X -direction at point clvd (upper figures) and at point clrg (bottom figures). The observation is in X -direction at point ccvug (figures on the left) and at point ccurg (figures on the right).

The next set of values for the dispersion coefficients correspond to higher statistical fluctuations on every block matrices that correspond to $[U_L]$, $[U_M]$, and $[U_H]$. Fig. 6.6 presents the confidence region for a probability level of 95% (yellow), the nominal FRF calculated by the deterministic computational model (blue), and the statistical mean value (red) for $\delta_{L,\mathcal{K}_{LMH}^s} = \delta_{M,\mathcal{K}_{LMH}^s} = \delta_{H,\mathcal{K}_{LMH}^s} = 0.25$, $\delta_{L,\mathcal{D}_{LMH}^s} = \delta_{M,\mathcal{D}_{LMH}^s} = \delta_{H,\mathcal{D}_{LMH}^s} = 0.3$, and $\delta_{L,\mathcal{M}_{LMH}^s} = \delta_{M,\mathcal{M}_{LMH}^s} = \delta_{H,\mathcal{M}_{LMH}^s} = 0.3$ for several FRFs. The excitation is in X -direction at point clvd (upper figures) and at point clrg (bottom figures). The observation is into X -direction at point ccvug (figures on the left) and at point ccurg (figures on the right).

6.7 Case 2: Stochastic multilevel reduced-order model with $\omega_L/2\pi = 200$ Hz

Case 2 corresponds to $\omega_L/2\pi = 200$ Hz. Several random FRFs are analyzed for an excitation in X -direction at points clvd and clvg, for observations in X -direction at points ccurg and ccvug, with $\delta_{\mathcal{C}_{LMH}} = 0.4$ for all the calculations performed in this case 2, and for several set of values of $\delta_{\mathcal{M}_{LMH}^s}$, $\delta_{\mathcal{D}_{LMH}^s}$, $\delta_{\mathcal{K}_{LMH}^s}$. The first set of values for the dispersion coefficients corresponds to higher

statistical fluctuations on the block matrix that corresponds to $[\mathcal{U}_L]$ and smaller statistical fluctuations on the block matrices that correspond to $[\mathcal{U}_M]$ and $[\mathcal{U}_H]$. Fig. 6.10 presents the confidence region for a probability level of 95% (yellow), the nominal FRF calculated by the deterministic computational model (blue), and the statistical mean value (red) for $\delta_L, \mathcal{K}_{LMH}^s = 0.25$, $\delta_L, \mathcal{D}_{LMH}^s = \delta_L, \mathcal{M}_{LMH}^s = 0.3$, and $\delta_M, \mathcal{K}_{LMH}^s = \delta_H, \mathcal{K}_{LMH}^s = \delta_M, \mathcal{D}_{LMH}^s = \delta_H, \mathcal{D}_{LMH}^s = \delta_M, \mathcal{M}_{LMH}^s = \delta_H, \mathcal{M}_{LMH}^s = 0.05$ for several FRFs. Figure 6.14 presents the confidence region for a probability level of 95% (yellow), the nominal FRF calculated by the deterministic vibroacoustic computational model (black), and the statistical mean value (red) for $\delta_L, \mathcal{K}_{LMH}^s = 0.25$, $\delta_L, \mathcal{D}_{LMH}^s = \delta_L, \mathcal{M}_{LMH}^s = 0.3$, and $\delta_M, \mathcal{K}_{LMH}^s = \delta_H, \mathcal{K}_{LMH}^s = \delta_M, \mathcal{D}_{LMH}^s = \delta_H, \mathcal{D}_{LMH}^s = \delta_M, \mathcal{M}_{LMH}^s = \delta_H, \mathcal{M}_{LMH}^s = 0.05$ for the excitation point clvg and the observation points (AVG, AVD, ARG and ARD). The excitation is in X -direction at point clvd (upper figures) and at point clrg (bottom figures). The observation is in X -direction at point ccvug (figures on the left) and at point ccurg (figures on the right).

The next set of values for the dispersion coefficients corresponds to higher statistical fluctuations on the block matrix that corresponds to $[\mathcal{U}_M]$ and smaller statistical fluctuations on the block matrices that correspond to $[\mathcal{U}_L]$ and $[\mathcal{U}_H]$. Fig. 6.11 presents the confidence region for a probability level of 95% (yellow), the nominal FRF calculated by the deterministic computational model (blue), and the statistical mean value (red) for $\delta_M, \mathcal{K}_{LMH}^s = 0.25$, $\delta_M, \mathcal{D}_{LMH}^s = 0.3$, $\delta_M, \mathcal{M}_{LMH}^s = 0.3$, and $\delta_L, \mathcal{K}_{LMH}^s = \delta_H, \mathcal{K}_{LMH}^s = \delta_L, \mathcal{D}_{LMH}^s = \delta_H, \mathcal{D}_{LMH}^s = \delta_L, \mathcal{M}_{LMH}^s = \delta_H, \mathcal{M}_{LMH}^s = 0.05$ for several FRFs. Figure 6.15 presents the confidence region for a probability level of 95% (yellow), the nominal FRF calculated by the deterministic vibroacoustic computational model (black), and the statistical mean value (red) for $\delta_M, \mathcal{K}_{LMH}^s = 0.25$, $\delta_M, \mathcal{D}_{LMH}^s = 0.3$, $\delta_M, \mathcal{M}_{LMH}^s = 0.3$, and $\delta_L, \mathcal{K}_{LMH}^s = \delta_H, \mathcal{K}_{LMH}^s = \delta_L, \mathcal{D}_{LMH}^s = \delta_H, \mathcal{D}_{LMH}^s = \delta_L, \mathcal{M}_{LMH}^s = \delta_H, \mathcal{M}_{LMH}^s = 0.05$ for the excitation point clvg and the observation points (AVG, AVD, ARG and ARD). The excitation is in X -direction at point clvd (upper figures) and at point clrg (bottom figures). The observation is in X -direction at point ccvug (figures on the left) and at point ccurg (figures on the right).

The next set of values for the dispersion coefficients corresponds to higher statistical fluctuations on the block matrix that corresponds to $[\mathcal{U}_H]$ and smaller statistical fluctuations on the block matrices that correspond to $[\mathcal{U}_L]$ and $[\mathcal{U}_M]$. Fig. 6.12 presents the confidence region for a probability level of 95% (yellow), the nominal FRF calculated by the deterministic computational model (blue), and the statistical mean value (red) for $\delta_H, \mathcal{K}_{LMH}^s = 0.25$, $\delta_H, \mathcal{D}_{LMH}^s = 0.3$, $\delta_H, \mathcal{M}_{LMH}^s = 0.3$, and $\delta_L, \mathcal{K}_{LMH}^s = \delta_H, \mathcal{K}_{LMH}^s = \delta_L, \mathcal{D}_{LMH}^s = \delta_M, \mathcal{D}_{LMH}^s = \delta_L, \mathcal{M}_{LMH}^s = \delta_M, \mathcal{M}_{LMH}^s = 0.05$ for several FRFs. Figure 6.16 presents the confidence region for a probability level of 95% (yellow), the nominal FRF calculated by the deterministic vibroacoustic computational model (black), and the statistical mean value (red) for $\delta_H, \mathcal{K}_{LMH}^s = 0.25$, $\delta_H, \mathcal{D}_{LMH}^s = 0.3$, $\delta_H, \mathcal{M}_{LMH}^s = 0.3$, and $\delta_L, \mathcal{K}_{LMH}^s = \delta_H, \mathcal{K}_{LMH}^s = \delta_L, \mathcal{D}_{LMH}^s = \delta_M, \mathcal{D}_{LMH}^s = \delta_L, \mathcal{M}_{LMH}^s = \delta_M, \mathcal{M}_{LMH}^s = 0.05$ for the excitation point clvg and the observation points (AVG, AVD, ARG and ARD). The excitation is in X -direction at point clvd (upper figures) and on point clrg (bottom figures). The observation is in X -direction at point ccvug (figures on the left) and at point ccurg (figures on the right).

The next set of values for the dispersion coefficients corresponds to higher statistical fluctuations on every block matrices that correspond to $[\mathcal{U}_L]$, $[\mathcal{U}_M]$, and $[\mathcal{U}_H]$. Fig. 6.13 presents the confidence region for a probability level of 95% (yellow), the nominal FRF calculated by the deterministic computational model (blue), and the statistical mean value (red) for $\delta_{L,\mathcal{K}_{LMH}^s} = \delta_{M,\mathcal{K}_{LMH}^s} = \delta_{H,\mathcal{K}_{LMH}^s} = 0.25$, $\delta_{L,\mathcal{D}_{LMH}^s} = \delta_{M,\mathcal{D}_{LMH}^s} = \delta_{H,\mathcal{D}_{LMH}^s} = 0.3$, and $\delta_{L,\mathcal{M}_{LMH}^s} = \delta_{M,\mathcal{M}_{LMH}^s} = \delta_{H,\mathcal{M}_{LMH}^s} = 0.3$ for several FRFs. The excitation is in X -direction at point clvd (upper figures) and at point clrg (bottom figures). The observation is in X -direction at point ccvvg (figures on the left) and at point ccurg (figures).

6.8 Discussions

In this section, we discuss about all the results presented in this chapter. The comments given below mainly concern the interpretation for all the results shown in Figs. 6.1 to 6.16.

It should be noted that the terminology "reference", which is sometimes used, corresponds to the "nominal configuration" (or also "mean configuration") of the vibroacoustic system. Then a reference FRF is a nominal FRF calculated by the deterministic computational vibroacoustic model. As a consequence, the value of a nominal FRF at a given frequency (blue for an acceleration output and black for a pressure output) may or may not belong to the confidence region (yellow) calculated with the classical nonparametric stochastic reduced-order computational model or with the nonparametric stochastic multilevel reduced-order computational model. Unfortunately, experimental measurements are not available for this vibroacoustic system allowing a direct validation.

The Nastran software was used with available computation servers, to compute the elastic eigenmodes and the acoustic modes, and to compute and export the generalized matrices of the vibroacoustic system, in particular the generalized full coupling matrix between the structure and the acoustic cavity. Taking into account the very large dimension of the computational vibroacoustic model, it has not been possible to do in one run, for all the frequency band of analysis (which would have made it possible to export the generalized full matrix of coupling), but had to be made frequency sub-band by sub-band. In this case, for a given sub-band, Nastran generates only the diagonal block of the generalized coupling matrix for the elastic modes and the acoustic modes that belong to this sub-band. Thus, it is not possible to obtain the full generalized coupling matrix for the entire band of analysis, but only the diagonal blocks, the extra-diagonal blocks then being zero, which is not correct. Under these conditions, the prediction of the acoustic response of the vibroacoustic system is an approximation whose level of approximation cannot be evaluated given the size of the problem. On the other hand, to test and validate the methodology and algorithms, the nonparametric probabilistic model of uncertainties has been developed in the general framework, which means that the random matrix germs are full as the theory of random matrices specifies for the ensembles of random matrices considered. However, as we have just

explained the generalized matrix of coupling of the nominal model, which should be full (taking into account of all the couplings between the structural and acoustic modes), is not and presents many extradiagonal blocks, which are zero matrices. The construction of the random matrices associated with this generalized coupling matrix of the nominal model, therefore substitutes the zero blocks of this nominal matrix by non-zero random blocks. Therefore, for the prediction of acoustic responses, the level of approximation used, between the nominal vibroacoustic model and the classical or multilevel nonparametric stochastic model, is not exactly the same. This could induce an additional small error in the interpretation of the acoustic results of the vibroacoustic system when comparing the acoustic response of the nominal system with the acoustic response of the classical or multilevel stochastic system. Despite these approximations, the errors induced remain low and do not modify quantitatively the results presented, both for the structural FRFs and for the acoustic FRFs.

In accordance with what we indicate in the perspectives of the chapter of conclusions, a necessary development would be to obtain the complete vibroacoustic coupling matrix and to see what is its influence on the vibroacoustic FRF. It should be noted that such a development is directly linked to the possibilities of the commercial software, here Nastran, used and not to the developments, strictly speaking, of the proposed method.

In the light of the comments, which have just been made, the results obtained are consistent and are the expected results. The stochastic multilevel ROM takes better into account the uncertainties as a function of the LF and MF frequency bands than the classical stochastic ROM.

An analysis of all the Figures (from Figs. 6.1 to 6.16) clearly shows that, the same conclusion can be made for the structural FRFs and the acoustic FRFs. From this point on, we will no longer differentiate between the acoustic and structural FRFs.

For each studied case, four different sets of dispersion coefficients (that is to say of uncertainty level) are used for the three complexity levels L, M, and H (see Chapter 4). A comparison of each set for each one of the two cases is done below.

The first set that features high level uncertainties for the L complexity level and low uncertainties for the M and H complexity levels can be seen in Figs. 6.3 and 6.7 for case 1, and in Figs. 6.10 and 6.14 for case 2. The first observation is that the confidence region is narrower for case 1 for all presented excitations and observations points, and the statistical mean is closer to the nominal response.

The results for the second set, which presents a high level of uncertainty for the M complexity level and a low level of uncertainty for the L and H complexity levels, are given in Figs. 6.4 and 6.8 for case 1, and in Figs. 6.11 and 6.15 for case 2. Case 2 yields a narrower confidence region than case 1. Also, the statistical mean is slightly closer to the nominal response for case 2. This

set of the uncertainties level gives narrow confidence regions in the LF band, which increase with the frequency.

The results for the third set, which deals with a high level of uncertainty for the H complexity level and a low level of uncertainty for the M and L complexity levels, are given in Figs. 6.5 and 6.9 for case 1, and in Figs. 6.12 and 6.16 for case 2. A quick observation shows that the results are really similar. Indeed, the thickness of the confidence region as well as the position of the statistical mean are nearly identical for cases 1 and 2. This attribution of the uncertainty level yields a very thin confidence region that grows with the frequency.

The structural FRFs for the last set, which introduces a high level of uncertainty for the three levels of complexity, L, M, and H, are shown in Figs. 6.6 for case 1 and in Figs. 6.13 for case 2. As observed for the third set, the similarities between the two cases are high (this is the reason why the acoustic FRFs are not shown for this set).

The main conclusion is the following concerning the stochastic multilevel ROM that is better than the classical stochastic ROM. First of all the robustness with regard to uncertainty level does not depend solely on the choice of the polynomial degrees but also of the three complexity levels. Finally, it is well known that MF domain is sensitive to uncertainties unlike the LF domain that has very little sensitivity to model uncertainties. It is therefore consistent in the multilevel method to consider a significant level of uncertainties for the M complexity levels (see the notion of complexity level in Chapter 4) and a very low level of uncertainty for the L complexity level. This situation corresponds to the second set of values for the coefficients of dispersion for which the results are given in Figs. 6.4 and 6.8 for case 1 and in Figs. 6.11 and 6.15 for case 2. We see by comparing case 1 and case 2 for this set of values of the coefficients of dispersion, that case 2 gives a better result in terms of taking into account of the uncertainties as a function of the frequency. This result is consistent with the fact that the value of $\omega_L/2\pi = 200$ Hz for case 2 gives a better separation of the 3 complexity levels: L, M, and H (see Chapter 4).

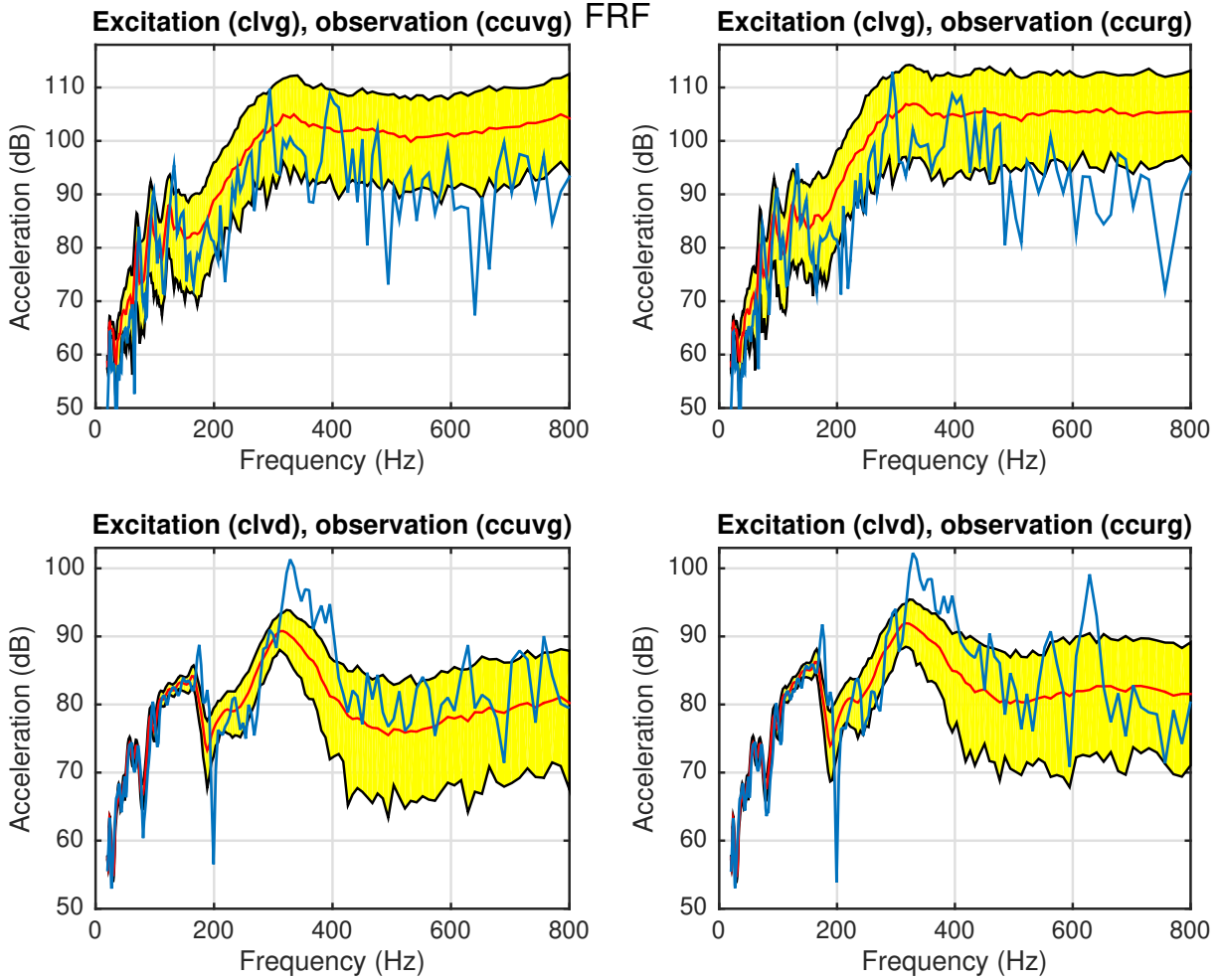


Figure 6.1 – Structural FRF estimated with the classical stochastic ROM in vibroacoustics for an excitation in X -direction at point $clvd$ and for an observation in X -direction at point $ccurg$ with $\delta_{\mathbf{c}_{LM}} = 0.4$, $\delta_{\mathbf{M}_{LM}^s} = \delta_{\mathbf{D}_{LM}^s} = \delta_{\mathbf{K}_{LM}^s} = 0.3$. Confidence region corresponding to a probability level of 95% (yellow), nominal (blue), and statistical mean value (red). In the upper part, the excitation point is $clvg$. In the lower part, the excitation point is $clvd$ while the observation points are $ccvug$ (on the left) and $ccurg$ (on the right). Horizontal axis: frequency $\omega/2\pi$ in Hz. Vertical axis: Acceleration in dB.

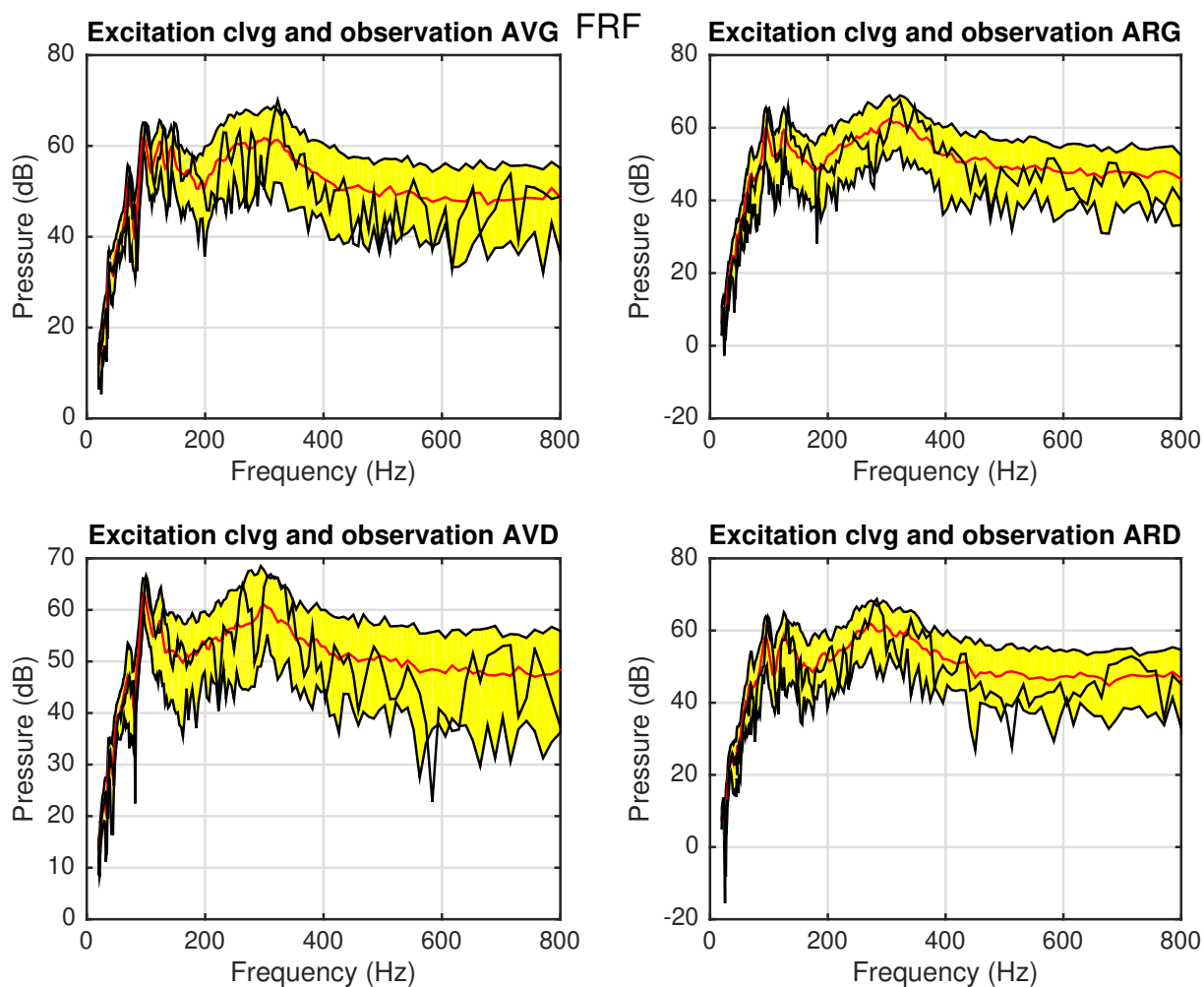


Figure 6.2 – Acoustic FRF estimated with the classical stochastic ROM in vibroacoustics for an excitation in X -direction at point $clvg$ with $\delta\mathbf{c}_{LM} = 0.4$, $\delta\mathbf{M}_{LM}^s = \delta\mathbf{D}_{LM}^s = \delta\mathbf{K}_{LM}^s = 0.3$. Confidence region corresponding to a probability level of 95% (yellow), nominal (black), and statistical mean value (red). The excitation point is always the same point noted $clvg$ and the observation points are the hearing points (AVG, AVD, ARG, and ARD). Horizontal axis: frequency $\omega/2\pi$ in Hz. Vertical axis: Pressure in dB.

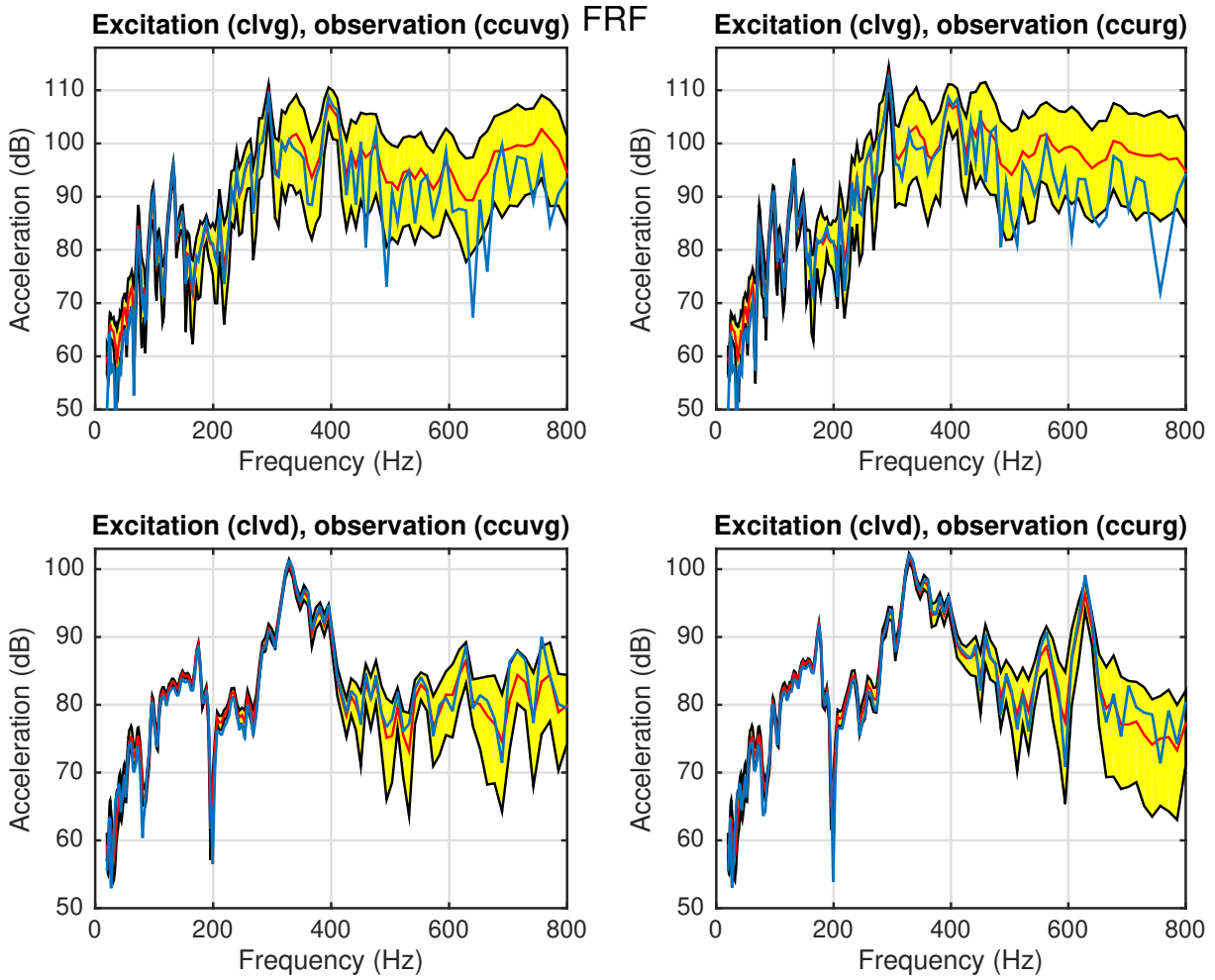


Figure 6.3 – Case 1, structural FRF for $\delta_{L,\mathcal{K}_{LMH}^s} = 0.25$, $\delta_{L,\mathcal{D}_{LMH}^s} = \delta_{L,\mathcal{M}_{LMH}^s} = 0.3$, and $\delta_{M,\mathcal{K}_{LMH}^s} = \delta_{H,\mathcal{K}_{LMH}^s} = \delta_{M,\mathcal{D}_{LMH}^s} = \delta_{H,\mathcal{D}_{LMH}^s} = \delta_{M,\mathcal{M}_{LMH}^s} = \delta_{H,\mathcal{M}_{LMH}^s} = 0.05$: Confidence region 95% (yellow), nominal (blue), and statistical mean (red).

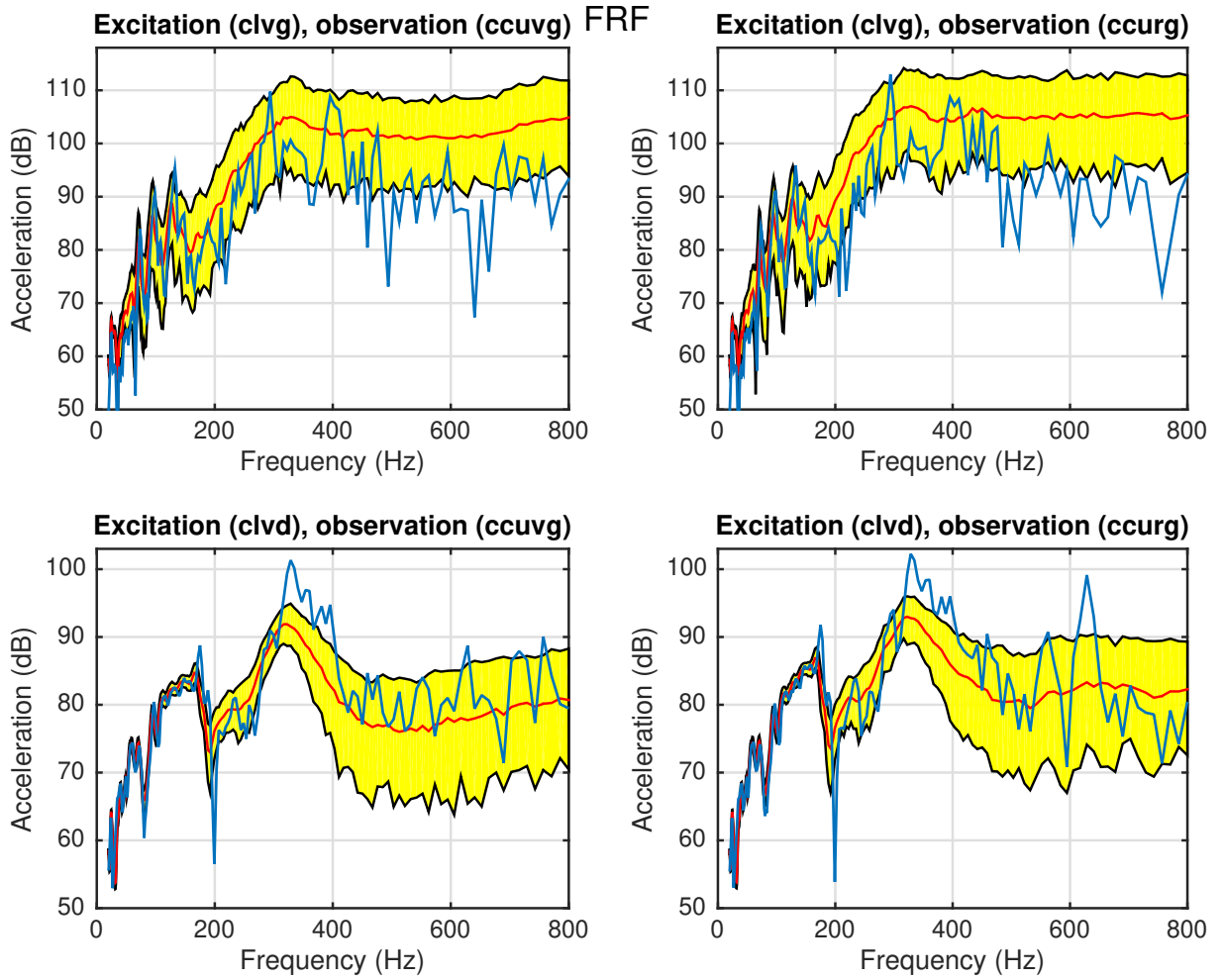


Figure 6.4 – Case 1, structural FRF for $\delta_{M, \mathcal{K}_{LMH}^s} = 0.25$, $\delta_{M, \mathcal{D}_{LMH}^s} = \delta_{M, \mathcal{M}_{LMH}^s} = 0.3$, and $\delta_{L, \mathcal{K}_{LMH}^s} = \delta_{H, \mathcal{K}_{LMH}^s} = \delta_{L, \mathcal{D}_{LMH}^s} = \delta_{H, \mathcal{D}_{LMH}^s} = \delta_{L, \mathcal{M}_{LMH}^s} = \delta_{H, \mathcal{M}_{LMH}^s} = 0.05$: Confidence region 95% (yellow), nominal (blue), and statistical mean (red).

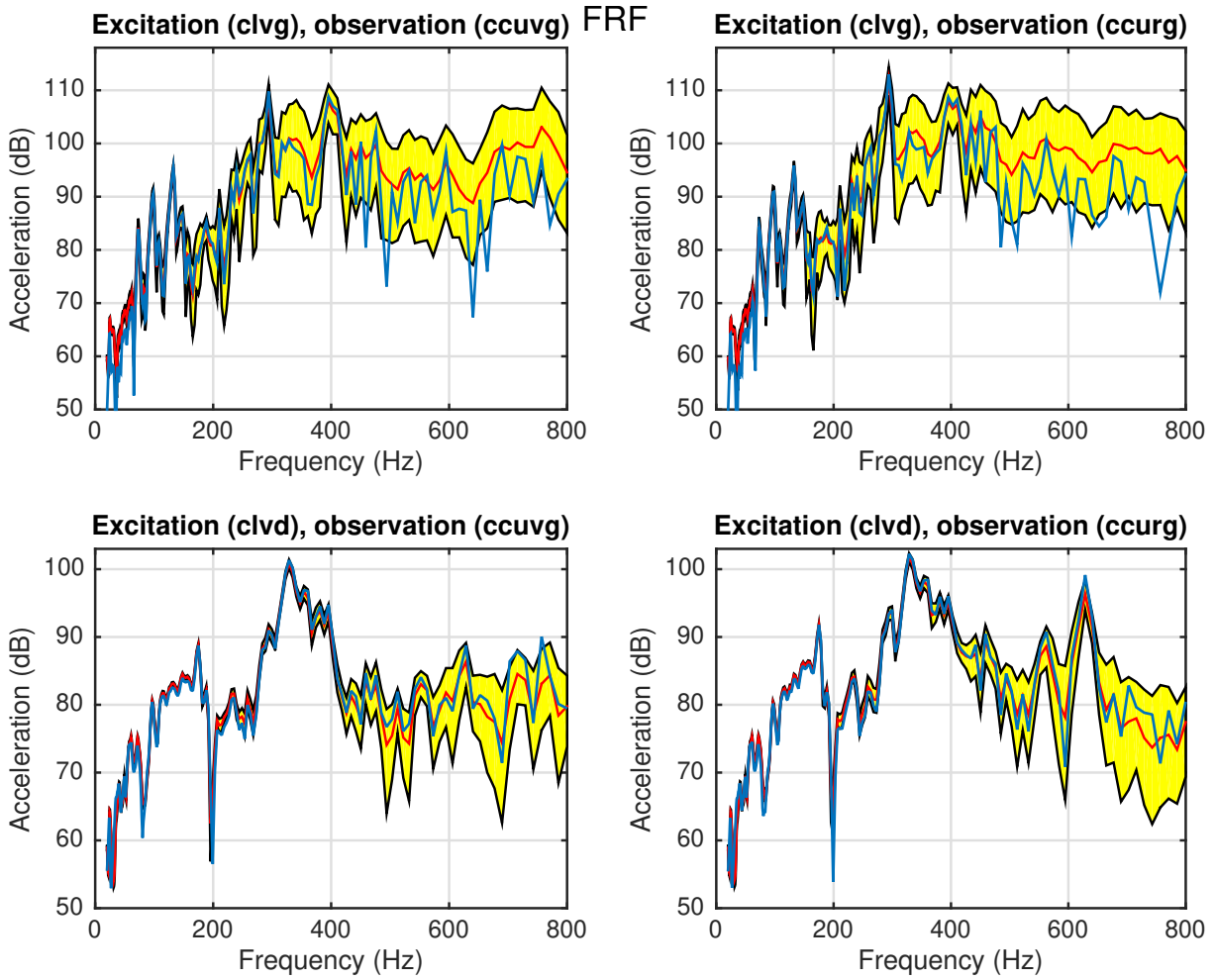


Figure 6.5 – Case 1, structural FRF for $\delta_{H,\mathcal{K}_{LMH}^s} = 0.25$, $\delta_{H,\mathcal{D}_{LMH}^s} = \delta_{H,\mathcal{M}_{LMH}^s} = 0.3$, and $\delta_{L,\mathcal{K}_{LMH}^s} = \delta_{M,\mathcal{K}_{LMH}^s} = \delta_{L,\mathcal{D}_{LMH}^s} = \delta_{M,\mathcal{D}_{LMH}^s} = \delta_{L,\mathcal{M}_{LMH}^s} = \delta_{M,\mathcal{M}_{LMH}^s} = 0.05$: Confidence region 95% (yellow), nominal (blue), and statistical mean (red).

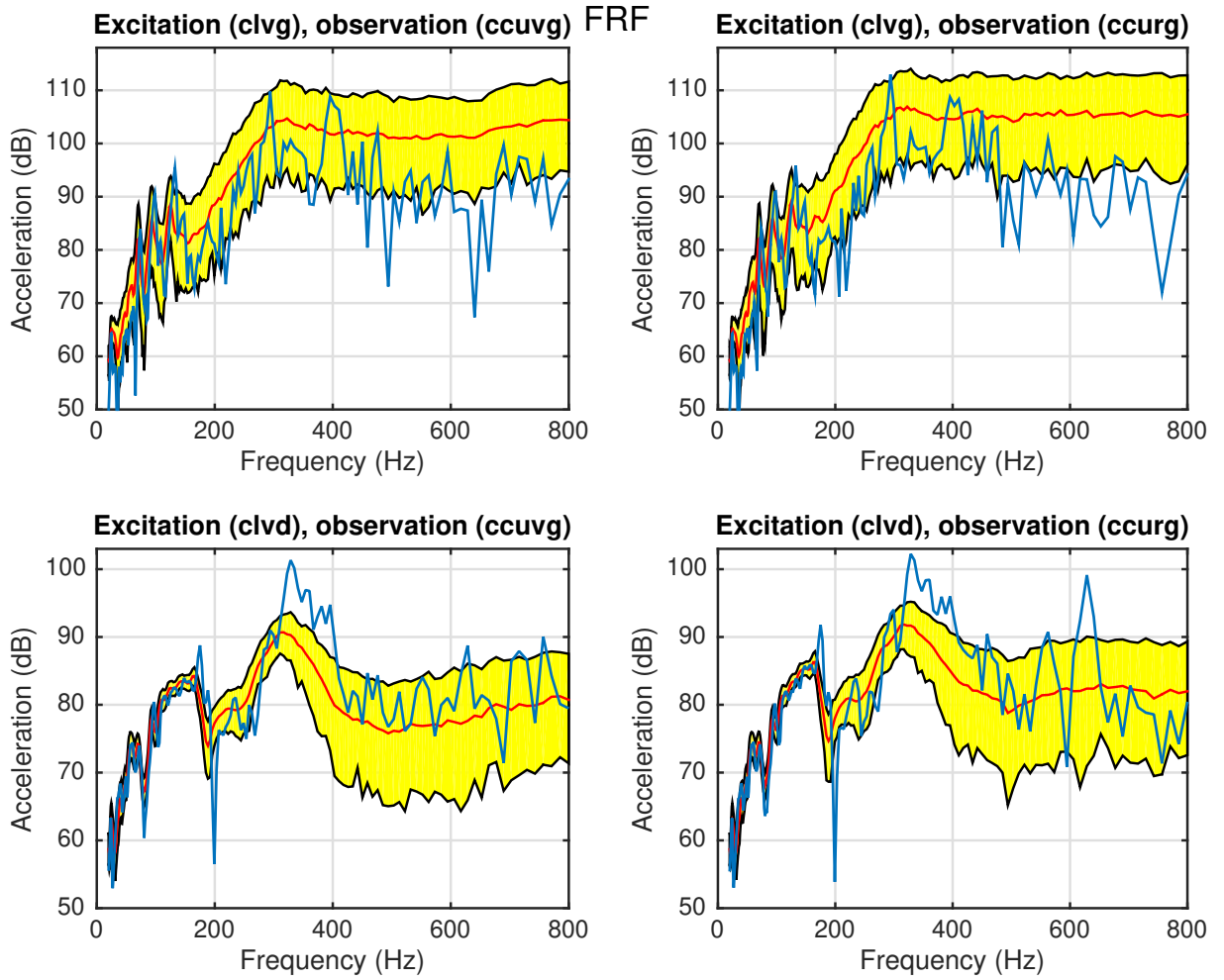


Figure 6.6 – Case 1, structural FRF for $\delta_{L,\mathcal{K}_{LMH}^s} = \delta_{M,\mathcal{K}_{LMH}^s} = \delta_{H,\mathcal{K}_{LMH}^s} = 0.25$, $\delta_{L,\mathcal{D}_{LMH}^s} = \delta_{M,\mathcal{D}_{LMH}^s} = \delta_{H,\mathcal{D}_{LMH}^s} = 0.3$, and $\delta_{L,\mathcal{M}_{LMH}^s} = \delta_{M,\mathcal{M}_{LMH}^s} = \delta_{H,\mathcal{M}_{LMH}^s} = 0.3$: Confidence region 95% (yellow), nominal (blue), and statistical mean (red).

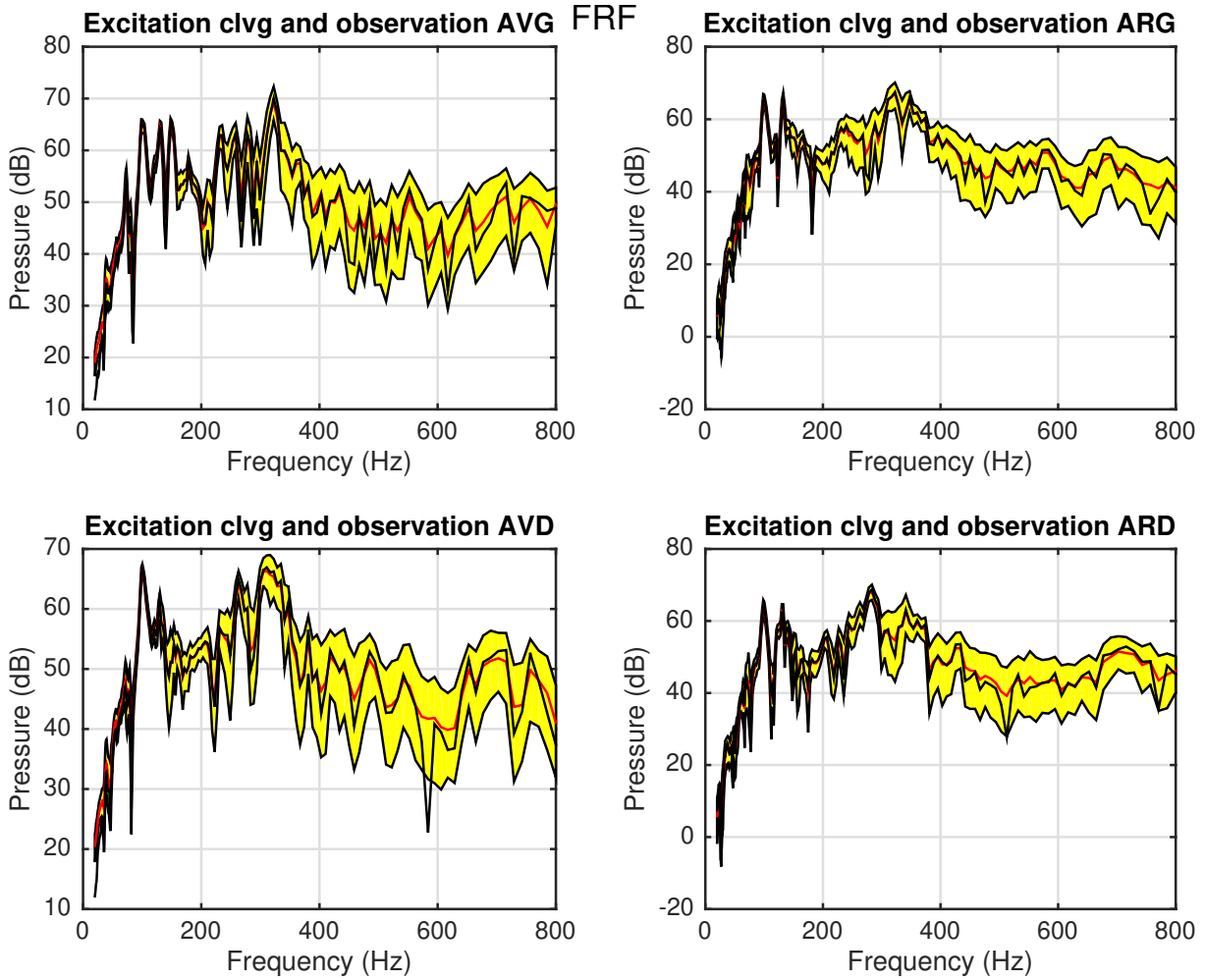


Figure 6.7 – Case 1, acoustic FRF for $\delta_{L,\mathcal{K}_{LMH}^s} = 0.2$, $\delta_{L,\mathcal{D}_{LMH}^s} = 0.3$, $\delta_{L,\mathcal{M}_{LMH}^s} = 0.3$, and $\delta_{M,\mathcal{K}_{LMH}^s} = \delta_{H,\mathcal{K}_{LMH}^s} = \delta_{M,\mathcal{D}_{LMH}^s} = \delta_{H,\mathcal{D}_{LMH}^s} = \delta_{M,\mathcal{M}_{LMH}^s} = \delta_{H,\mathcal{M}_{LMH}^s} = 0.05$: Confidence region 95% (yellow), nominal (black), and statistical mean (red).

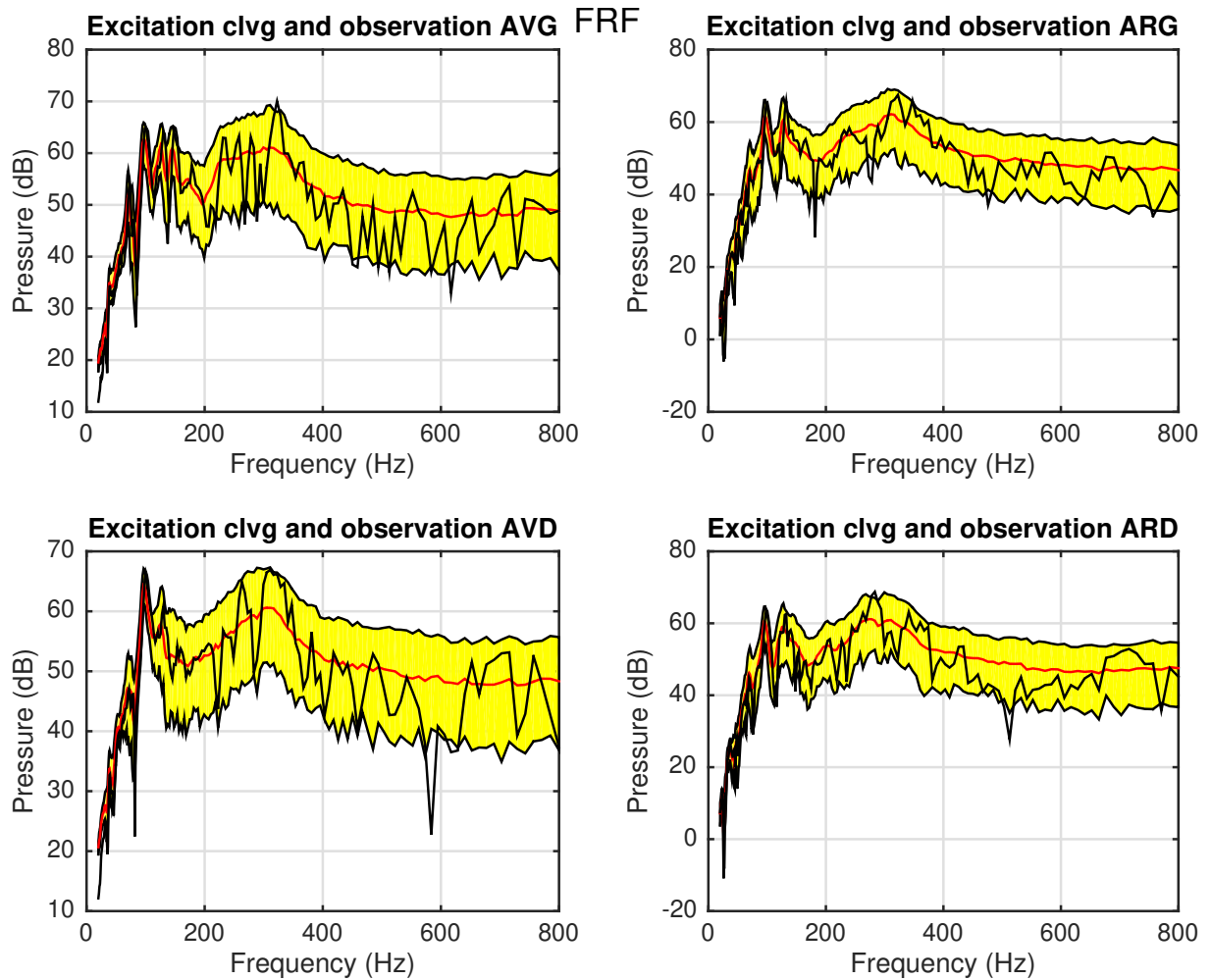


Figure 6.8 – Case 1, acoustic FRF for $\delta_{M,\mathcal{K}_{LMH}^s} = 0.25$, $\delta_{M,\mathcal{D}_{LMH}^s} = \delta_{M,\mathcal{M}_{LMH}^s} = 0.3$, and $\delta_{L,\mathcal{K}_{LMH}^s} = \delta_{H,\mathcal{K}_{LMH}^s} = \delta_{L,\mathcal{D}_{LMH}^s} = \delta_{H,\mathcal{D}_{LMH}^s} = \delta_{L,\mathcal{M}_{LMH}^s} = \delta_{H,\mathcal{M}_{LMH}^s} = 0.05$: Confidence region 95% (yellow), nominal (black), and statistical mean (red).

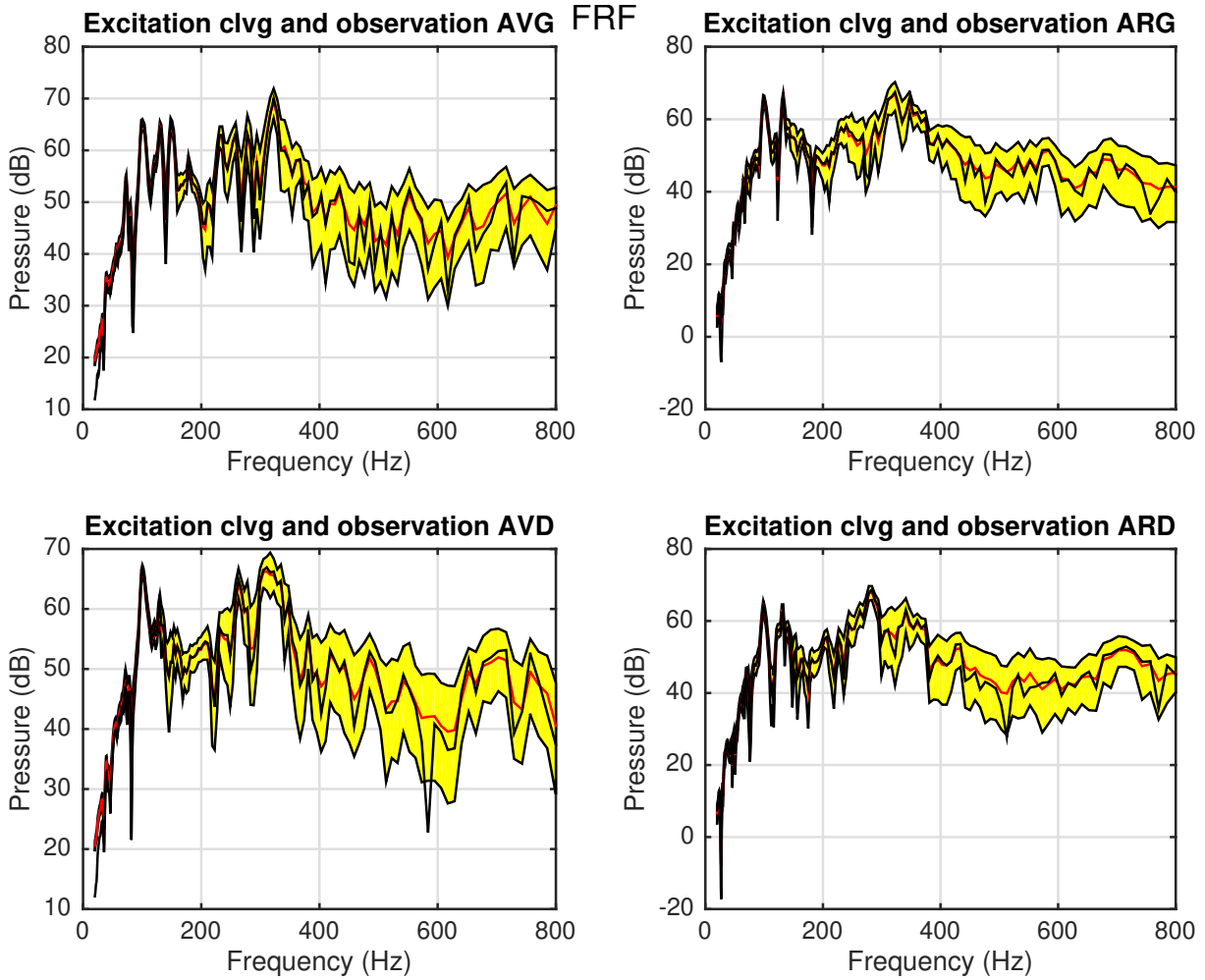


Figure 6.9 – Case 1, acoustic FRF for $\delta_{H,\mathcal{K}_{LMH}^s} = 0.25$, $\delta_{H,\mathcal{D}_{LMH}^s} = \delta_{H,\mathcal{M}_{LMH}^s} = 0.3$, and $\delta_{L,\mathcal{K}_{LMH}^s} = \delta_{M,\mathcal{K}_{LMH}^s} = \delta_{L,\mathcal{D}_{LMH}^s} = \delta_{M,\mathcal{D}_{LMH}^s} = \delta_{L,\mathcal{M}_{LMH}^s} = \delta_{M,\mathcal{M}_{LMH}^s} = 0.05$: Confidence region 95% (yellow), nominal (black), and statistical mean (red).

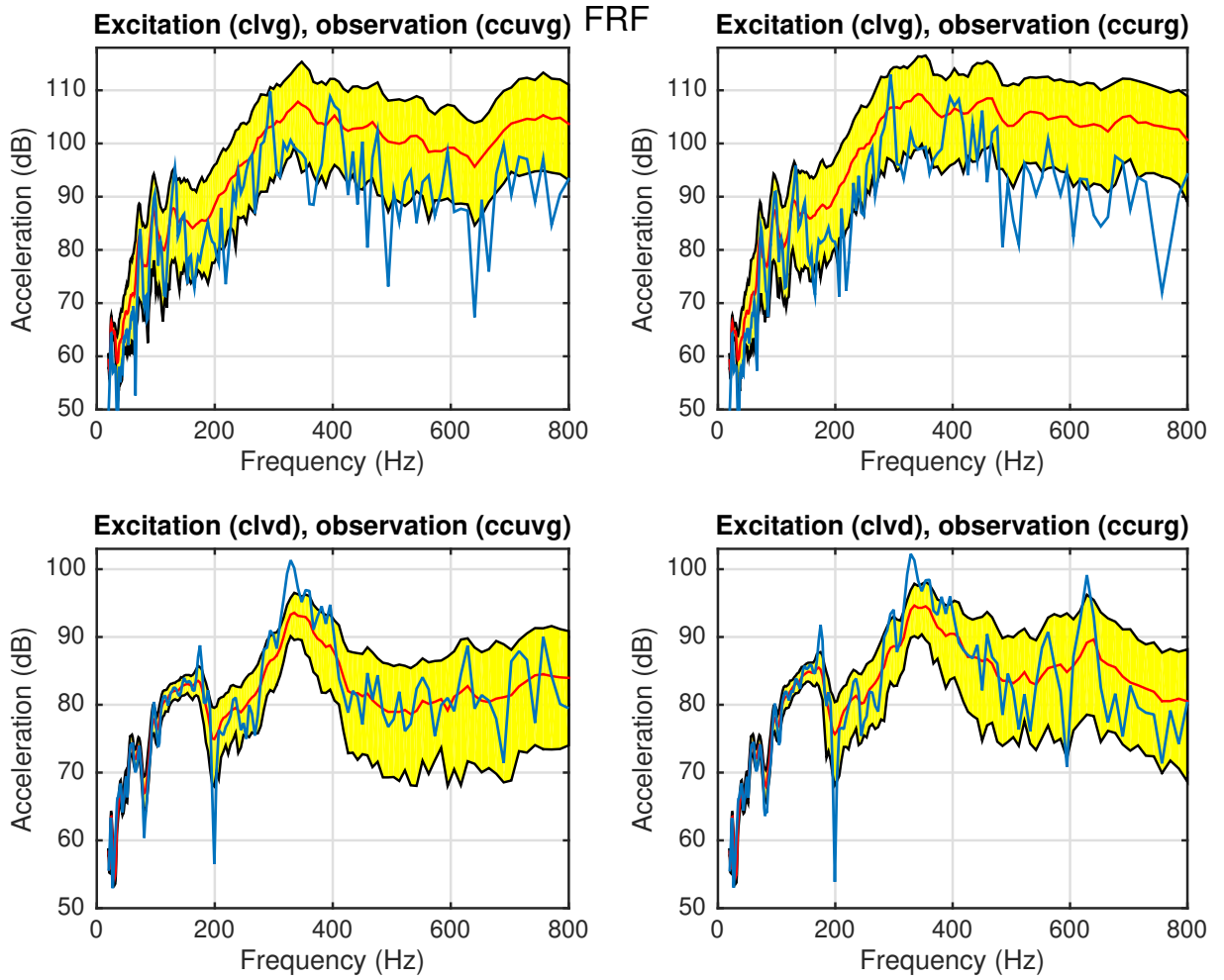


Figure 6.10 – Case 2, structural FRF for $\delta_{L,\mathcal{K}_{LMH}^s} = 0.25$, $\delta_{L,\mathcal{D}_{LMH}^s} = \delta_{L,\mathcal{M}_{LMH}^s} = 0.3$, and $\delta_{M,\mathcal{K}_{LMH}^s} = \delta_{H,\mathcal{K}_{LMH}^s} = \delta_{M,\mathcal{D}_{LMH}^s} = \delta_{H,\mathcal{D}_{LMH}^s} = \delta_{M,\mathcal{M}_{LMH}^s} = \delta_{H,\mathcal{M}_{LMH}^s} = 0.05$: Confidence region 95% (yellow), nominal (blue), and statistical mean (red).

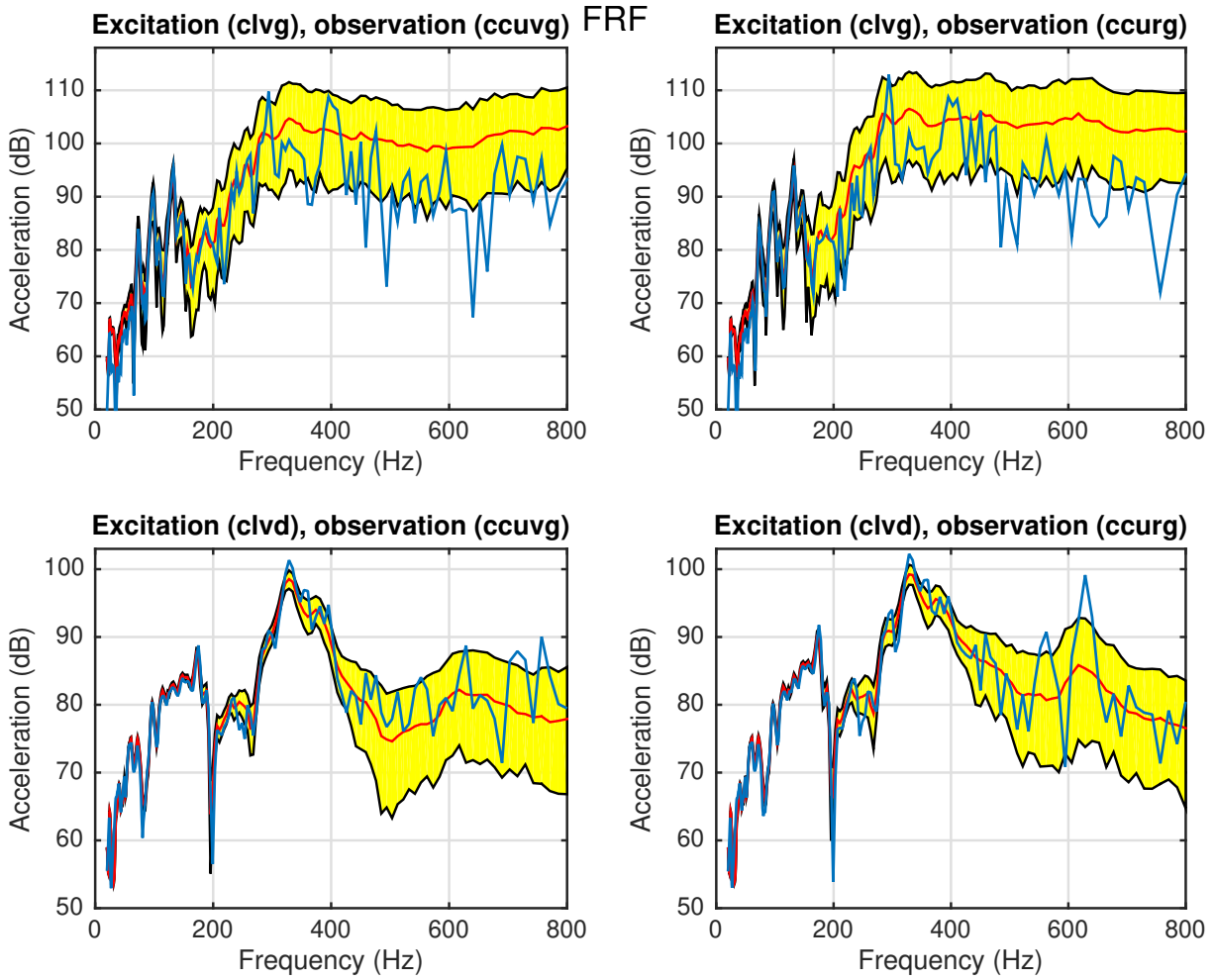


Figure 6.11 – Case 2, structural FRF for $\delta_{M,\mathcal{K}_{LMH}^s} = 0.25$, $\delta_{M,\mathcal{D}_{LMH}^s} = \delta_{M,\mathcal{M}_{LMH}^s} = 0.3$, and $\delta_{L,\mathcal{K}_{LMH}^s} = \delta_{H,\mathcal{K}_{LMH}^s} = \delta_{L,\mathcal{D}_{LMH}^s} = \delta_{H,\mathcal{D}_{LMH}^s} = \delta_{L,\mathcal{M}_{LMH}^s} = \delta_{H,\mathcal{M}_{LMH}^s} = 0.05$: Confidence region 95% (yellow), nominal (blue), and statistical mean (red).

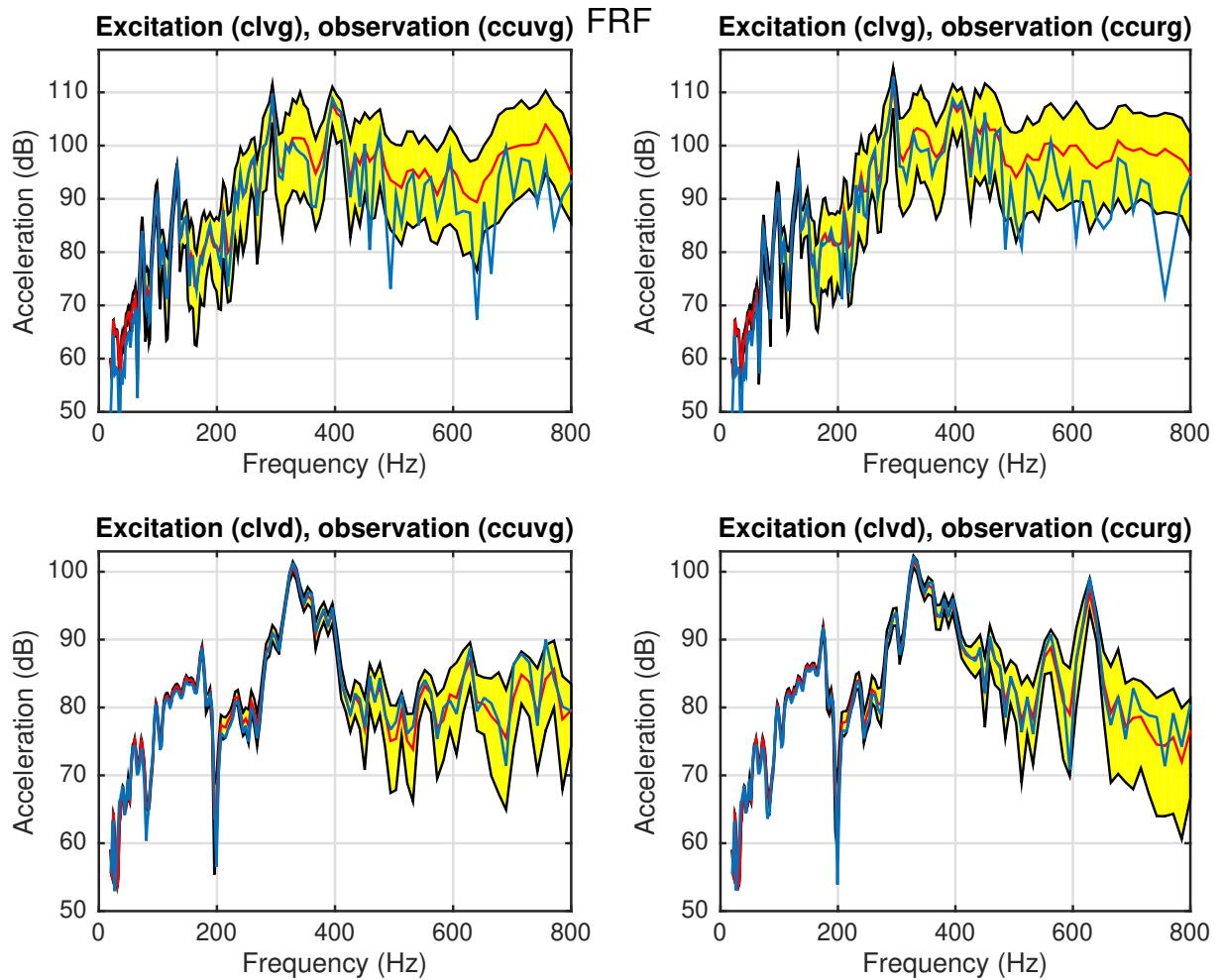


Figure 6.12 – Case 2, structural FRF for $\delta_{H, \mathcal{K}_{LMH}^s} = 0.25$, $\delta_{H, \mathcal{D}_{LMH}^s} = \delta_{H, \mathcal{M}_{LMH}^s} = 0.3$, and $\delta_{L, \mathcal{K}_{LMH}^s} = \delta_{M, \mathcal{K}_{LMH}^s} = \delta_{L, \mathcal{D}_{LMH}^s} = \delta_{M, \mathcal{D}_{LMH}^s} = \delta_{L, \mathcal{M}_{LMH}^s} = \delta_{M, \mathcal{M}_{LMH}^s} = 0.05$: Confidence region 95% (yellow), nominal (blue), and statistical mean (red).

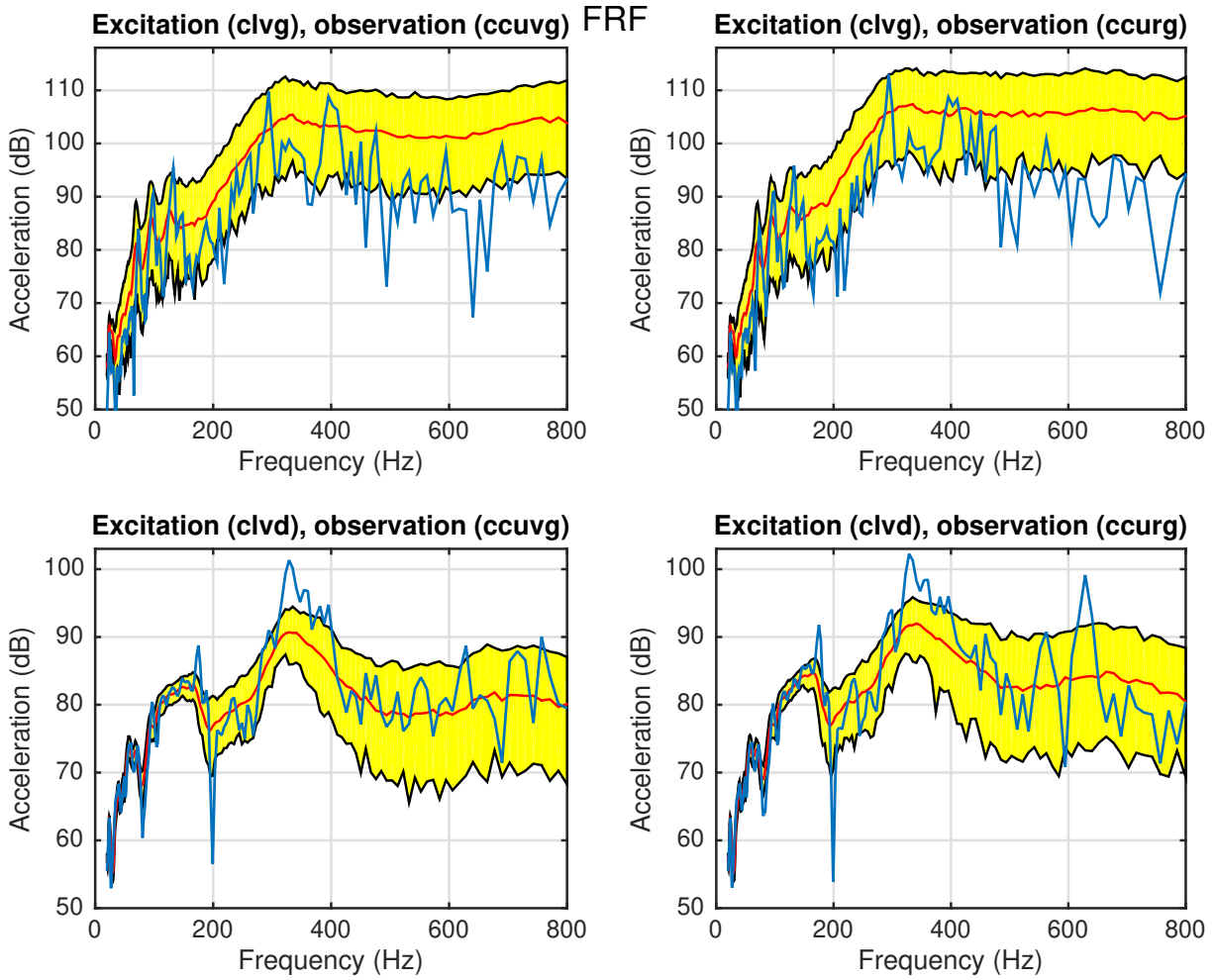


Figure 6.13 – Case 2, structural FRF for $\delta_{L,\mathcal{K}_{LMH}^s} = \delta_{M,\mathcal{K}_{LMH}^s} = \delta_{H,\mathcal{K}_{LMH}^s} = 0.25$, $\delta_{L,\mathcal{D}_{LMH}^s} = \delta_{M,\mathcal{D}_{LMH}^s} = \delta_{H,\mathcal{D}_{LMH}^s} = 0.3$, and $\delta_{L,\mathcal{M}_{LMH}^s} = \delta_{M,\mathcal{M}_{LMH}^s} = \delta_{H,\mathcal{M}_{LMH}^s} = 0.3$: Confidence region 95% (yellow), nominal (blue), and statistical mean (red).

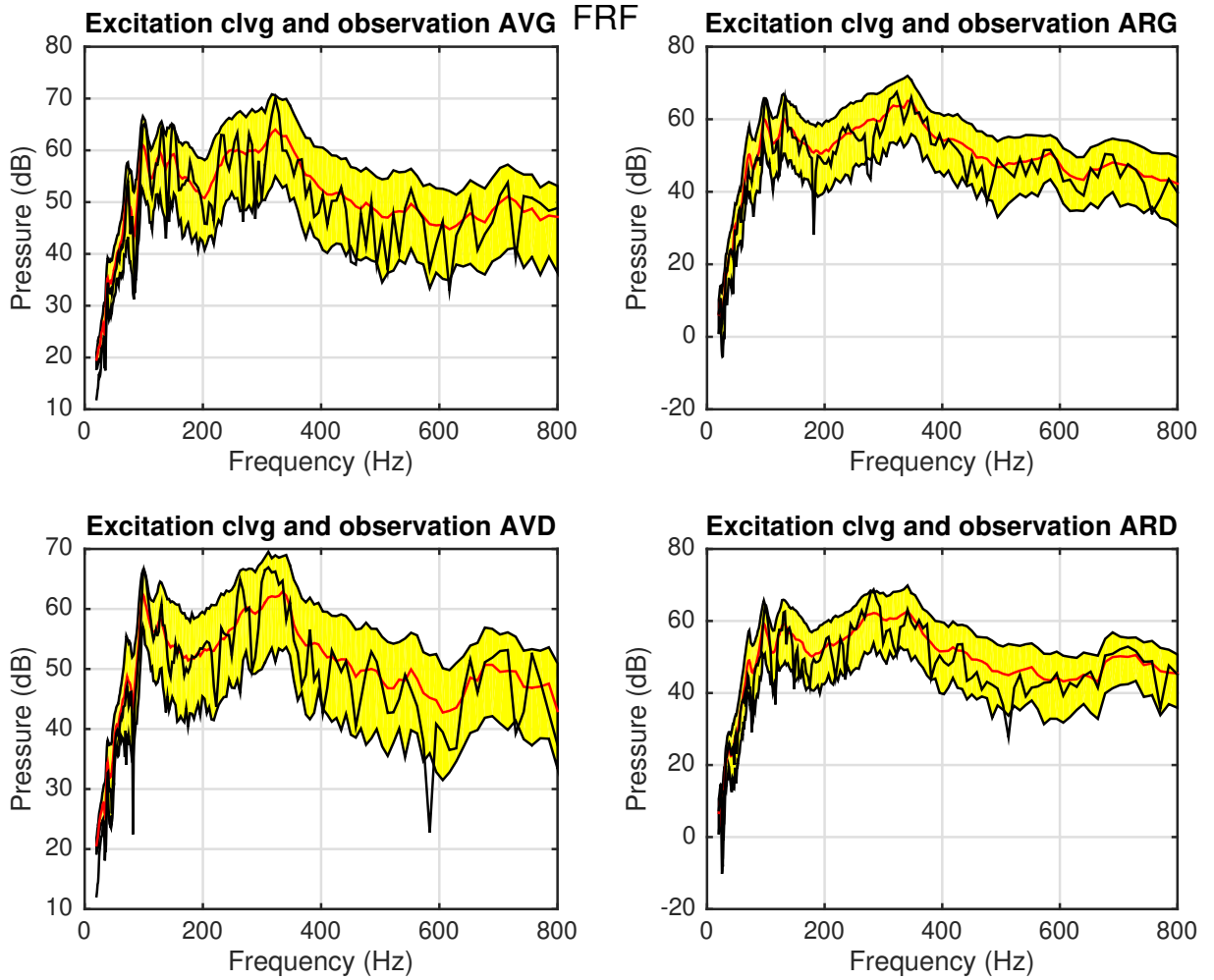


Figure 6.14 – Case 2, acoustic FRF for $\delta_{L,\mathcal{K}_{LMH}^s} = 0.2$, $\delta_{L,\mathcal{D}_{LMH}^s} = 0.3$, $\delta_{L,\mathcal{M}_{LMH}^s} = 0.3$, and $\delta_{M,\mathcal{K}_{LMH}^s} = \delta_{H,\mathcal{K}_{LMH}^s} = \delta_{M,\mathcal{D}_{LMH}^s} = \delta_{H,\mathcal{D}_{LMH}^s} = \delta_{M,\mathcal{M}_{LMH}^s} = \delta_{H,\mathcal{M}_{LMH}^s} = 0.05$: Confidence region 95% (yellow), nominal (black), and statistical mean (red).

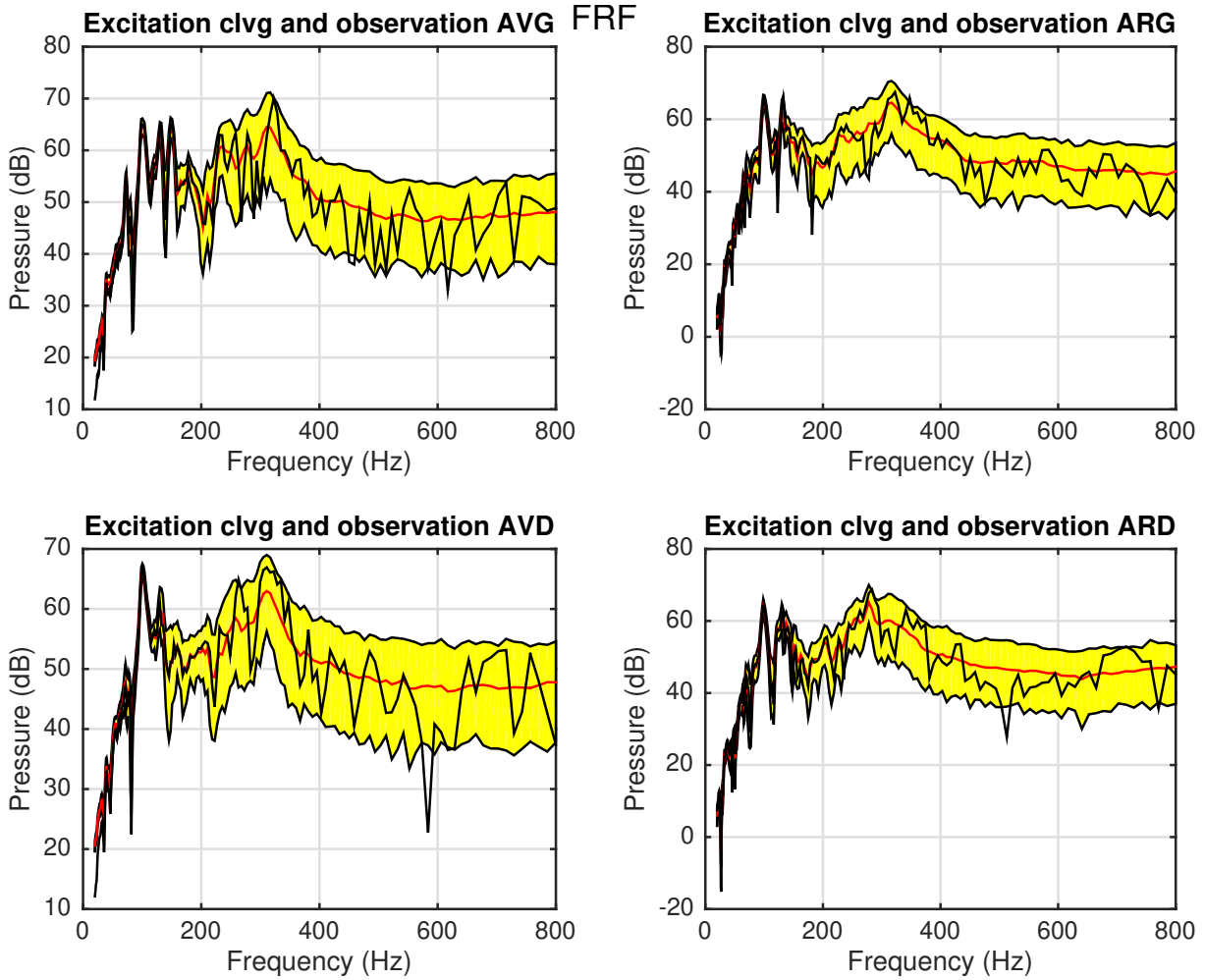


Figure 6.15 – Case 2, acoustic FRF for $\delta_{M, \mathcal{K}_{LMH}^s} = 0.25$, $\delta_{M, \mathcal{D}_{LMH}^s} = \delta_{M, \mathcal{M}_{LMH}^s} = 0.3$, and $\delta_{L, \mathcal{K}_{LMH}^s} = \delta_{H, \mathcal{K}_{LMH}^s} = \delta_{L, \mathcal{D}_{LMH}^s} = \delta_{H, \mathcal{D}_{LMH}^s} = \delta_{L, \mathcal{M}_{LMH}^s} = \delta_{H, \mathcal{M}_{LMH}^s} = 0.05$: Confidence region 95% (yellow), nominal (black), and statistical mean (red).

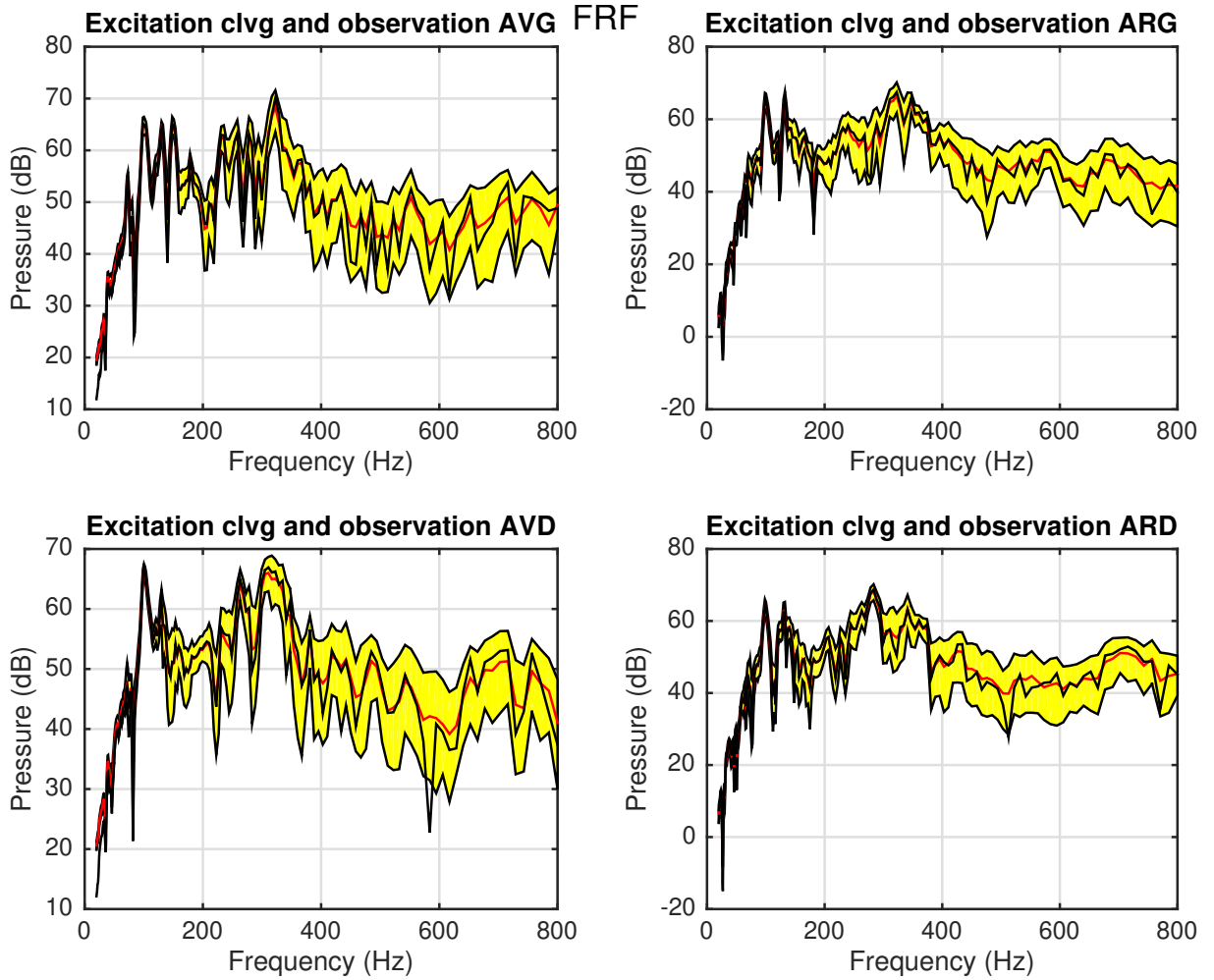


Figure 6.16 – Case 2, acoustic FRF for $\delta_{H,\mathcal{K}_{LMH}^s} = 0.25$, $\delta_{H,\mathcal{D}_{LMH}^s} = \delta_{H,\mathcal{M}_{LMH}^s} = 0.3$, and $\delta_{L,\mathcal{K}_{LMH}^s} = \delta_{M,\mathcal{K}_{LMH}^s} = \delta_{L,\mathcal{D}_{LMH}^s} = \delta_{M,\mathcal{D}_{LMH}^s} = \delta_{L,\mathcal{M}_{LMH}^s} = \delta_{M,\mathcal{M}_{LMH}^s} = 0.05$: Confidence region 95% (yellow), nominal (black), and statistical mean (red).

Conclusion and Perspectives

Summary

This thesis has proposed an improvement of the general method of spatial filtering previously developed for complex structures and has presented an extension to vibroacoustic systems made up of a complex structure coupled with an internal acoustic cavity. The systems studied are all the more complex as the number of degrees of freedom increases with the frequency band of analysis. The modified method has been made to construct a multi-complexity-level displacements basis in order to obtain the multilevel ROM. The principal use is for robust dynamical analysis of complex vibroacoustic systems over a broad frequency band for which the model uncertainties induced by modeling errors can be adapted to each one of the three vibration regimes, LF, MF, and HF. For that, a multilevel stochastic ROM has been developed for the structure, which is able to take into account the variability induced by the overlap in the three vibration regimes.

The work starts from the Ezvan's works for which a complete reformulation of the method is proposed, for which a novel presentation and developments are performed, and for which novel interpretations are given. For large scale computational vibroacoustic model, we have constructed a predictive stochastic multilevel ROM whose dimension is inferior to the usual ROM constructed by using the classical modal analysis. Algorithms have specifically been developed to be used for very large computational models without encountering problems related to the limitation of Random Access Memory (RAM) and with numerical costs that remain low. This capability of the proposed method has required in-depth methodological and algorithmic reflection. In particular, the numerical analysis and the developed algorithm have been written to improve the existing codes. The high dimension of the computational model compelled us to propose an efficient computation to optimize time calculation (CPU) and data storage limitations (RAM). The database (modal analysis, lumped mass matrix, vibroacoustic modal coupling matrix) has been computed from a dedicated software (Nastran). All the proposed approach and the post-processing have been implemented in Matlab. Consequently, the approach proposed is nonintrusive with respect to commercial software. We have automated some parameters like the range of the first eigenvalue problem and not use the cutoff frequency in the process of the filtering.

The applications have been performed for an automobile whose computational vibroacoustic

model is made up an acoustic cavity (cockpit) of 600 000 DOFs coupled with a complex structure (car) (of nearly 19 000 000 DOFs). Several cases have been considered in order to test the method, the numerical analysis, and the algorithms. The validation has been given and the capability of the proposed approach has been tested, for the stochastic multilevel reduced-order computational vibroacoustic model. This nonparametric stochastic multilevel ROM gives better results than the classical nonparametric stochastic ROM with respect to the taking into account of the uncertainties as a function of the frequency. In addition, it allows a significative reducing of the CPU time with respect to the use of the classical ROM constructed by modal analysis.

Perspectives

In addition to technical refinements that could be proposed here and there, some future research directions can be identified as follows.

The first development would be to obtain the complete vibroacoustic coupling matrix and to see what is its influence on the vibroacoustic FRF. Such a development is directly linked to the possibilities of the commercial software used and not to the developments, strictly speaking, of the proposed method.

The second development would be to propose an adapted visualization of the filtered modes. The study of these visualizations could be quite interesting to improve the method.

A third point would be to perform further test over other complex vibroacoustic systems.

Appendix A

Independent Component Analysis using Nastran

Improvement of vibroacoustic models prediction capabilities in a probabilistic context requires an adapted metric to compare experimental measurements with stochastic computations. The likelihood appears as the natural tool to compare experiments with probabilistic computations as soon as the probability of a given result may be computed. Since the vibroacoustic analysis mainly relies on complex matrix-valued Frequency Response Functions ($[FRF] = \{\omega \rightarrow [FRF(\omega)]\}$) that can be measured and computed, the likelihood of such complex and frequency dependent matrices is investigated. A two stage statistical reduction, based on Independent Components Analysis [146], is proposed in order to separate statistically independent components with complex amplitudes for which the probability may be computed independently one from each others. Bi-dimensional probability density functions of the complex components amplitudes are deduced from a Monte-Carlo simulation of the nonparametric stochastic computational model, using MSC/NASTRAN. The proposed statistical reduction presents many interesting properties regarding the physical understanding of FRF matrices as well as a numerical aspects.

A.1 Introduction

In the automotive industry, computational vibroacoustic models are used for designing automobiles. The acoustic comfort and the vibrations of vehicles constitute a major issue. In the vibroacoustic analysis, FRFs are widely used to control the structure borne noise transmission in the case of multiple transmission paths. However, the computational structural model considered in this Appendix has about fifteen million of degrees-of-freedom (DOFs) and the coupled acoustic cavity has about eight million of DOFs. The high dimension of the computational model brings great difficulties. The advantage of the FRF is that, even for such complex structures such as automobiles, it always provides a simple system of one vector-valued input (excitation) and one vector-valued output (observation). The vibroacoustic computational model allows the computation of the FRF matrices. The same FRF matrices can also be measured experimentally.

A.2 Statistical reduction using ICA

An Independent Component Analysis (ICA) is performed. The main difference with the Principal Component Analysis (PCA) is that the components will be statistically independent. This approach has been widely used and can be seen in [147]. The ICA can lead to an interesting physical interpretation of the extract components as shown from the Monte-Carlo simulation of the nonparametric stochastic model. It should be noted that the PCA and ICA use the same space. The only difference is the constraint imposed on the components, which is a linear decorrelation for the PCA and the independence for the ICA. We use the Joint Approximation Diagonalization of Eigen-matrices (JADE) algorithm as presented in [148], which is based on a fourth-order moments formulation. JADE computes the matrix such as the sum of all nondiagonal terms of the fourth-order matrix are equal to zero.

In this Appendix, $\mathbb{M}_{n,m}(\mathbb{C})$ denotes the set of all the $(n \times m)$ complex matrices. Let $\omega_1, \dots, \omega_{N_f}$ be the frequency sampling. The number of observations DOFs are denoted by N_o and the number of excitations DOFs by N_e . The complex matrix-valued random FRF is written as $[\text{FRF}(\omega_j)]$ with value in $\mathbb{M}_{N_o, N_e}(\mathbb{C})$, with $j = 1, \dots, N_f$. Let $N = N_o \times N_e$ be the spatial dimension. Let $\mathbf{F}(\omega_j)$ be the random vector with values in \mathbb{C}^N , which is the reshaping by columns of the complex random matrix $[\text{FRF}(\omega_j)]$. Let $[\mathbf{Y}] = [\mathbf{F}(\omega_1) \dots \mathbf{F}(\omega_{N_f})]$ be the complex random matrix with values in $\mathbb{M}_{N, N_f}(\mathbb{C})$. Let $\{[Y_n], n = 1, \dots, N_{MC}\}$ be N_{MC} independent realizations of $[\mathbf{Y}]$ computed by using the stochastic computational model for a fixed value δ of the vector-valued hyperparameter of the random matrices of the nonparametric probabilistic approach of model uncertainties.

A.2.1 First statistical reduction based on ICA

We introduce the positive Hermitian matrix

$$[R] = \frac{1}{N_{MC}} \sum_{n=1}^{N_{MC}} [Y_n]^* [Y_n] \in \mathbb{M}_{N_f, N_f}(\mathbb{C}) \quad , \quad (\text{A.1})$$

in which $[Y_n]^* = [\overline{Y_n}]^T$. We solve the eigenvalue problem $[R]\mathbf{x}^\alpha = \lambda_\alpha \mathbf{x}^\alpha$ of $[R]$ with $\alpha = 1, \dots, N_f$. The positive eigenvalues λ_α are ordered in a decreasing order. We can approximate $[R]$ with a lower number N_p of terms. Let $N_p \leq N_f$ such that $[R] \simeq \sum_{\alpha=1}^{N_p} \lambda_\alpha \mathbf{x}^\alpha (\mathbf{x}^\alpha)^*$, which is rewritten as

$$[R] = [x][\Lambda][x]^* \quad , \quad (\text{A.2})$$

in which $[\Lambda]$ is the diagonal matrix in $\mathbb{M}_{N_p}(\mathbb{R})$ of the decreasing eigenvalues $\lambda_1, \dots, \lambda_{N_p}$ and $[x] = [\mathbf{x}^1, \dots, \mathbf{x}^{N_p}]$ is the complex matrix in $\mathbb{M}_{N_f, N_p}(\mathbb{C})$ of the associated complex eigenvectors that are normalized in order that

$$[x]^* [x] = [I_{N_p}] \quad . \quad (\text{A.3})$$

It can be seen that each realization $[Y_n]$ can be written as

$$[Y_n] = [A_n][x]^* \quad , \quad (\text{A.4})$$

where $[A_n] \in \mathbb{M}_{N,N_p}(\mathbb{C})$ is given by the projection on $[Y_n]$, which is written, by using Eq.(A.3), as

$$[A_n] = [Y_n][x] \quad . \quad (\text{A.5})$$

Let

$$[c] = [x]^* \quad (\text{A.6})$$

be the complex $(N_p \times N_f)$ matrix, for which its columns are denoted by \mathbf{c}^j with $j = 1, \dots, N_f$: $[c] = [\mathbf{c}^1, \dots, \mathbf{c}^{N_f}]$. Let us introduce the random vector \mathbf{C} with values in \mathbb{C}^{N_p} whose realizations are $\mathbf{c}^1, \dots, \mathbf{c}^{N_f}$. The Independent Component Analysis of random vector \mathbf{C} is carried out and yields,

$$[c] = [b][s] \quad , \quad (\text{A.7})$$

in which $[b]$ is a $(N_p \times N_p)$ complex matrix and where $[s]$ is a $(N_p \times N_f)$ complex matrix whose rows $\mathbf{s}^1, \dots, \mathbf{s}^{N_p}$, which belong to $\mathbb{M}_{1,N_f}(\mathbb{C})$, are independent realizations of a random vector \mathbf{S}^T with values in \mathbb{C}^{N_f} . From Eqs.(A.4), (A.6), and (A.7), it can be deduced that

$$[Y_n] = [\hat{A}_n][s] \quad , \quad (\text{A.8})$$

in which $[\hat{A}_n]$ is written as

$$[\hat{A}_n] = [A_n][b] \in \mathbb{M}_{N,N_p}(\mathbb{C}) \quad . \quad (\text{A.9})$$

On the frequency basis $[c]$, there are N_p independent components. Figure A.1 shows the N_p independent components issued from the ICA. It can be seen peaks all along the frequency band \mathcal{B} and that each component has a different contribution over the frequency band. Consequently, for each sub-band of \mathcal{B} , only the components that have the main contributions are kept. This means that the reductions is performed by sub-band and not globally for all the frequency band of analysis. We have taken the frequency value at the maximum of each independent component from the first ICA statistical reduction from Fig. A.1. It can be seen that the sub-bands are narrower for the lowest frequencies. As the frequency increases, the width of the sub-bands increases.

A.2.2 Second statistical reduction based on ICA

In the second statistical reduction, we construct a spatial basis over the observations and excitations DOFs. From the N_p independent components obtained from the first statistical reduction over the frequency band, we determine the components that have contributions on the spatial basis. We use exactly the same methodology that the one previously presented. The ICA is then reused for constructing the second statistical reduction of the random matrix $[\hat{\mathbf{A}}]$ whose realizations are $\{[\hat{A}_n], n = 1, \dots, N_{MC}\}$ that are defined by Eq.(A.9). The following representation is

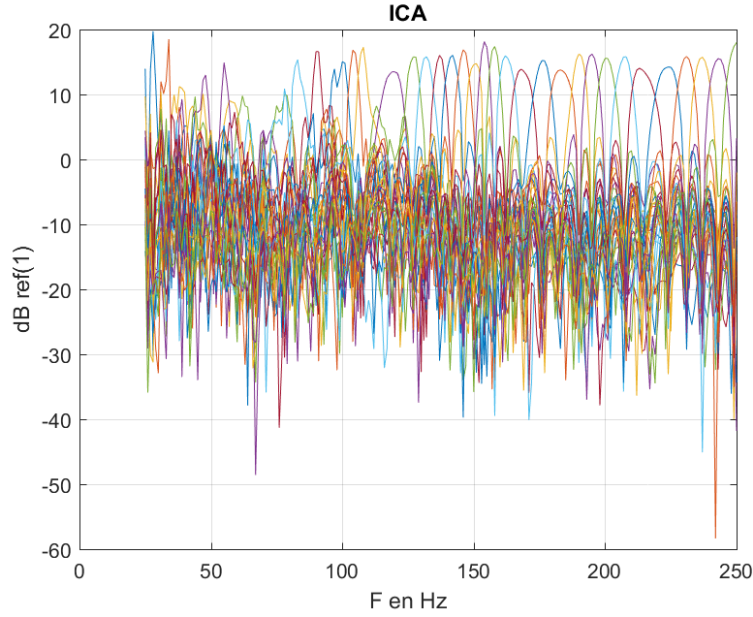


Figure A.1 – Frequency independent components from JADE algorithm with ICA.

obtained,

$$[\hat{A}_n]_{k\alpha} = \sum_{\beta=1}^{\hat{N}_p(\alpha)} [\hat{F}(\alpha)]_{k\beta} [\chi_n(\alpha)]_{\beta\alpha} \quad , \quad (\text{A.10})$$

in which $k = 1, \dots, N$ and $\alpha = 1, \dots, N_p$, where $\hat{N}_p(\alpha) \leq N$, and where $[\hat{F}(\alpha)]$ and $[\chi_n(\alpha)]$ are complex matrices of dimension $(N \times \hat{N}_p(\alpha))$ and $(\hat{N}_p(\alpha) \times N_p)$, respectively. The matrix $[\chi_n(\alpha)]$ represents the basis. Substituting Eq. (A.10) into Eq. (A.8) yields

$$[Y_n]_{kj} = \sum_{\alpha=1}^{N_p} \sum_{\beta=1}^{\hat{N}_p(\alpha)} [\hat{F}(\alpha)]_{k\beta} [\chi_n(\alpha)]_{\beta\alpha} [s]_{\alpha j} \quad . \quad (\text{A.11})$$

The statistical reduction is efficient if $\hat{N}_p(\alpha) \ll N$. Let us define γ such that for all $\gamma = 1, \dots, N_{\text{comp}}$ with $N_{\text{comp}} = \sum_{\alpha=1}^{N_p} \hat{N}_p(\alpha)$, representing all independent components from the two filterings.

The probability density function of the random variable $[\chi(\alpha)]_{\beta\alpha}$ is estimated with its realizations $[\chi_n(\alpha)]_{\beta\alpha}$. Such a probability density function is shown in the bottom right of each block in Fig. A.2. Moreover, it shows the contribution of each excitation point for each observation point (left figures up and bottom). The upper-right figure represents the frequency independent component of the first statistical reduction.

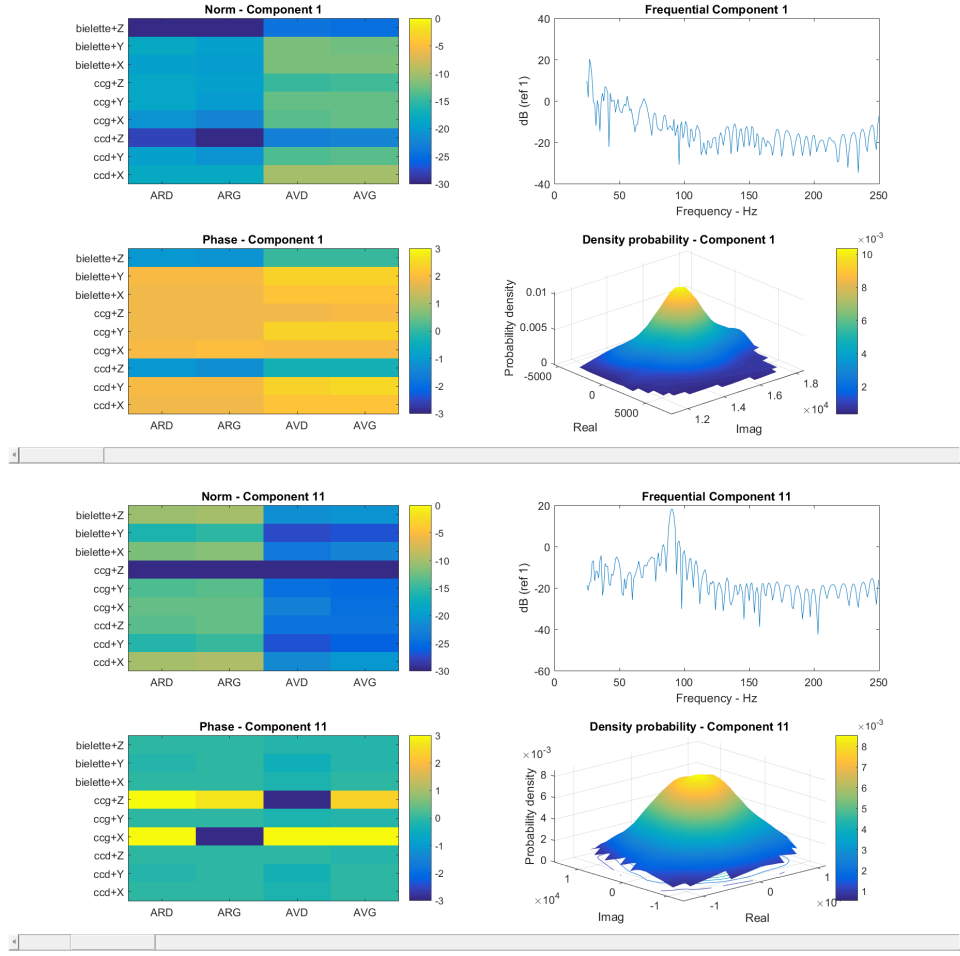


Figure A.2 – Reading the figure as a (4×2) -matrix of sub-figures. For $\gamma = 1$, $\alpha = 1$, and $\beta = 1$: modulus (1,1), phase (2,1), frequency component (1,2), and probability density function (2,2). For $\gamma = 11$, $\alpha = 2$, and $\beta = 1$: modulus (3,1), phase (4,1), frequency component (3,2), and probability density function (4,2).

A.2.3 Projection of an experimental measurement

In this section, the experimental measurements are projected by using the two statistical reductions in order to obtain the $(\hat{N}_p(\alpha) \times N_p)$ complex matrix $[\chi^{exp}(\alpha)]$, for $\alpha = 1, \dots, N_p$. For all $\ell = 1, \dots, \nu_{exp}$, let $[Y^{exp}]$ be the $(N \times N_f)$ complex matrix related to the experimental measurements,

$$[Y^{exp, \ell}] = [\hat{A}^{exp, \ell}][s] \quad , \quad (\text{A.12})$$

$$[\hat{A}^{exp, \ell}]_{k\alpha} = \sum_{\beta=1}^{\hat{N}_p(\alpha)} [\hat{F}(\alpha)]_{k\beta} [\chi^{exp, \ell}(\alpha)]_{\beta\alpha} \quad . \quad (\text{A.13})$$

Equation (A.10) yields

$$[\hat{A}^{exp, \ell}] = [Y^{exp, \ell}][\mathcal{S}] \quad , \quad (\text{A.14})$$

in which $[\mathcal{S}] = [s]^*([s][s]^*)^{-1}$ is the right pseudo-inverse of $[s]$. For α fixed in $\{1, \dots, N_p\}$, let $[\mathbb{H}(\alpha)]$ be the $(\widehat{N}_p(\alpha) \times \widehat{N}_p(\alpha))$ complex matrix defined by

$$[\mathbb{H}(\alpha)]_{\beta'\beta} = \sum_{k=1}^N [\widehat{F}(\alpha)]_{k\beta'} [\widehat{F}(\alpha)]_{k\beta} \quad . \quad (\text{A.15})$$

The projection of Eq. (A.11) on $[\widehat{F}(\alpha)]$ yields, for α fixed in $\{1, \dots, N_p\}$ and β' in $\{1, \dots, \widehat{N}_p(\alpha)\}$, the expression of $[\chi^{\text{exp},\ell}(\alpha)]$ written as

$$[\chi^{\text{exp},\ell}(\alpha)]_{\beta'\alpha} = \sum_{k=1}^N [\widehat{\mathcal{F}}(\alpha)]_{\beta'k} [\widehat{A}^{\text{exp},\ell}]_{k\alpha} \quad , \quad (\text{A.16})$$

in which $[\widehat{\mathcal{F}}(\alpha)]$ is such that

$$[\widehat{\mathcal{F}}(\alpha)]_{\beta'k} = \sum_{\beta=1}^{\widehat{N}_p(\alpha)} \{[\mathbb{H}(\alpha)]^{-1}\}_{\beta'\beta} [\widehat{F}(\alpha)]_{k\beta} \quad . \quad (\text{A.17})$$

A.3 Calculation of the likelihood

The likelihood function is estimated using the kernel density estimation method. The family $\{[\chi(\alpha)]_{\beta\alpha}, \alpha = 1, \dots, N_p, \beta = 1, \dots, \widehat{N}_p(\alpha)\}$ of independent random variables (due to the use of the ICA) are gathered in a random vector $\mathbf{W} = (W_1, \dots, W_{N_{\text{comp}}})$ of independent components with $N_{\text{comp}} = \sum_{\alpha=1}^{N_p} \widehat{N}_p(\alpha)$. The corresponding experimental values of \mathbf{W} are denoted

by $\{\mathbf{w}^{\text{exp},\ell}, \ell = 1, \dots, \nu_{\text{exp}}\}$. Let $(w_1, \dots, w_{N_{\text{comp}}}) \mapsto p_{\mathbf{W}}(w_1, \dots, w_{N_{\text{comp}}}) = \prod_{\gamma=1}^{N_{\text{comp}}} p_{W_\gamma}(w_\gamma)$ be the probability density function of \mathbf{W} on $\mathbb{R}^{N_{\text{comp}}}$. The log-likelihood \mathcal{L} of \mathbf{W} for $\{\mathbf{w}^{\text{exp},\ell}, \ell = 1, \dots, \nu_{\text{exp}}\}$ is written as

$$\mathcal{L} = \sum_{\ell=1}^{\nu_{\text{exp}}} \sum_{\gamma=1}^{N_{\text{comp}}} \mathcal{L}_{\gamma,\ell} \quad , \quad (\text{A.18})$$

in which, for all $\gamma = 1, \dots, N_{\text{comp}}$,

$$\mathcal{L}_{\gamma,\ell} = 10 \log_{10} p_{W_\gamma}(w_\gamma^{\text{exp},\ell}) \quad . \quad (\text{A.19})$$

In order to visualize the log-likelihood of the components from the first statistical reduction, Eq.(A.18) is rewritten as a function of the frequency,

$$\mathcal{L} = \sum_{\ell=1}^{\nu_{\text{exp}}} \sum_{\alpha=1}^{N_p} \mathcal{L}_\alpha \quad , \quad (\text{A.20})$$

in which

$$\mathcal{L}_\alpha = \sum_{\beta=1}^{\hat{N}_p(\alpha)} \mathcal{L}_\beta \quad . \quad (\text{A.21})$$

Figure A.3 shows the maximum and the minimum of the log-likelihood for $[\chi(\alpha)]_{\alpha\beta}$. It can

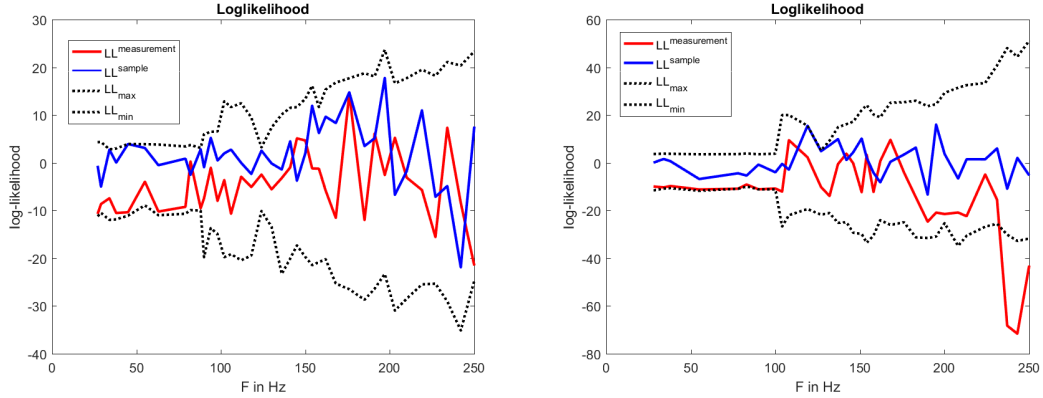


Figure A.3 – On the left, log-likelihood of the experimental measurements (red), one sample from Monte Carlo (blue), the minimum and the maximum of the stochastic basis (black dotted). On the right, log-likelihood of the experimental measurements (red), one sample from Monte Carlo (blue), the minimum and the maximum of the stochastic basis (black dotted)

be noticed that the realizations computed with the stochastic ROM are within the range of the maximum and the minimum. A verification step has been carried out to make sure that all realizations are within the range. The experimental measurements are also within the range of the maximum and the minimum, which means that the nonparametric stochastic model is sufficiently good. Some results and further details can be found in [15]

A.4 Discussion

It should be noted that this approach yields a significant reduction factor that is not negligible for the models studied. The proposed statistical reduction offers many perspectives in different fields. First, considering the data reduction capabilities, compressed model could be handled in NVH synthesis tools in order to propagate uncertainties for various vibration sources and operating conditions. Second, the deep physical meaning of the independent component analysis has not yet been investigated.

We have mostly presented a methodology for constructing a statistical reduction of a complex matrix-valued random FRF. At a given frequency, the random FRF complex matrix is represented by a large collection of realizations computed using the Nonparametric Variability Modeling in MSC/NASTRAN (nonparametric probabilistic approach of uncertainties). Since we

consider the complex matrix-valued random FRF, the use of two statistical reductions is efficient. The first reduction provides a decomposition of the studied frequency range in independent frequency sub-bands, while the second reduction deals with the DOFs interaction in each of these frequency sub-bands. Statistical independence of the reduction components is guaranteed by the Independent Component Analysis as implemented in the JADE algorithm. Once the components have been characterized, the PDF of their complex amplitude can be estimated, later allowing the likelihood computation. The model reduction is performed according to a requested precision: the lower the precision, the lower the number of components, and the higher the reduction.

Appendix A

Bibliography

- [1] L. Gagliardini, L. Houillon, G. Borello, and L. Petrinelli. Virtual sea-fea-based modeling of mid-frequency structure-borne noise. *Sound and Vibration*, 39(1):22–28, 2005.
- [2] JF. Durand, C. Soize, and L. Gagliardini. Structural-acoustic modeling of automotive vehicles in presence of uncertainties and experimental identification and validation. *The Journal of the Acoustical Society of Americam*, 123(3):1513–1525, 2008.
- [3] M. Arnst, D. Clouteau, and M. Bonnet. Inversion of probabilistic structural models using measured transfer functions. *Computer Methods in Applied Mechanics and Engineering*, 197(6-8):589–608, 2008.
- [4] M. Kassem, C. Soize, and L. Gagliardini. Structural partitioning of complex structures in the medium-frequency range. an application to an automotive vehicle. *Journal of Sound and Vibration*, 330(5):937–946, 2011.
- [5] J. Antoni. A bayesian approach to sound source reconstruction: Optimal basis, regularization, and focusing. *The Journal of the Acoustical Society of America*, 131(4):2873–2890, 2012.
- [6] A. Arnoux, C. Soize, and L. Gagliardini. Reduced-order computational model for low-frequency dynamics of automobiles. *Advances in Mechanical Engineering*, 31036:1–12, 2013.
- [7] A. Arnoux, A. Batou, C. Soize, and L. Gagliardini. Stochastic reduced order computational model of structures having numerous local elastic modes in low frequency dynamics. *Journal of Sound and Vibration*, 332(16):3667–3680, 2013.
- [8] D. Clouteau, R. Cottureau, and G. Lombert. Dynamics of structures coupled with elastic media - a review of numerical models and methods. *Journal of Sound and Vibration*, 332(10):2415–2436, 2013.

- [9] G. Brogna, J. Antoni, N. Totaro, L. Gagliardini, and O. Sauvage. Modelling vehicles nvh performances: a probabilistic approach. In *Inter-Noise and Noise-Con Congress and Conference Proceedings*, volume 255, pages 1400–1411. Institute of Noise Control Engineering, 2017.
- [10] G. Brogna, J. Antoni, N. Totaro, L. Gagliardini, and O. Sauvage. Identification of sources through a probabilistic approach: application to vehicles in real usage conditions. In *Inter-Noise and Noise-Con Congress and Conference Proceedings*, volume 257, pages 399–410. Institute of Noise Control Engineering, 2018.
- [11] A. Diez-Ibarbia, M. Battarra, J. Palenzuela, G. Cervantes, S. Walsh, M. De-la Cruz, S. Theodossiades, and L. Gagliardini. Comparison between transfer path analysis methods on an electric vehicle. *Applied Acoustics*, 118:83–101, 2017.
- [12] O. Ezvan, A. Batou, C. Soize, and L. Gagliardini. Multilevel model reduction for uncertainty quantification in computational structural dynamics. *Computational Mechanics*, 59(2):219–246, 2017.
- [13] L. Gagliardini. An efficient input mobility mapping computational method. *SAE International Journal of Vehicle Dynamics, Stability, and NVH*, 1(2017-01-1806):439–444, 2017.
- [14] C. Soize. *Uncertainty Quantification*. Interdisciplinary Applied Mathematics 47, Springer, 2017.
- [15] L. Gagliardini, C. Soize, and J. Reyes. Vibroacoustic model’s likelihood computation based on a statistical reduction of random frf matrices. Technical report, SAE Technical Paper, 2019.
- [16] X. Li, J. Antoni, M. Brennan, T. Yang, and Z. Liu. A frequency domain blind identification method for operational modal analysis using a limited number of sensors. *Journal of Vibration and Control*, page 1077546319897218, 2020.
- [17] J. Reyes, C. Desceliers, C. Soize, and L. Gagliardini. Multi-frequency model reduction for uncertainty quantification in computational vibroacoustics of automobiles. *SAE International conference, virtual conference, September 15-17*, pages 1–7, 2020.
- [18] KJ. Bathe. *Finite Element Procedures*. Klaus-Jurgen Bathe, 2006.
- [19] TJR. Hughes. *The Finite Element Method: Linear Static and Dynamic Finite Element Analysis*. Dover Publications, 2000.
- [20] OC. Zienkiewicz and RL. Taylor. *The Finite Element Method*. Butterworth-Heinemann, 2000.
- [21] C. Soize. Medium frequency linear vibrations of anisotropic elastic structures. *La Recherche Aéropatiale (English edition)*, 5:65–87, 1982.

-
- [22] KJ. Bathe and EL. Wilson. *Numerical Methods in Finite Element Analysis*. Englewood Cliffs, New Jersey: Prentice-Hall, 1976.
- [23] L. Meirovitch. *Dynamics and Control of Structures*. Wiley, New York, 1990.
- [24] J. Argyris and HP. Mlejnek. *Dynamics of Structures*. North-Holland, Amsterdam, 1991.
- [25] M. Geradin and D. Rixen. *Mechanical Vibrations, Second edition: Theory and Applications to Structural Dynamics*. Wiley, Chichester, 1997.
- [26] R. Ohayon and C. Soize. *Structural Acoustics and Vibration*. Academic Press, San Diego, 1998.
- [27] RR. Craig and AJ. Kurdila. *Fundamentals of Structural Dynamics*. John Wiley and Sons, Hoboken, 2006.
- [28] KJ. Bathe. The subspace iteration method - revisited. *Computers & Structures*, 126:177–183, 2013.
- [29] S. Casciati and L. Faravelli. Quantity vs quality in the model order reduction (MOR) of a linear dynamical system. *Smart Structures and Systems*, 136:99–109, 2014.
- [30] R. Rumpler, A. Legay, and J-F. Deü. Performance of a restrained-interface substructuring fe model for reduction of structural-acoustic problems with poroelastic damping. *Computers & structures*, 89(23-24):2233–2248, 2011.
- [31] R. Rumpler, P. Göransson, and J-F. Deü. A residue-based mode selection and sorting procedure for efficient poroelastic modeling in acoustic finite element applications. *The Journal of the Acoustical Society of America*, 134(6):4730–4741, 2013.
- [32] R. Ohayon and Soize. C. *Advanced Computational Vibroacoustics - Reduced-Order Models and Uncertainty Quantification*. Cambridge University Press, New York, 2014.
- [33] RH. Lyon and RG. DeJong. *Theory and Application of Statistical Energy Analysis*. Butterworths-Heimann, Boston, 1995.
- [34] RS. Langley and P. Bremner. A hybrid method for the vibration analysis of complex structural-acoustic systems. *The Journal of the Acoustical Society of America*, 105(3):1657–1671, 1999.
- [35] A. LeBot. Energy transfer for high frequencies in built-up structures. *Journal of Sound and Vibration*, 250(2):247–275, 2002.
- [36] L. Maxit and JL. Guyader. Extension of sea model to subsystems with non-uniform modal energy distribution. *Journal of Sound and Vibration*, 265(2):337–358, 2003.

- [37] RS. Langley and V. Cotoni. Response variance prediction in the statistical energy analysis of built up systems. *The Journal of the Acoustical Society of America*, 115(2):706–718, 2004.
- [38] RS. Langley. On the diffuse field reciprocity relationship and vibrational energy variance in a random subsystem at high frequencies. *The Journal of the Acoustical Society of America*, 121(2):913–921, 2007.
- [39] V. Cotoni, R. Langley, and P. Shorter. A statistical energy analysis subsystem formulation using finite element and periodic structure theory. *Journal of Sound and Vibration*, 318(4-5):1077–1108, 2008.
- [40] P. Ragnarsson, B. Pluymers, S. Donders, and W. Desmet. Subcomponent modelling of input parameters for statistical energy analysis by using a wave-based boundary condition. *Journal of Sound and Vibration*, 329(1):96–108, 2010.
- [41] S. Besset, MN. Ichchou, and L. Jezequel. A coupled bem and energy flow method for mid-high frequency internal acoustic. *Journal of Computational Acoustics*, 18(01):69–85, 2010.
- [42] V. Cotoni, A. LeBot, and L. Jezequel. High-frequency radiation of l-shaped plates by a local energy flow approach. *Journal of Sound and Vibration*, 250(3):431–444, 2002.
- [43] FS. Sui, MN. Ichchou, and L. Jezequel. Prediction of vibroacoustics energy using a discretized transient local energy approach and comparison with tsea. *Journal of Sound and Vibration*, 251(1):163–180, 2002.
- [44] HJ-P. Morand. A modal hybridization method for vibroacoustic studies at medium frequencies. *The Journal of the Acoustical Society of America*, 92(4):2365–2366, 1992.
- [45] C. Soize. Reduced models in the medium frequency range for general dissipative structural-dynamics systems. *European Journal of Mechanics-A/Solids*, 17(4):657–685, 1998.
- [46] C. Farhat, I. Harari, and U. Hetmaniuk. A discontinuous galerkin method with lagrange multipliers for the solution of helmholtz problems in the mid-frequency regime. *Computer Methods in Applied Mechanics and Engineering*, 192(11-12):1389–1419, 2003.
- [47] E. De Bel, Ph. Villon, and Ph. Bouillard. Forced vibrations in the medium frequency range solved by a partition of unity method with local information. *International Journal for Numerical Methods in Engineering*, 62(9):1105–1126, 2005.
- [48] PJ. Shorter and RS. Langley. Vibro-acoustic analysis of complex systems. *Journal of Sound and Vibration*, 288(3):669–699, 2005.
- [49] L. Zhang, R. Tezaur, and C. Farhat. Vibro-acoustic analysis of complex systems. *International Journal for Numerical Methods in Engineering*, 66(13):2086–2114, 2006.

-
- [50] L. Ji, BR. Mace, and RJ. Pinnington. A mode-based approach for the mid-frequency vibration analysis of coupled long- and short-wavelength structures. *Journal of Sound and Vibration*, 289(1-2):148–170, 2006.
- [51] C. Soize. A model and numerical method in the medium frequency range for vibroacoustic predictions using the theory of structural fuzzy. *The Journal of the Acoustical Society of America*, 94(2):849–865, 1993.
- [52] A. Sarkar and R. Ghanem. Mid-frequency structural dynamics with parameter uncertainty. *Computer Methods in Applied Mechanics and Engineering*, 191(47-48):5499–5513, 2002.
- [53] L. Gagliardini, L. Houillon, G. Borello, and L. Petrinelli. Virtual sea: Mid-frequency structure-borne noise modeling based on finite element analysis. *In: Noise & Vibration Conference*, 2003-01-1555:22–28, 2003.
- [54] R. Ghanem and A. Sarkar. Mid-frequency structural dynamics with parameter uncertainty. *The Journal of the Acoustical Society of America*, 113(2):834–846, 2003.
- [55] C. Soize. Uncertain dynamical systems in the medium-frequency range. *Journal of Engineering Mechanics*, 129(9):1017–1027, 2003.
- [56] E. Capiez-Lernout and C. Soize. Robust updating of uncertain damping models in structural dynamics for low- and medium-frequency ranges. *Mechanical System and Signal Processing*, 22(8):1774–1792, 2008.
- [57] L. Gagliardini. Dispersed vibroacoustic responses of industrial products: What are we able to predict? *The 26th International Conference on Noise and Vibration engineering (ISMA2014), Leuven, 15-17 September*, 2003-01-1555:17–37, 2014.
- [58] Braun SG. Bucher, I. Left eigenvectors: Extraction from measurements and physical interpretation. *Journal of Applied Mechanics ASME*, 64(1):97–105, 1997.
- [59] PC. Hansen. The truncatedsvd as a method for regularization. *BIT Numerical Mathematics*, 27(4):534–553, 1987.
- [60] RJ. Guyan. Reduction of stiffness and mass matrices. *AIAA Journal*, 3(2):380–380, 1965.
- [61] RJ. Guyan. A method for selecting master dof in dynamic substructuring using the guyan condensation method. *Computers & Structures*, 45(5-6):941–946, 1992.
- [62] RJ. Guyan. Flexural wave-propagation behavior of lumped mass approximations. *Computers & Structures*, 12(6):805–812, 1980.
- [63] HC. Chan, CW. Cai, and YK. Cheung. High convergence order finite elements with lumped mass matrix. *Journal of Sound and Vibration*, 165(2):193–207, 1993.

- [64] MS. Jensen. Convergence studies of dynamic analysis by using the finite element method with lumped mass matrix. *International Journal for Numerical Methods in Engineering*, 139(11):1879–1888, 1996.
- [65] Y. Hahn and N. Kikuchi. Identification of global modeshape from a few nodal eigenvectors using simple free-form deformation. *Engineering with Computers*, 21(2):115–128, 2005.
- [66] JL. Guyader. Characterization and reduction of dynamic models of vibrating systems with high modal density. *Journal of Sound and Vibration*, 328(4-5):488–506, 2009.
- [67] JL. Guyader. Modal sampling method for the vibration study of systems of high modal density. *The Journal of the Acoustical Society of America*, 88(5):2269–2276, 1990.
- [68] A. Noor, M. Anderson, and W. Greene. Continuum models for beam- and platelike-lattice structures. *AIAA Journal*, 16(12):1219–1228, 1978.
- [69] J. Planchard. Vibrations of nuclear fuel assemblies: a simplified model. *Nuclear Engineering and Design*, 86(3):383–391, 1985.
- [70] J. Sigrits and D. Broc. Dynamic analysis of a tube bundle with fluid-structure interaction modelling using a homogenisation method. *Computer Methods in Applied Mechanics and Engineering*, 197(9-12):1080–1099, 2008.
- [71] RR. Craig. *A Review of Time Domain and Frequency Domain Component Mode Synthesis Method in Combined Experimental-Analytical Modeling of Dynamic Structural Systems*. D.R. Martinez and A.K. Miller, New York, 1985.
- [72] D. de Klerk, DJ. Rixen, and SN. Voormeeren. General framework for dynamic substructuring: History, review, and classification of techniques. *AIAA Journal*, 4:1169–1181, 2008.
- [73] AYT. Leung. *Dynamic Stiffness and Substructures*. Springer-Verlag, Berlin, 1993.
- [74] R. Ohayon, C. Soize, and R. Sampaio. Variational-based reduced-order model in dynamic substructuring of coupled structures through a dissipative physical interface: Recent advances. *Archives of Computational Methods in Engineering*, 21(3):321–329, 2014.
- [75] JH. Argyris and S. Kelsey. The analysis of fuselages of arbitrary cross-section and taper: A dsir sponsored research program on the development and application of the matrix force method and the digital computer. *Aircraft Engineering and Aerospace Technology*, 31(3):62–74, 1959.
- [76] JS. Przemieniecki. Matrix structural analysis of substructures. *AIAA Journal*, 1(1):138–147, 1963.
- [77] B. Irons. Structural eigenvalue problems - elimination of unwanted variables. *AIAA Journal*, 3(5):961–962, 1965.

-
- [78] WC. Hurty. Vibrations of structural systems by component mode synthesis. *Journal of Engineering Mechanics ASCE*, 86(4):51–70, 1960.
- [79] WC. Hurty. Dynamic analysis of structural systems using component modes. *AIAA Journal*, 3(4):678–685, 1965.
- [80] RR. Craig and MC. Bampton. Coupling of substructures for dynamic analyses. *AIAA Journal*, 6(7):1313–1319, 1968.
- [81] KJ. Bathe and S. Gracewski. On nonlinear dynamic analysis using substructuring and mode superposition. *Computers & Structures*, 13(5):699–707, 1981.
- [82] C. Farhat and M. Geradin. On a component mode synthesis method and its application to incompatible substructures. *Computers & Structures*, 51(5):459–473, 1994.
- [83] L. Meirovitch and AL. Hale. On the substructure synthesis method. *AIAA Journal*, 19(7):940–947, 1981.
- [84] L. Meirovitch and MK. Kwak. Rayleigh-ritz based substructure synthesis for flexible multi-body systems. *AIAA Journal*, 29(10):1709–1719, 1991.
- [85] SN. Voormeeren, PL. van der Valk, and DJ. Rixen. Generalized methodology for assembly and reduction of component models for dynamic substructuring. *AIAA Journal*, 49(5):1010–1020, 2011.
- [86] SN. Voormeeren, PL. van der Valk, and DJ. Rixen. Vibration analysis of structures by component mode substitution. *AIAA Journal*, 9(7):1255–1261, 1971.
- [87] R. Mac Neal. Vibration analysis of structures by component mode substitution. *Computers & Structures*, 1(4):581–601, 1971.
- [88] S. Rubin. Improved component-mode representation for structural dynamic analysis. *AIAA Journal*, 13(8):995–1006, 1975.
- [89] D. Markovic, KC. Park, and A. Ibrahimbegovic. Reduction of substructural interface degrees of freedom in flexibility-based component mode synthesis. *International Journal for Numerical Methods in Engineering*, 70(2):163–180, 2007.
- [90] Sampaio R. Ohayon, R. and C. Soize. Dynamic substructuring of damped structures using singular value decomposition. *Journal of Applied Mechanics ASME*, 64(2):292–298, 1997.
- [91] KC. Park and YH. Park. Dynamic substructuring of damped structures using singular value decomposition. *AIAA Journal*, 42(6):1236–1245, 2004.
- [92] DJ. Rixen. A dual craig–bampton method for dynamic substructuring. *Journal of Computational and Applied Mathematics*, 168(1-2):383–391, 2004.

- [93] RA. Ibrahim. *Parametric Random Vibration*. John Wiley and Sons, New York, 1985.
- [94] RA. Ibrahim. *Stochastic Finite Elements: A Spectral Approach*. Revised edition, Dover Publications, New York, 1991.
- [95] JL. Beck and LS. Katafygiotis. Updating models and their uncertainties - i: Bayesian statistical framework. *Journal of Engineering Mechanics ASCE*, 124(4):455–461, 1998.
- [96] C. Soize and R. Ghanem. Physical systems with random uncertainties: chaos representations with arbitrary probability measure. *SIAM Journal on Scientific Computing*, 26(2):395–410, 2004.
- [97] R. Mace, W. Worden, and G. Manson. Physical systems with random uncertainties: Chaos representation with arbitrary probability measure. *Journal of Sound and Vibration*, 288(3):431–790, 2005.
- [98] GI. Schuëller. Computational methods in stochastic mechanics and reliability analysis. *Computer Methods in Applied Mechanics and Engineering*, 194(12-16):1251–1795, 2005.
- [99] GI. Schuëller. Uncertainties in structural mechanics and analysis - computational methods. *Computer & Structures*, 83(14):1031–1150, 2005.
- [100] GI Schuëller. Developments in stochastic structural mechanics. *Archive of Applied Mechanics*, 75(10-12):755–773, 2006.
- [101] G. Deodatis and PD. Spanos. Developments in stochastic structural mechanics. *Probabilistic Engineering Mechanics*, 23(2-3):103–346, 2008.
- [102] GI. Schuëller and HJ. Pradlwarter. Uncertain linear systems in dynamics: Retrospective and recent developments by stochastic approaches. *Engineering Structures*, 31(11):2507–2517, 2009.
- [103] OP. Le Maitre and OM. Knio. *Spectral Methods for Uncertainty Quantification with Applications to Computational Fluid Dynamics*. Springer, Heidelberg, 2010.
- [104] C. Soize. Stochastic modeling of uncertainties in computational structural dynamics - recent theoretical advances. *Journal of Sound and Vibration*, 332(10):2379–2395, 2013.
- [105] R. Ghanem, D. Higdon, and H. Owhadi. *Handbook of Uncertainty Quantification*. Springer International Publishing Switzerland, 2017.
- [106] T. Bui-Thanh, K. Willcox, and O. Ghattas. Parametric reduced-order models for probabilistic analysis of unsteady aerodynamic applications. *AIAA Journal*, 46(10):2520–2529, 2008.

-
- [107] J. Degroote, J. Vierendeels, and K. Willcox. Interpolation among reduced-order matrices to obtain parameterized models for design, optimization and probabilistic analysis. *International Journal for Numerical Methods in Engineering*, 63(2):207–230, 2010.
- [108] Y. Marzouk, HN. Najm, and LA. Rahn. Stochastic spectral methods for efficient bayesian solution of inverse problems. *Journal of Computational Physics*, 224(2):560–586, 2007.
- [109] D. Galbally, K. Fidkowski, K. Willcox, and O. Ghattas. Non-linear model reduction for uncertainty quantification in large scale inverse problems. *International Journal for Numerical Methods in Engineering*, 81(12):1581–1608, 2010.
- [110] C. Lieberman, K. Willcox, and O. Ghattas. Parameter and state model reduction for large scale statistical inverse problems. *SIAM Journal on Scientific Computing*, 32(5):2523–2542, 2010.
- [111] A. Nouy and C. Soize. Random field representations for stochastic elliptic boundary value problems and statistical inverse problems. *European Journal of Applied Mathematics*, 25(3):339–373, 2014.
- [112] T. Cui, YM. Marzouk, and KE. Willcox. Data-driven model reduction for the bayesian solution of inverse problems. *International Journal for Numerical Methods in Engineering*, 102(5):966–990, 2015.
- [113] R. Ghanem, D. Higdon, and H. Owhadi. *Handbook for Uncertainty Quantification*, chapter Random vectors and random fields in high dimension. Parametric model-based representation, identification from data. Springer: Heidelberg, 2017.
- [114] C. Soize. A nonparametric model of random uncertainties for reduced matrix models in structural dynamics. *Probabilist Engineering Mechanics*, 15(3):277–299, 2000.
- [115] CE. Shannon. A mathematical theory of communication. *The Bell system technical journal*, 27(3):379–423, 1948.
- [116] ET. Jaynes. Information theory and statistical mechanics. *Physical review*, 106(4):620, 1957.
- [117] MP. Mignolet and C. Soize. Nonparametric stochastic modeling of linear systems with prescribed variance of several natural frequencies. *Probabilistic Engineering Mechanics*, 23(2-3):267–278, 2008.
- [118] R. Ghanem, D. Higdon, and H. Owhadi. *Handbook for Uncertainty Quantification*, chapter Random matrix models and nonparametric method for uncertainty quantification. Springer International Publishing Switzerland, 2017.

- [119] C. Chen, D. Duhamel, and C. Soize. Probabilistic approach for model and data uncertainties and its experimental identification in structural dynamics: Case of composite sandwich panels. *Journal of Sound and Vibration*, 294(1-2):64–81, 2006.
- [120] R. Capillon, C. Desceliers, and C. Soize. Uncertainty quantification in computational linear structural dynamics for viscoelastic composite structures. *Computer Methods in Applied Mechanics and Engineering*, 305:154–172, 2016.
- [121] C. Soize and H. Chebli. Random uncertainties model in dynamic substructuring using a nonparametric probabilistic model. *Journal of Engineering Mechanics ASCE*, 129(4):449–457, 2003.
- [122] MP. Mignolet, C. Soize, and J. Avalos. Nonparametric stochastic modeling of structures with uncertain boundary conditions / coupling between substructures. *AIAA Journal*, 51(6):1296–1308, 2013.
- [123] M. Arnst, D. Clouteau, H. Chebli, R. Othman, and G. Degrande. A non-parametric probabilistic model for ground-borne vibrations in buildings. *Probabilistic Engineering Mechanics*, 21(1):18–34, 2006.
- [124] E. Capiez-Lernout and C. Soize. Robust design optimization in computational mechanics. *Journal of Applied Mechanics ASME*, 75(2):1–11, 2008.
- [125] M. Arnst and C. Soize. Identification and sampling of bayesian posteriors of high-dimensional symmetric positive-definite matrices for data-driven updating of computational models. *Computer Methods in Applied Mechanics and Engineering*, 352:300–323, 2019.
- [126] MP. Mignolet and C. Soize. Stochastic reduced order models for uncertain geometrically nonlinear dynamical systems. *Computer Methods in Applied Mechanics and Engineering*, 197(45-48):3951–3963, 2008.
- [127] E. Capiez-Lernout, C. Soize, and Mignolet MP. Post-buckling nonlinear static and dynamical analyses of uncertain cylindrical shells and experimental validation. *Computer Methods in Applied Mechanics and Engineering*, 271(1):210–230, 2014.
- [128] C. Soize and C. Farhat. Uncertainty quantification of modeling errors for nonlinear reduced-order computational models using a nonparametric probabilistic approach. *International Journal for Numerical Methods in Engineering*, 30(2016):96, 2016.
- [129] O. Ezvan, A. Batou, and C. Soize. Multilevel reduced-order computational model in structural dynamics for the low-and medium-frequency ranges. *Computers & Structures*, 160:111–125, 2015.

-
- [130] C. Soize and A. Batou. Stochastic reduced-order model in low-frequency dynamics in presence of numerous local elastic modes. *Journal of Applied Mechanics ASME*, 78(6):1–9, 2011.
- [131] JA. Sethian. A fast marching level set method for monotonically advancing fronts. *Proceedings of the National Academy of Sciences*, 93(4):1591–1595, 1996.
- [132] R. Kimmel and JA. Sethian. Computing geodesic paths on manifolds. *Proceedings of the national academy of Sciences*, 95(15):8431–8435, 1998.
- [133] A. Batou and C. Soize. Uncertainty quantification in low-frequency dynamics of complex beam-like structures having a high-modal density. *International Journal for Uncertainty Quantification*, 1(1):475–485, 2013.
- [134] A. Batou, C. Soize, and N. Brie. Reduced-order computational model in nonlinear structural dynamics for structures having numerous local elastic modes in the low-frequency range. application to fuel assemblies. *Nuclear Engineering and Design*, 262:276–284, 2013.
- [135] A. Arnoux. *RÉduction des ModÈles NumÉriques en Dynamique LinÉaire Basse FrÉquence des Automobiles*. PhD thesis, Université Paris-Est Marne-la-Vallée, 2012.
- [136] O. Ezvan, A. Batou, and C. Soize. Reduced-order model for the dynamical analysis of complex structures with a high modal density. *The 21st International Congress on Sound and Vibration (ICSV21), Beijing, China, July 13-17*, 2:1396–1403, 2014.
- [137] O. Ezvan, A. Batou, and C. Soize. Stochastic reduced-order model for the dynamical analysis of complex structures with a high modal density. *International Conference on Uncertainty in Structural Dynamics, USD2014, Katholieke Universiteit Leuven, Belgium, September 15-17*, 15–17:4653–4664, 2014.
- [138] O. Ezvan, A. Batou, and C. Soize. Global reduced-order model adapted to the low- and medium-frequency analysis of complex dynamical structures. *PANACM 2015, 1st Pan-American Congress on Computational Mechanics, Buenos Aires, Argentina, April 27-29*, 27–29:1022–1028, 2015.
- [139] O. Ezvan, A. Batou, and C. Soize. Multilevel stochastic reduced-order model in linear structural dynamics for complex structures. *7th European Congress on Computational Methods in Applied Sciences and Engineering, ECCOMAS Congress 2016, the Island of Crete, Greece, June 5-10*, 2016.
- [140] G. Karypis and K. Vipin. A fast and high quality multilevel scheme for partitioning irregular graphs. *SIAM J Sci Comput*, 20(1):359–392, 1998.
- [141] JK. Bennighof and RB. Lehoucq. An automated multilevel substructuring method for eigenspace computation in linear elastodynamics. *SIAM Journal on Scientific Computing*, 25(6):2084–2016, 2004.

- [142] W. Gao, X.S. Li, C. Yang, and Z. Bai. An implementation and evaluation of the amls method for sparse eigenvalue problems. *ACM Transactions on Mathematical Software (TOMS)*, 34(4):1–28, 2008.
- [143] J. Reyes, C. Soize, L. Gagliardini, and G. Brogna. Nonparametric probabilistic vibroacoustic analysis with nastran: a computational tool for estimating the likelihood of automobiles experimental FRF measurements. *28th Conference on Noise and Vibration Engineering (ISMA 2018)*, pages 1–12, 2018.
- [144] J. Reyes, C. Desceliers, C. Soize, and L. Gagliardini. Réduction de modèle multi-niveau pour la quantification de l’incertitude dans le cas de la dynamique vibroacoustique. *Actes du 14ème Colloque National en Calcul des Structures (CSMA 2019)*, pages 1–7, 2019.
- [145] J. Reyes, C. Desceliers, C. Soize, and L. Gagliardini. Multilevel model reduction for uncertainty quantification in computational vibro-acoustical dynamics. *3rd International Conference on Uncertainty Quantification in Computational Sciences and Engineering (UNCECOMP 2019), Island of Crete, Greece, June 2019*.
- [146] G. Brogna, J. Antoni, N. Totaro, L. Gagliardini, and O. Sauvage. Reduction and interpretation of matrices of frequency response functions by bayesian independent component analysis. *Journal of Sound and Vibration*, 458:238–261, 2019.
- [147] A. Hyvarinen, J. Karhunen, and E. Oja. *Independent Component Analysis*. John Wiley and Sons, Hoboken, New Jersey, 2004.
- [148] J-F. Cardoso and A. Souloumiac. Blind beam forming for non-gaussian signals. *IEEE Proceedings F*, 140(6):362–370, 1993.